ISTANBUL TECHNICAL UNIVERSITY ★ GRADUATE SCHOOL OF SCIENCE ENGINEERING AND TECHNOLOGY

SEISMIC PERFORMANCE OF STEEL-CONCRETE COMPOSITE BUILDING WITH REINFORCED CONCRETE SHEAR WALLS

M.Sc. THESIS

Ragibe Ece YÜKSELEN

Department of Civil Engineering

Structure Engineering Programme

Thesis Advisor: Prof. Dr. Cavidan YORGUN

JANUARY 2015

ISTANBUL TECHNICAL UNIVERSITY ★ GRADUATE SCHOOL OF SCIENCE ENGINEERING AND TECHNOLOGY

SEISMIC PERFORMANCE OF STEEL-CONCRETE COMPOSITE BUILDING WITH REINFORCED CONCRETE SHEAR WALLS

M.Sc. THESIS

Ragibe Ece YÜKSELEN
(501111068)

Department of Civil Engineering

Structure Engineering Programme

Thesis Advisor: Prof. Dr. Cavidan YORGUN

19 JANUARY 2015

İSTANBUL TEKNİK ÜNİVERSİTESİ ★ FEN BİLİMLERİ ENSTİTÜSÜ

BETONARME PERDELİ ÇELİK-BETON KOMPOZİT BİNANIN DEPREM PERFORMANSININ İNCELENMESİ

YÜKSEK LİSANS TEZİ

Ragibe Ece YÜKSELEN
(501111068)

İnşaat Mühendisliği Anabilim Dalı

Yapı Mühendisliği Programı

Tez Danışmanı: Prof. Dr. Cavidan YORGUN

19 OCAK 2015

Ragibe Ece Yükselen, a **M.Sc.** student of ITU **Graduate School of Science Engineering and Technology** student ID 501111068, successfully defended the **thesis** entitled "**SEISMIC PERFORMANCE OF STEEL-CONCRETE COMPOSITE BUILDING WITH SHEAR WALLS**", which she prepared after fulfilling the requirements specified in the associated legislations, before the jury whose signatures are below.

Thesis Advisor :	**Prof. Dr. Cavidan YORGUN** Istanbul Technical University	....
Jury Members :	**Prof. Dr. A. Zafer ÖZTÜRK** Yıldız Technical University	....
	Asst. Prof. Dr. Cüneyt VATANSEVER Istanbul Technical University	....

Date of Submission : 15 December 2014
Date of Defense : 19 January 2015

To my beloved parents and brother,

PREFACE

This thesis is submitted in partial fulfillment of the requirements for M.Sc. degree in structural engineering. This thesis journey is started with the idea of doing research in Europe. The path was rough, but everytime overcoming a difficulty makes the feeling of self-improvement and having experience.

The case study of this thesis is done in University of Trento, Italy, as a part of the research that inspired by the European Project ATTEL, with counseling of Professor Oreste S. Bursi. The opportunity of joining this research is provided by Erasmus Programme. The full-text of the thesis is prepared with supervision of Professor Cavidan Yorgun.

I would like to express my sincere gratitude to my supervisor Prof. Dr. Cavidan Yorgun, who never gives up to share her profound knowledge and experience during my academic life. I would like to thank Asst. Prof. Dr. Cüneyt Vatansever for leading up the comunication with Italy and supporting me in the scientific sense.

Special thanks and appreciation go to Prof. Dr. Oreste S. Bursi for his hospitability and sharing his erudition. Research of this thsesis is actualised with support of him by accepting to coroparete me to the research conducted in Universty of Trento, Italy. I would like to thank Asst. Prof. Dr. Nicola Tondini due to his patience, encouragement and teaching me during the study. It has been pleasure for me to know and be able to have a chance to work with them.

I wish to express my thanks to Dr. Gabriele Zanon for his support and sharing his knowledge. I would also like to thank Ph.D candidates Manuel Fassin and Pavel Sozonov. I am glad that I had the change to work with all of them.

I am deeply grateful to my mother and my father, who have been supportive from the moment of my first steps until these M.Sc. thesis days, for their patience and understanding. I would also like to thank my brother, who has been always helpful, supportive and cheering.

I want to express my thankfulness to Metin, who provides full support in every respect, from the moment we have met.

Finally, I would like to thank to all my dear colleagues and friends. I am very glad that I had the chance to meet with them during my education life.

December 2014 Ragibe Ece YÜKSELEN

TABLE OF CONTENTS

Page

PREFACE ix
TABLE OF CONTENTS xi
ABBERVIATIONS xiii
SYMBOLS xv
LIST OF TABLES xix
LIST OF FIGURES xxi
SUMMARY xxv
ÖZET xxvii
1. INTRODUCTION 1
1.1 Objective 1
1.2 Scope of Thesis 3
2. BASICS OF NONLINEAR ANALYSIS 5
2.1 Modeling of Reinforced Concrete Elements 6
2.1.1 Material models for concrete 6
2.1.2 Material models for steel 18
2.1.3 Material model for the effect of shear and shear strength 21
2.1.4 Material model for the effect of torsion and torsional capacity 21
2.1.5 Fiber beam-column elements: distributed plasticity 23
2.1.5.1 Fiber section 24
2.1.5.2 Difference between forced-based and displacement-based beam column elements 25
2.2 Modeling Steel-Concrete Composite Moment Frames 27
2.2.1 Elastic beam-column elements 28
2.2.2 Modeling of lumped plasticity 29
3. METHODS FOR PERFORMANCE ASSESSMENT OF BUILDINGS 33
3.1 Performance Assessment With Nonlinear Static Analysis Per Eurocode 8 33
3.2 Performance Assessment With Nonlinear Dynamic Analysis 39
4. MODEL BUILDING FOR CASE STUDY 43
4.1 Structural System of the Building 43
4.2 Analytical Models of the Moment Frames and Shear Walls 54
4.3 Analyses Of The Shear Wall and Building 60
4.3.1 Analysis of the shear wall 61
4.3.1.1 Static monotonic nonlinear (pushover) analysis 63
4.3.1.2 Static cyclic nonlinear (ECCS) analysis 64
4.3.2 Analyses of the building 66
4.4 Analyses Results 66
4.4.1 Moment-curvature analysis results of shear wall 67
4.4.2 Pushover analysis results of shear wall 68
4.4.3 Cyclic nonlinear analysis results of shear wall 70
4.4.4 Pushover analysis results of the building 75

4.4.5 Modal analysis results of the building..77
4.4.6 Time-history analysis results of the building..78
4.5 Target displacement of the building according to Eurocode 8.........................79
5. CONCLUSIONS AND RECOMMENDATIONS...85
REFERENCES...87
APPENDICES...91
APPENDIX A: Drawings of the Structure...92
APPENDIX B: Input Data...96
APPENDIX C: Analyses Results...98
CURRICULUM VITAE...101

ABBERVIATIONS

ATTEL	**:** Performance-based approaches for high strength tubular columns and connections under earthquake and fire loadings
CFT	**:** Concrete Filled Tube
CHS	**:** Circular Hollow Section
ECCS	**:** European Convention for Constructional Steelwork
HSS	**:** High Strength Steel
MDOF	**:** Multi Degree of Freedom
RC	**:** Reinforced Concrete
SDOF	**:** Single Degree of Freedom
SIMQKE	**:** Conditioned earthquake ground motion simulator
2D	**:** Two dimensional
3D	**:** Three dimensional

SYMBOLS

$\boldsymbol{A_c}$: Area of core of section enclosed by centerlines of the perimeter hoop
$\boldsymbol{A_{cc}}$: Area of concrete core
$\boldsymbol{A_e}$: Area of effective confined concrete core at hoop level
$\boldsymbol{A_g}$: Gross section area of the shear wall section
$\boldsymbol{a_g}$: Ground acceleration
$\boldsymbol{A_i}$: Total plan area of ineffectually confined core concrete at the level of the hoops
$\boldsymbol{A_{sl}}$: Total area of longitudinal reinforcement
$\boldsymbol{A_{sx}}$: The total area of transverse bars running in the x direction
$\boldsymbol{A_{sy}}$: The total area of transverse bars running in the y direction
$\boldsymbol{b}$: Strain hardening ratio
$\boldsymbol{b_c}$: Core length to centerlines of perimeter hoop in x direction for RC sections
$\boldsymbol{c}$: Damping coefficient
$\boldsymbol{c_0}$: Constant
$\boldsymbol{d^*}$: The displacement of the SDOF system
$\boldsymbol{d_c}$: Core width to centerlines of perimeter hoop in y direction for RC sections
$\boldsymbol{d_d}$: Average displacement of three accelerograms according to time-history analyses
$\boldsymbol{d^*_{et}}$: The target displacement of the structure with period T^*
$\boldsymbol{d_{Fmax}}$: Displacement at maximum shear force reaction of the building
$\boldsymbol{d_l}$: Diameter of longitudinal reinforcement
$\boldsymbol{d^*_m}$: The displacement at plastic mechanism of the equivalent SDOF system
$\boldsymbol{d_n}$: Displacement of the control node of the MDOF system (top displacement)
$\boldsymbol{d_{Pmax}}$: Displacement at maximum shear force reaction of shear wall for pushover
$\boldsymbol{d_t}$: Target displacement of the MDOF system
$\boldsymbol{d^*_t}$: Target displacement of the idealized equivalent SDOF system
$\boldsymbol{d_{time}}$: Time step
$\boldsymbol{d_{tr}}$: Diameter of transverse reinforcement
$\boldsymbol{d_w}$: Thickness of the shear wall section
$\boldsymbol{d^*_y}$: Yield displacement of the idealized SDOF system
$\boldsymbol{E}$: Elastic modulus of reinforcing steel
$\boldsymbol{E_c}$: Elastic modulus of confined concrete
$\boldsymbol{E_{c0}}$: Initial elastic tangent for steel material
$\boldsymbol{e_{cc}}$: Strain of confined concrete at compressive strength
$\boldsymbol{e_{ccu}}$: Strain of confined concrete at ultimate strength
$\boldsymbol{E_{cm}}$: Modulus of elasticity of concrete

e_{cu} : Strain of unconfined concrete at ultimate compressive strength
e_{c0} : Strain of unconfined concrete at characteristic compressive strength
$(EI)_{eff}$: Charactreristic value of effective flexural stiffness of composite sections
E_H : Hysteretic energy of the MDOF system
E_H^* : Hysteretic energy of equivalent SDOF system
E_m^* : The actual deformation energy, up to the formation of the plastic mechanism
e_{su} : Ultimate strain of reinforcing steel
e_{sy} : Yielding strain of reinforcing steel
e_y : Yielding displacement
F^* : The base shear force of the equivalent SDOF system
F_b : The base shear force of the MDOF system
f'_{cc} : Compressive strength of confined concrete
f'_{c0} : Characteristic compressive strength of unconfined concrete
$\overline{F}_i$: Normalized lateral forces
f_l : Lateral pressure from the transverse reinforcement
f'_l : Effective lateral confining pressure
f_{lx} : Lateral confining stress on the concrete in the x direction
f_{ly} : Lateral confining stress on the concrete in the y direction
F_{max} : Maximum shear force reaction of the building
f_s : Elastic force or inelastic resisting force
f_{tk} : Tensile strength of the reinforcement
f_u : Ultimate strength of the reinforcement
$F_{ultimate}$: Ultimate shear strength of the building
F_y^* : Yield force which represents also ultimate strength of idealized system
f_{yh} : Yield strength of transverse reinforcement
f_{yk} : Yielding strength of the reinforcement
g : Gravitational acceleration
G_{c0} : Shear modulus
$G_{c0}J$: Torsional stiffness
h_s : Story height
h_w : Height of the shear walls
I_a : Second moment of area of the structural steel section
I_c : Second moment of area of the uncracked concrete section
I_s : Second moment of area of the reinforcement for bending plane
J : Polar moment of inertia
k_e : Confinement effectiveness coefficient
K_e : Correction factor
l_{max} : Length from further point to the center for the shear wall section
l_w : Length (width) of the shear walls
m : Mass matrix
m^* : The mass of the equivalent SDOF system
m_i : Concentrated mass in the i^{th} story
M_{Gelfi} : Moment capacity of shear wall section acc. to calculations with Gelfi
M_{max} : Moment capacity of shear wall section acc. to pushover analysis

$\boldsymbol{M_{MC}}$	: Moment capacity of shear wall section according to moment-curvature analysis
$\boldsymbol{M_T}$	: Torsional moment capacity of the section
$\boldsymbol{m_1}$	: Concentrated masses at nodes 3, 4, 5 and 6 of shear wall model
$\boldsymbol{m_2}$	: Concentrated mass at node 7 of shear wall model
$\boldsymbol{N_R}$	: Vertical support reaction of shear wall
$\boldsymbol{N_0}$	: Gravity load of the shear wall
$\boldsymbol{P_{crushing}}$	: Shear force reaction at failure of shear wall according to pushover
$\boldsymbol{P_{max}}$	: Maximum shear force reaction of shear wall according to pushover analysis
$\boldsymbol{p(t)}$	: Exitation vector
$\boldsymbol{P_1}$	: Axial (gravity) loads at nodes 3,4,5 and 6 of shear wall model
$\boldsymbol{P_2}$	: Axial (gravity) load at node 7 of shear wall model
$\boldsymbol{q_u}$	: Ratio between acc. in the struct. with unlimited behaviour and limited strength
$\boldsymbol{R}$	: Quantities in the equivalent SDOF system
$\boldsymbol{R^*}$	: Quantities in the MDOF system
$\boldsymbol{R_0, cR_1, cR_2}$	: Values that control the transition from elastic to plastic (R parameter)
$\boldsymbol{S}$	: Soil factor
$\boldsymbol{s}$	: Center to center spacing of hoops
$\boldsymbol{s'}$	: Clear vertical spacing between hoop bars
$\boldsymbol{S_e(T^*)}$	: The elastic acceleration response spectrum at the period T^*
$\boldsymbol{T^*}$	: The period of the idealized equivalent SDOF system
$\boldsymbol{T_C}$	: The corner period between the short and medium-long period range
$\boldsymbol{T_{max}}$	: Maximum duration of ground motion
$\boldsymbol{T_S}$	: Minimum duration of ground motion
$\boldsymbol{T_1}$	: Fundamental period of the structure
$\boldsymbol{u}$	: Displacement vector
$\boldsymbol{\dot{u}}$	: Velocity
$\boldsymbol{\ddot{u}}$	: Acceleration
$\boldsymbol{V}$	: Reduced shear capacity of shear wall section
$\boldsymbol{w'_i}$	: i^{th} clear distance between adjacent longitudinal bars
$\boldsymbol{\rho_{cc}}$	: Ratio of area of longitudinal reinforcement to area of core of section
$\boldsymbol{\rho_x}$	: Ratio of the transversal confining steel volume to the volume of confined concrete core in x direction
$\boldsymbol{\rho_y}$	: Ratio of the transversal confining steel volume to the volume of confined concrete core in y direction
$\boldsymbol{\Gamma}$	: Transformation factor
$\boldsymbol{\gamma}$	: Density of reinforced concrete
$\boldsymbol{\tau_{max}}$	: Maximum shear stress
$\boldsymbol{\tau_y}$	: Shear stress at yielding in a simple tension test
$\boldsymbol{\sigma_{max}}$	: Maximum principle stress
$\boldsymbol{\sigma_{min}}$	: Minimum principle stress
$\boldsymbol{\upsilon}$	: Poisson ratio
$\boldsymbol{\varphi}$	: Curvature
$\boldsymbol{\Phi_i}$	: Normalized displacements
$\boldsymbol{\Phi_n}$	: Displacement shape

LIST OF TABLES

Page

Table 2.1 : Properties of reinforcement according to Eurocode 2 [17]. 19
Table 4.1 : Moadal analysis results of 3D structure. 77
Table 4.2 : Periods of the building. 78
Table 4.3 : Maximum displacements. 78
Table 4.4 : Max. displacements for top of the building according to time-history analysis. 78
Table 4.5 : Mass distribution to the floors for 3D structure model. 79
Table 4.6 : Normalization of predominant (4th) mode shape. 80
Table 4.7 : Comparison of displacements 83

LIST OF FIGURES

Page

Figure 2.1 : Modeling structural components. [12] 6
Figure 2.2 : Typical uniaxial compresion and tension stress-strain curve for concrete, [16]. 7
Figure 2.3 : Cyclic loading of concrete according to Karsan and Jirsa [18], cited from Bangash, [16]....... 8
Figure 2.4 : Stress-strain curve of concrete01 model, [12]....... 9
Figure 2.5 : Typical hysteretic stress-strain relation of concrete01 material, [12]. 9
Figure 2.6 : Stress-strain curve of concrete02 material, [12]....... 10
Figure 2.7 : Typical hysteretic stress-strain relation of concrete02 model, [12]. 10
Figure 2.8 : Comparison of hysteretic behaviour of concrete01 and concrete02, [12]. 11
Figure 2.9 : Calculated relative stress-strain diagrams for normal-weight concretes of various compressive strengths and for cement paste, [19]....... 12
Figure 2.10 : An example cyclic tension-compression response envelope of concrete generated using the concrete04 model, [12]....... 12
Figure 2.11 : A representation of stress-strain relation for RC sections with and without confinement....... 13
Figure 2.12 : Stress-strain curve of confined and unconfined concrete proposed by Saatcioglu and Razvi, [15]. 14
Figure 2.13 : Stress-strain model proposed for monotonic loading of confined and unconfined concrete [14]....... 15
Figure 2.14 : Effectively confined core for rectangular hoop reinforcement, [14]... 17
Figure 2.15 : Stress-strain relationship for typical reinforcing steel....... 19
Figure 2.16 : Stress-strain relationship under cyclic loading for Giuffré-Menegotto-Pinto steel material model [21]....... 20
Figure 2.17 : Stress-strain relationship for Steel02 model, [12]. 20
Figure 2.18 : Stress-strain relationship of elastic material model, [12]. 21
Figure 2.19 : Steel 01 material parameters of monotonic envelop [12]....... 22
Figure 2.20 : An example for fiber beam-column element model. 24
Figure 2.21 : An example for fiber section, [12]. 25
Figure 2.22 : Obtaining curvature of forced-based and displacement-based elements, [26]. 26
Figure 2.23 : Fiber type beam-column element, [20]. 26
Figure 2.24 : A representation for composite beams. 28
Figure 2.25 : A representation for composite columns. 29
Figure 2.26 : Representation of ZeroLength element. 30
Figure 2.27 : Schematic model of hysteretic SDOF system, [27]....... 30
Figure 2.28 : Stress-strain curve for one-member truss with degrading Bouc-Wen material, [30]. 31

Figure 2.29 : Definition of pinchin4 uniaxial material model, [12]. 31
Figure 2.30 : Graphically represented parallel material, [12]. 32
Figure 3.1 : Input data for pushover, [3]. 34
Figure 3.2 : Represetation for evaluation of pushover (capacity) curve [3]. 35
Figure 3.3 : Transformation from MDOF sytem to SDOF system. 35
Figure 3.4 : Determination of the idealized elasto-perfectly plastic force-displacement relationship, [10]. 37
Figure 3.5 : Determination of the target displacement for the equivalent SDOF system [10]. 39
Figure 4.1 : Plan view of the ground floor. 44
Figure 4.2 : Sectional view of axis C-C. 45
Figure 4.3 : Sectional view of composite slab. 46
Figure 4.4 : A representation of shear wall. 46
Figure 4.5 : Reinforcement details of ground floor shear wall section. 47
Figure 4.6 : Stress-strain relationship for reinforcing steel. 48
Figure 4.7 : Representation of fibers of sections. 49
Figure 4.8 : A vertical section of RC shear wall at ground floor. 51
Figure 4.9 : Comparison between confined and unconfined stress-strain relationship. 53
Figure 4.10 : Comparison of stress-strain curves of concrete01 and concrete04 material models for confined concrete fibers. 56
Figure 4.11 : Comparison of pushover-curves for shear walls with concrete 01 and concrete04 material models. 57
Figure 4.12 : Representation of section aggregator for 2D model. 58
Figure 4.13 : Representation of section aggregator for 3D model. 59
Figure 4.14 : Representation of forced-based beam-column element model. 60
Figure 4.15 : Mass distribution of shear wall. 61
Figure 4.16 : Gravity loading of shear wall. 62
Figure 4.17 : Representation of loadig for moment-curvature analysis. 63
Figure 4.18 : Representation of static monotonic loading. 64
Figure 4.19 : Evaluation of yielding displacement (e_y). 65
Figure 4.20 : ECCS loading procedure. 65
Figure 4.21 : Moment-curvature of shear wall section. 67
Figure 4.22 : Moment capacity calculations of shear wall section. 68
Figure 4.23 : Pushover (capacity) curve. 69
Figure 4.24 : Moment capacity diagram according to pushover analysis. 70
Figure 4.25 : Force-displacement curve of shear wall under ECCS loading. 71
Figure 4.26 : Representation of fiber names. 71
Figure 4.27 : Stress-strain relationship of confined concrete fibers. 72
Figure 4.28 : Stress-strain relationship of unconfined concrete fibers. 72
Figure 4.29 : Stress-strain assesment of confined concrete fibers on the left edge of the section. 74
Figure 4.30 : Stress-strain assesment of confined concrete fibers on the right edge of the section. 74
Figure 4.31 : Pushover curve of 3D structure model. 75
Figure 4.32 : Pushover curves of shear walls and columns. 76
Figure 4.33 : Moment reaction of 3D structure model. 76
Figure 4.34 : Moment reactions of shear walls and columns. 77
Figure 4.35 : Force displacement curve of equivalent SDOF system. 81

Figure 4.36 : Determination of idealized elasto-perfectly force-displacement relationship. 82
Figure 4.37 : Determination of target displacement. 83

SEISMIC PERFORMANCE OF STEEL-CONCRETE COMPOSITE BUILDING WITH REINFORCED CONCRETE SHEAR WALLS

SUMMARY

Reinforced concrete walls are commonly used components for earthquake resistant design of structures. Composite structures become widespread too in seismic regions. Additionally, performance based apporaches for structures is often placed in design codes of countries, which are located in seismic zones. Eurocode 8 composes procedures for performance based design.

In general seismic performance assesment is possible with both linear and nonlinear methods. This study is interested in nonlinear approaches. Nonlinear static method is investigated according to Eurocode 8 in this study. Modeling and numerical analysis of shear walls are examined. Study for modeling and analysis of steel-concrete composite structures followed and performance-based approaches are investigated. Finally, a case study is perfomed.

The case study of this thesis is perfomed as a part of a project that was carried out in University of Trento, Italy. A three-dimensional (3D) steel-concrete composite building with reinforced concrete (RC) shear walls is analyzed and results are discussed. Target displacement of the buildig, which is the limit displacement of the structure under the applied seismic hazard level, is determined due to nonlinear static analysis results in terms of Eurocode 8. Additionally, maximum top displacement of the structure is obtained with nonlinear dynamic (time-history) analysis.

The thesis consists of five chapters. The first chapter presents an introduction and definition of the topic of the thesis, a short review of literature, the scope and purpose of the study.

In the second chapter, a detailed explanation of nonlinear analysis using software is given. Since the software named Opensees is used in this study, this chapter contains explanations about this program. The chapter composes material models and definition of materials in Opensees, methods to define nonlinearty of the elements and comparison of methods (lumped or distributed plasticity) and fiber section models.

Third chapter covers general information about the methods for performance assessment of the structures. Performance assessment with nonlinear static analysis is explained and the procedure for calculation of target displacement according to Eurocode 8 is represented in this chapter. Seismic performance assesment of the structures with nonlinear dynamic analysis is described too. Advantages and disadvantages of nonlinear dynamic methods are shortly explained.

Fourth chapter is the chapter where the seismic performance assessment of a steel-concrete composite structure with shear walls takes place. Detailed representation of

the properties of the structure, modeling with OpenSEES, definition of perfomed analysis, explanation of analysis results are presented in this chapter.

Analyses of two-dimensional (2D) shear walls and three dimensional (3D) structure that are exposed to earthquake loads are carried through. Modeling and analysis of shear walls are performed. Then shear wall model is combined with 3D model of the structure. This chapter contains analysis of 2D shear wall and performance assessment of 3D building on the shear wall direction.

The conclusions and discussions of this study take place in fifth chapther. Convenient methods for practical modeling and performance assessment are expressed according to previous studies and this research. The performance assessment is performed with comparison of the target displacement obtained in terms of Eurocode 8 and displacements obtained with time history analysis. This comparison is presented in chapter five. Possible researches in the future are also recommended in this chapter.

BETONARME PERDELİ ÇELİK-BETON KOMPOZİT BİNANIN DEPREM PERFORMANSININ İNCELENMESİ

ÖZET

Yapıların deprem performansanın incelenmesi son yıllarda yaygın bir yöntem haline geldi. Özellikle deprem bölgelerinde yer alan ülkelerin yönetmelik ve strandartlarında performansa dayalı yapısal tasarıma yer verilmektedir. Eurocode 8 de bu hesap metoduna yer veren tasarım standartlardan biridir. Bu çalışmada Eurocode 8'de bulunan hesap yöntemlerinin incelenmesine de yer verilmiştir.

Bilindiği üzere betonarme perdeler yatay yük taşıyıcı sistemlerde oludukça yaygın kullanılan elemanlardan biridir. Dolayısıyle deprem bölgelerindeki yapılarda sık rastalanan bir elemandır. Kompozit yapıların kullanımı ise gerek ülkemizde gerekse dünyada giderek artmaktadır. Bu çerçevede bu tez çalışması hem yapı hem de deprem mühendisliği alanlarında güncel konuları kapsamaktadır.

Yapıların deprem performansının değerlendirilmesi için genel olarak doğrusal veya doğrusal olmayan hesap yöntemleri kullanılabilir. Bu çalışmada yanlızca doğrusal olmayan hesap yöntemleri incelenmiştir. Öncelikle betonarme perdelerin modellenmesi ve analizleri için uygun olan yöntemler araştırılmış, daha sonra üç boyutlu çelik-beton kompozit yapının değerlendirilebilmesi için uygun modelleme ve hesap yöntemleri incelenmiştir. Son olarak da performansa dayalı heseplamalar, doğrusal olmayan statik analiz ve doğrusal olmayan dinamik analiz gibi yöntemlere değinilmiştir.

Bu tez çalışmasında sayısal incelemelere de yer verilmiştir. Bu sayısal incelemelerde kullanılan örnek bina ve yapılmış çalışmalar Università Degli Studi di Trento, İtalya'da gerçekleştirlen projenin bir kısmından oluşmaktadır. Betonarme perdeli çelik-beton kompozit bir bina bilgisayar ortamında Opensees programı ile modellenmiş, analizleri gerçekleştirilmiş ve elde edilen sonuçlar değerlendirilmiştir.

Örnek çalışma olarak betonarme perdeli çelik-beton kompozit bir binanın üç boyutlu modelinin performans seviyesi belirlenmiştir Binanın yatay yük taşıyıcı sistemi bir doğrultuda betonarme perdeli sistemden diğer doğrultuda ise çelik-beton kompozit elemanlardan oluşan moment aktaran çerçevelerden oluşmaktadır. Bu çalışma kapsamında betonarme perdeler ve üç boyutlu yapının perde doğrultusunda ki davranışı incelenmiştir.

Binada birbinin aynısı olmak üzere dört adet betonarme perde bulunmaktadır. Öncelikle perdeler Opensees ile modellenip bu modelin doğru çalışıp çalışmadığı bazı analizler yapılarak kontrol edilmiş, daha sonra perde modeli üç boyutlu binaya entegre edilmiştir. Perde kesitleri için fiber modelleme, elemanı modellemek için ise beam-column element modeli kullanılmıştır. Perdelerde bulunan sargılı betonun karakteristik özellikleri ise Mander malzeme modeline göre hesaplamıştır.

Perde modelinin doğruluğunu kontrol etmek amacıyla moment-eğrilik, monotonik itme (pushover) ve periyodik itme (ECCS prosedürüne göre) analizleri gerçekleştirilmiştir. Bu anlizlerle ilgili detyalı açıklamalara ve sonuçlarına dördüncü bölümde yer verilmiştir.

Çelik-beton kompozit çerçevelerde perde modellerinin aksine yığılı plastisite kullanılmıştır. Bu şekilde elemanların doğrusal olmayan davranışları elaman uçlarında tanımlanan bölgelere plastik mafsal atanması ile gerçekleştirilmiştir. Plastik mafsal modellerine bouc-wen malzeme modeli ve pinching etkisi tanımlanmıştır. Elemanların diğer kısımları ise elastik olarak modellenmiştir.

Üç boyutlu modele bu çalışma kapsamında uygulanan analizler ise modal analiz, pushover analiz ve zaman tanım alanında hesap yöntemidir. Modal analiz yapının perdeli doğrultudaki baskın mod şeklini berlirlemek amacıyla yapılmıştır. İtme analizi sonucu üç boyutlu binanın kapasite eğrisi elde edilmiş. Göçmenin betonarme perdelerin göçmesi sonucunda gerçekleştiği gösterilmiştir. Burada elde edilen sonuçlara göre perdelerin göçmesinin ardından yapıda yüksek oranda dayanım kaybı meydana gelmektedir. Son olarak zaman tanım alanında analizler gerçekleştirilmiştir. Bu analizler binanın davranış spektrumu ile uyumlu üç adet yapay ivme kaydı kullanılarak yapılmıştır. Sonuç olarak yapının en büyük tepe deplasmanları elde edilmiştir.

Performans seviyesi şu şekilde belirlenmiştir; Eurocode 8'de belirtilen yöntemle hedef deplasman yani binanın uygulanan deprem seviyesi altında yapmasına izin verilen en büyük deplasman değeri, hesaplanmıştır. Bu yöntemde kullanılmak üzere doğrusal olmayan statik (pushover) analiz ile binanın kapasite (pushover) eğrisi elde edilmiştir. Binanın davranış spektrum ile uyumlu olarak üç adet yapay ivme kaydı kullanılarak doğrusal olmayan dinamik analizler (zaman tanım alanında hesap) gerçekleştirilmiş ve binada meydana gelen en büyük tepe deplasmanları elde edilmiştir. Hedef deplasman ile dinamik analiz sonuçları karşılaştırılmışır. Bu karşılaştırmaya beşinci bölümde yer verilmiştir.

Bu yüksek lisans tezi beş bölümden oluşmaktadır. Birinci bölümde tez konusu açıklanmış, bu konu ile ilgili daha önce yapılmış çalışmalar hakkında kısa bilgiler verilmiş ve tezin kapsam ve amacı belirtilmiştir.

Tezin ikinci bölümünde bilgisayar programı kullanılarak doğrusal olmayan analizlerin gerçekleştirilmesi ile ilgili detaylı açıklamalara yer verilmiştir. Bu bölümde malzeme modelleri, yapı elemanlarının modellenmesi (doğrusal ve doğrusal olmayan modeller) ve Opensees programı hakkında yapılmış çalışmalar ve gerekli bilgiler yer almaktadır. Bu program kullanılıcılara yapısal sistemlerinin deprem etkisi altındaki tepkilerini gözlemlemek amacıyla, yapıların bilgisayar ortamında simulasyonunu gerçekteştirme olanağı sağlamaktadır.

Üçüncü bölüm yapıların deprem performansının değerlendirilmesinde kullanınlan doğrusal olmayan hesap yöntemleri incelenmektedir. İtme analizi ile ilgili açıklamalar yer almaktadır. Aynı zamanda Eurocode 8'de gösterilen hesap yöntemleri bu bölümde açıklanmıştır. Bu yöntem, aynı zamanda dinamik hesap yöntemlerine alternatif olarak ortaya çıkmıştır. Şöyle ki zaman tanım alanında (time-history) hesap gibi yöntemler hem karmaşık hem de zaman alıcı olmaları sebebiyle daha pratik bir yönteme ihtiyaç duyulmuştur.

Üçüncü bölümde aynı zamanda doğrusal olmayan dinamik (zaman tanım alanında) hesap yöntemlerine yer verilmiştir. Bu yöntem hakkında genel bilgiler ve daha önce yapılmış çalışmalar açıklanmıştır.

Sayısal incelemelere dördüncü bölümde yer verilmiştir. Burada incelenen binanın yapısal özellikleri detaylıca anlatılmış. Modellemede kullanılan yöntemler sebepleri ile birlikte açıklanmıştır. Aynı zamanda binaya uygulanan analizler, analiz sonuçları ve sonuçların değerlendirilmesi bu bölümde anlatılmaktadır.

Beşinci bölümde bu tez çalışmasının sonuçları ve bu sonuçlarla ilgili açıklamalar verilmiştir. İtme analizi ve zaman tanım alanında analizin karşılaştırmaları ve örnek çalışmada elde edilen deplasmanların karşılaştırılarak yapının performans seviyesinin tespit edilmesi bu bölümde yapılmışıtr. Son olarak bu çalışmanın genişletilebileceği yönlerlerinden ve ileride yapılabilecek çalışmalardan bahsedilmiştir.

1. INTRODUCTION

1.1 Objective

Earthquake has been one of the major engineering problems for centuries. Accordingly, seismic performance approaches for structural systems become a common topic. Priestly expresses in 12th WCEE that, in the last 70 years, which traces to time before design codes ask for seismic resistance evaluation of structures, it has been assumed that strength and performance have the same meaning. On the other hand understanding safety or reduction of damage is not definitely possible with strength improvement, has changed this situation progressively in last 25 years. As it is seen, earthquake-resistant design has been seriously changing from "strength" to "performance" in recent years, [1]. Consequently performance based design of structures significantly takes part in design codes of countries that are located in earthquake zones.

Seismic design of structures could be developed with linear or nonlinear analysis methods. Linear elastic procedures used to be common for a long time. However, these procedures neither are applicable for high-rise or irregular structures, which may have high predominant mode shapes, nor satisfy performance requirements. In other words, generally linear methods are appropriate when the structure remains nearly elastic under earthquake loading, but seismic performance assessment includes and mostly interested with nonlinear behavior of the structure and structural elements. Besides, nonlinear and nonelastic methods become widespread with the development of the technology that enables suitable analysis tools for non-linear static and nonlinear dynamic analysis.

In order to evaluate seismic response of structures, inelastic dynamic analysis is an influential method. Seismic performance of the structure can be evaluated accurately in case of using a suite of delicately chosen ground motion records. A set of representative acceleration time–histories, which causes a significant increment in computational effort, have to be selected because the input ground motions quietly affects computed inelastic dynamic response. Additionally, improvement in the technology causes the development of computing tools in sense of accuracy and efficiency; however, dynamic inelastic analysis causes doubts about simplicity and applicability in practical design. Evaluation of strength capacity after the elastic behavior and pointing out the probable poor regions in the structure are possible with the inelastic static pushover analysis. Pushover analysis requires the definition of lateral load pattern, which is distributed throughout the structure height. Lateral loads monotonically increase with constant increments until the control node at the top of the structure reaches to specified deformations. When the objective is design of a new structure, target top displacement can be the deformation supposed in the design earthquake. On the other hand, for performance evaluation of existing structures it might be the drift corresponding to structural collapse. Determination of yielding and failure ranges both on the member and the structure levels are possible with inelastic static pushover analysis. Furthermore, stages of general capacity curve of the structure can be estimated with this method, [2].

Fajfar and Gaspersic have developed and described a detailed and quite simple nonlinear method for seismic performance assessment of reinforced concrete buildings, which is called N2 method, in 1996. It is stated that, the procedures that are defined in building codes for design of new structures or assessment of current structures under earthquake loadings consider forms of the structures only in the linear elastic range. Acceptable evaluation of demand of a structure according to energy dissipation, ductility, strength and structural stiffness, is not possible with these procedures. Although the dynamic time-history analysis of Multi-Degree-Of-Freedom (MDOF) systems leads to more accurate results in terms of uncertainties of the model, it needs additional data such as time-histories of several ground motions and the hysteretic behavior of structural members. Accordingly, from the point of practical design applications this method is not convenient. Consequently there is a requirement for a simple procedure, which is enough due to uncertainties of the input data and satisfies the requirements given above, [3].

Although time-history analysis procedure is general and accurate for the purposes of seismic design and assessment, earthquake-engineering community has been studying on a simpler and more convenient method for everyday use. Consequently, many studies have performed in this field for decades for instance Saiidi and Sozen in 1981 [4], Fajfar and Gaspersic in 1996 [3] and Priestly [1] in 2000 published their studies. Applied Technology Council (ATC) has published Guidelines and Commentary for Seismic Rehabilitation of Buildings - ATC 40 in 1996 [5] and NEHRP Guidelines for the Seismic Rehabilitation of Buildings- FEMA 273[6] has been prepared by Federal Emergency Management Agency (FEMA) as well. Prestandart and Commentary for the Seismic Rehabilitation of Buildings (FEMA-356) [7] and Improvement of Nonlinear Static Seismic Analysis Procedures (FEMA-440) [8] has followed these studies. FEMA-440 implies the results of project ATC-55. In parallel with these developments Seismic Rehabilitation of Existing Buildings (ASCE 41-06) [9] has been prepared by American Society of Civil Engineers (ASCE). Additionally Design of Structures for Earthquake Resistance-Assessment and Retrofitting of Buildings Eurocode 8 [10], which is one of the main topics of this study, comprises results of studies carried by European Committee for Standardization about performance based approaches.

In the light of previous studies, performance assessment with nonlinear methods is performed. Comparison of performance evaluation with time-history and pushover procedures is the main purpose of this study. Accordingly, displacements, which are obtained with time-history and pushover analysis, are compared in order to evaluate performance of the structure.

1.2 Scope of Thesis

Nonlinear structural analysis of shear walls and steel-concrete composite structures with shear walls, performance assessment of such structural systems and comparison of performance evaluation with pushover analysis according to Eurocode 8 [10] and performance evaluation with time-history analysis is the purpose of this thesis. This study comprises non-linear analysis of structural systems; modeling and analysis of shear walls and steel-concrete composite structures with shear walls using Opensees and performance assessment of structures in the shear wall direction according to Eurocode 8.

As a case study, analyses of a two-dimensional (2D) shear wall and a three dimensional (3D) structure, which are exposed to earthquake loads are performed within the scope of this study. Modeling and analysis of shear walls are performed. Then shear wall model is combined with 3D model of the structure. The case study contains analysis of 2D shear wall and performance assessment of 3D building on the shear wall direction according to Eurocode 8.

The followed path of the study is given below.

a) Non linear structural analysis

b) Non linear analysis of shear walls and steel-concrete composite structures

c) Non linear structural analysis using OpenSEES

d) Performance assessment of structures according to Eurocode 8

e) Evaluation of a case study.

f) Explanation of the analysis results

g) Comparison of pushover and time-history analyses

2. BASICS OF NONLINEAR ANALYSIS

Performance assessment comes into prominence in earthquake and structural engineering, this also yields requirement for software that is sufficient to simulate seismic structural response of nonlinear constitutive systems in terms of large displacement theories, robust solution algorithms. Traditional codes are computationally adequate, but they have restrictions in the sense of extension of the system. For example, variable time integration and root-finding algorithms for solving equilibrium equations or improvement of a different analysis types are not available [11]. In order to answer this purpose Open System for Earthquake Engineering Simulation (OpenSEES), which is a software platform for research and application for simulation of structural systems with finite element method, has been developed by Pacific Earthquake Engineering Research Center (PEER) with support of National Science Foundation (NFS). Opensees is an open source software framework that is available for simulation of seismic response of structural and geotechnical systems.

The analyses covered by this study is carried out with Opensees in order to build structural models and analyze structures and structural members since it fulfills requirements of this study as follows:

- It is a powerful tool for non-linear numerical analysis,
- It is suitable for variable input data,
- The consisting open source allows comprehensible analysis and models
- Possible to create material or element according to needs
- It allows the description of the structural input on the basis of diffrent levels; element level, section level or fiber level.
- It enables simulations of static pushover analyses, static reversed-cyclic analyses and dynamic time-series analyses

- Network for Earthquake Engineering Simulation (NEES) supports improvement of Opensees with laboratory testing that cause reliance on it.

2.1 Modeling of Reinforced Concrete Elements

In finite element analysis analyst initially separates the components of the structure into nodes and elements. The definition of the component is possible in three levels with Opensees, element level, section level and fiber level (Figure 2.1).

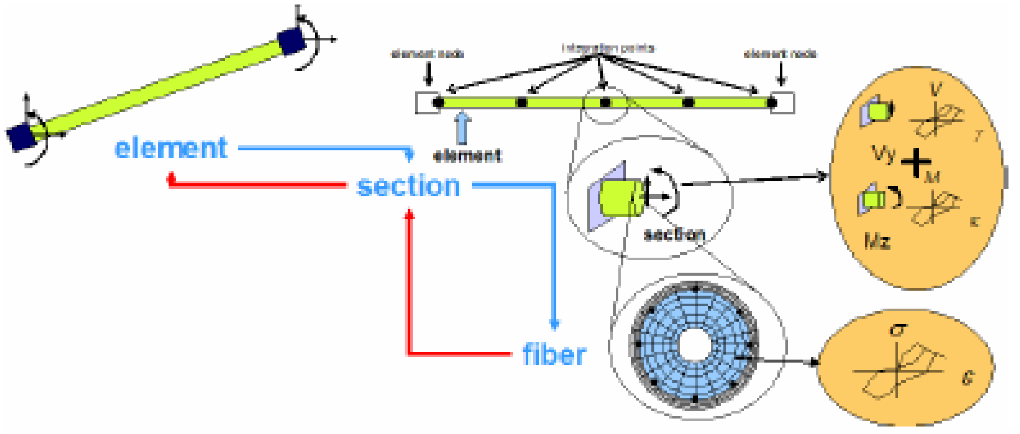

Figure 2.1 : Modeling structural components. [12]

According to this study, modeling of a reinforced concrete (RC) shear wall consists of three steps. Material definition is the first step same as any structural modeling. Section definition in fiber level follows as second step, and element definition is the final step of building shear wall model. This section contains description of these steps and explanations of used model-building objects and models in respect of literature.

As is known definition of concrete and reinforcement steel is necessary for RC components. Opensees give the opportunity of material definition to the analyst. This study implies assessment of uniaxial material objects of Opensees. For concrete material concrete01 concrete02 and concrete04, for reinforcement steel material steel02 and for other definitions of material properties (like torsion or shear strength) elastic material and steel01 commands are investigated.

2.1.1 Material models for concrete

A RC element usually has two different kind of concrete region; confined concrete region and unconfined concrete region. Concrete cover is the unconfined concrete part. Confined concrete is the concrete that is wrapped with trasversal reinforcement named stirrup or hoop. Several studies are performed in order to explain behavior of confined concrete [13-15]. Most common ones are investigated in scope of this study.

Unconfined concrete is the concrete without transversal reinforcements. Cover part of a RC section is usually consideres as unconfined concrete. Additionally analyst could assume the concrete unconfined in case of large sections with rare transversal reinforcements. The characteristic properties of the concrete, which is given by design codes, can be implemented for this type of concrete. In this study, characteristic properties of materials are taken from Eurocode 2, [17].

This section contains repectively assessment of Opensees uniaxial concrete material commands and confined concrete material models. Assumption about the material is that plane sections remain plane and perpendicular to the neutral axis of the section (uniaxial material). According to experimental results, concrete shows an extremely nonlinear behavior under uniaxial compressive loading. A Typical uniaxial compresion and tension stress-stain curve for concrete is shown in Figure 2.2.

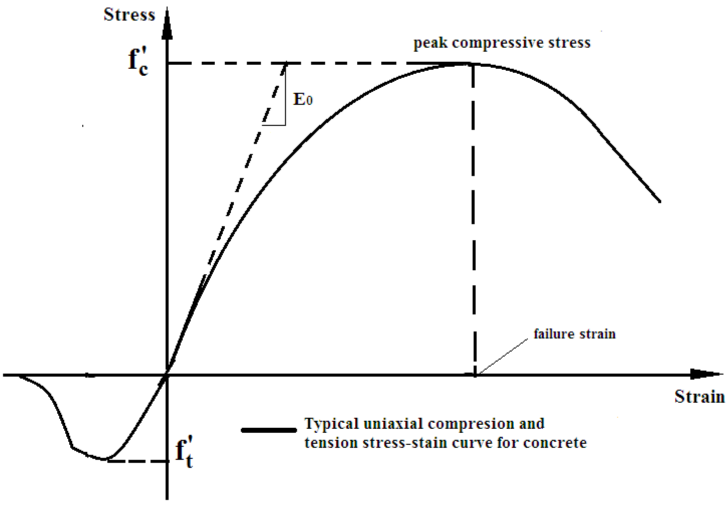

Figure 2.2 : Typical uniaxial compresion and tension stress-strain curve for concrete, [16].

This section contains repectively assessment of Opensees uniaxial concrete material commands and confined concrete material models. Assumption about the material is that plane sections remain plane and perpendicular to the neutral axis of the section (uniaxial material). According to experimental results, concrete shows an extremely nonlinear behavior under uniaxial compressive loading.

Concrete01 command in Opensees builts a uniaxial concrete material object that has degraded linear unloading and reloading stiffness with respect to Karsan and Jirsa [18] concrete material model (uniaxial Ken-Scott-Park concrete material). Karsan and Jirsa examined that degradation of the concrete can be observed from the trace of a long narrow region on the stress-strain plane under cyclic loading. This region is reduce to a single curve and named “locus of common points” (Figure 2.3). Accordingly, a stress strain model for concrete material is defined, [18].

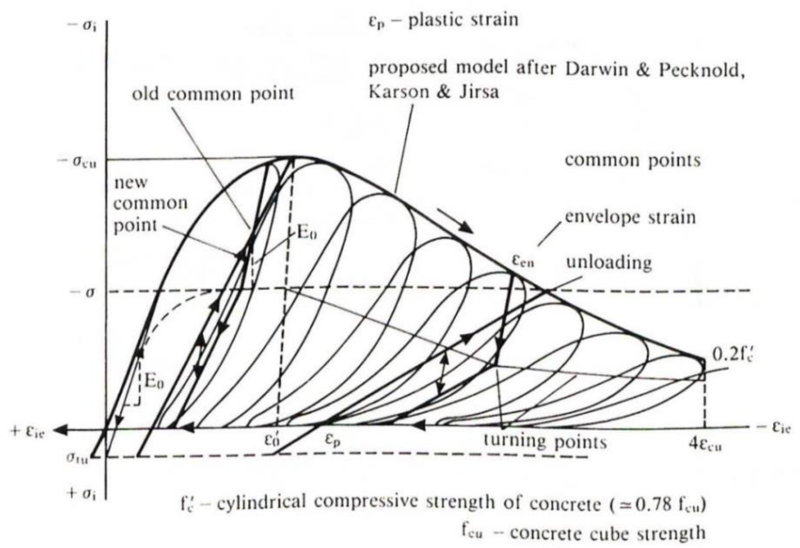

Figure 2.3 : Cyclic loading of concrete according to Karsan and Jirsa [18], cited from Bangash, [16].

Concrete01 material command also neglects tensile strength of concrete. It defines a material model with zero-tensile strength. Stress-strain relationships of concrete01 material under linear and cyclic loadings are shown respectively in Figure 2.4 and Figure 2.5. This command requires the information about characteristic properties of concrete as compressive strength at 28 days, strain at maximum strength, crushing strength and strain at crushing strength.

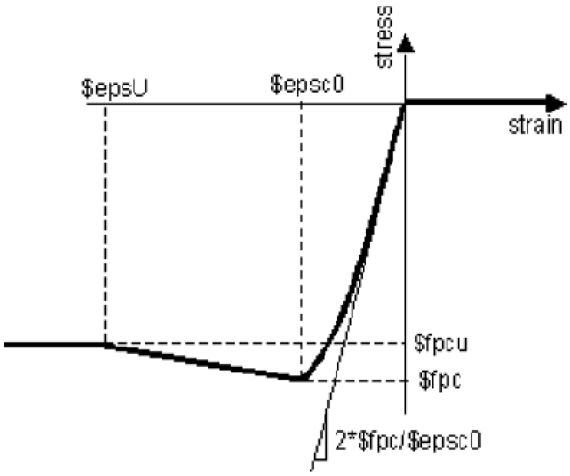

Figure 2.4 : Stress-strain curve of concrete01 model, [12].

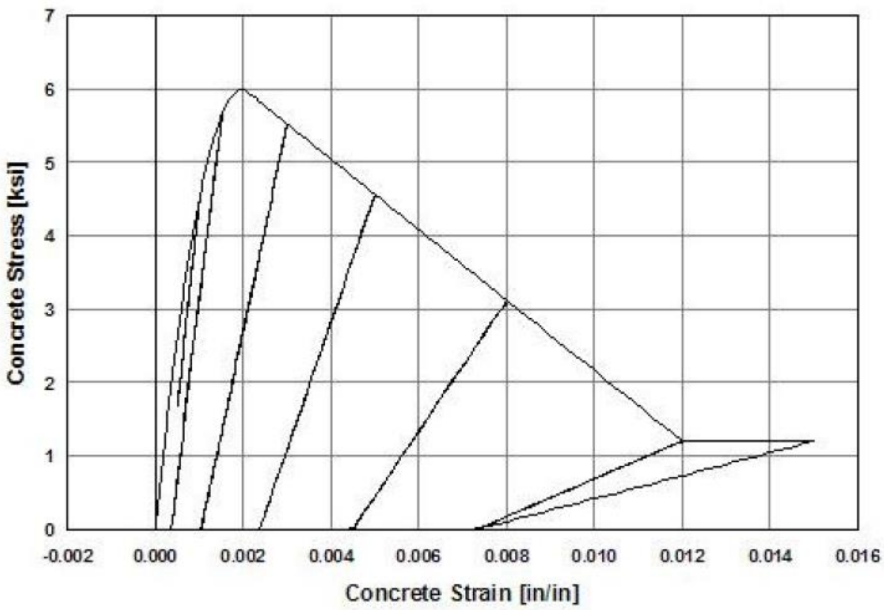

Figure 2.5 : Typical hysteretic stress-strain relation of concrete01 material, [12].

Differently from concrete01, concrete02 command has developed in order to define concrete material with tensile strength. It builts a uniaxial concrete material object with tensile strength and linear tension softening. Definition the material with concrete02 model needs knowledge of tensile strength of the concrete, tension softening stiffness (slope of the linear tension softening branch) and ratio between unloading slope and initial slope in addition to the required information of concrete01 . Stress-strain relations of concrete02 model are shown in Figure 2.6 and Figure 2.7. Additionally Figure 2.8 represents comparison of hysteretic behaviour of concrete01 and concrete02.

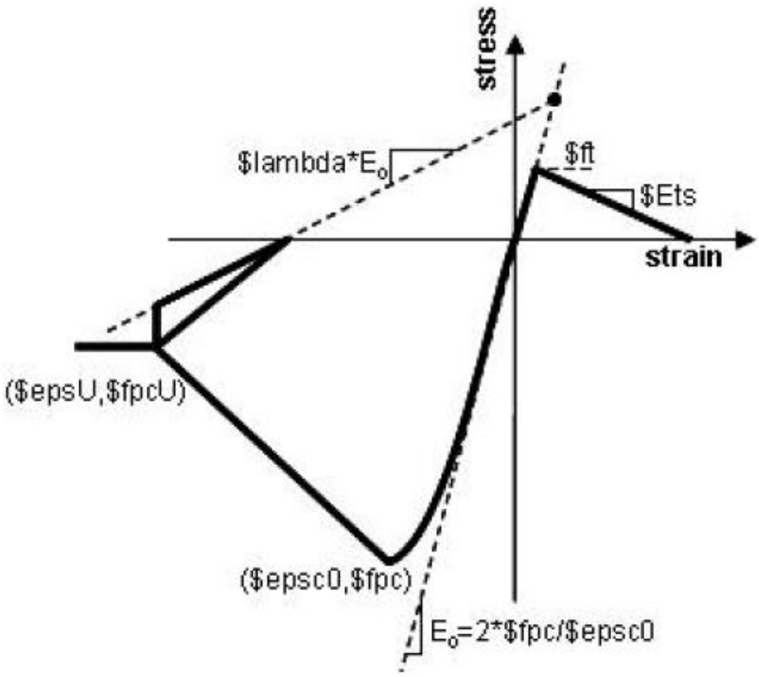

Figure 2.6 : Stress-strain curve of concrete02 material, [12].

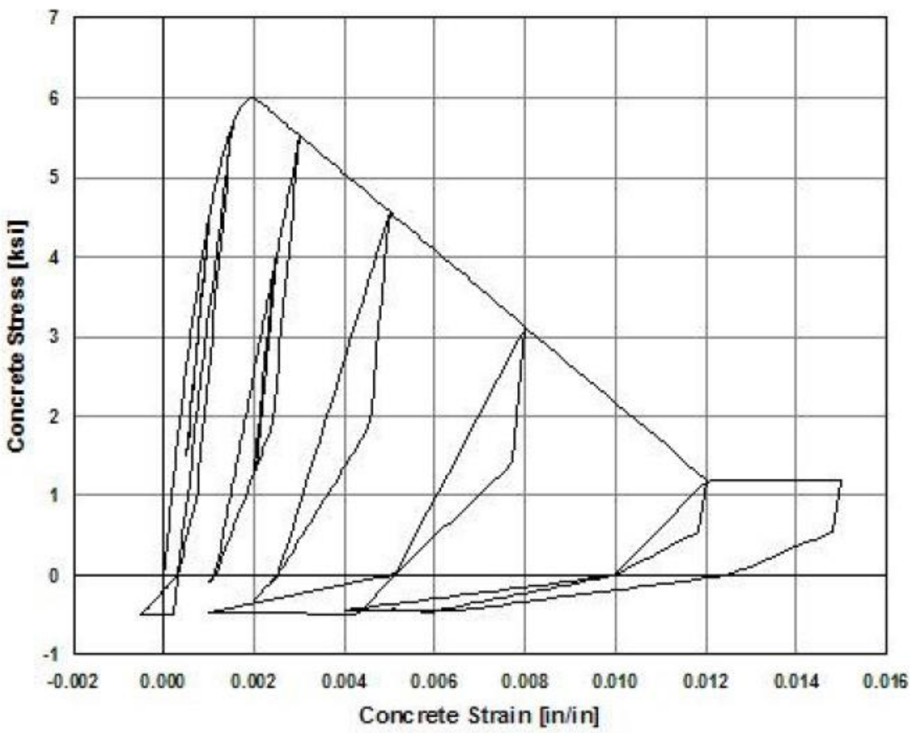

Figure 2.7 : Typical hysteretic stress-strain relation of concrete02 model, [12].

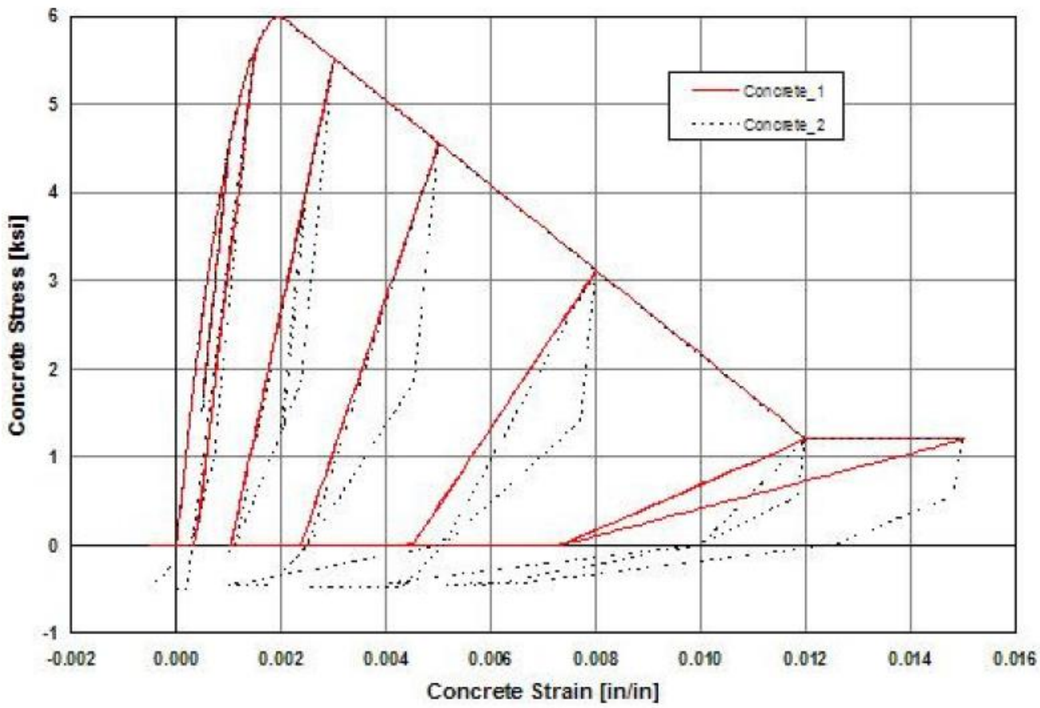

Figure 2.8 : Comparison of hysteretic behaviour of concrete01 and concrete02, [12].

Concret02 is a command of the Fedeas ML1D library developed by F.C. Filippou. Fedeas. It is a structural element library for the linear and nonlinear static and dynamic analysis of buildings and bridges that works under the general-purpose finite element analysis program FEAP, which is developed by Professor Robert L. Taylor. Fedeas structures library consists of several uniaxial stress-strain relations and Concret02 command is one of them.

Concrete04 model implies the same definition of degradation at linear unloading/reloading stiffness, which is found by Karsan and Jirsa [18], with the concrete01 model. It constructs uniaxial Popovics concrete material object and it displays tensile strength of concrete with exponential decay that differs from concrete01 model.

In 1973 Popovic proposed formulations in order to complete stress-strain curve of concrete. These formulas were suitable with relevant experimental results. Popovic's work is shown in Figure 2.9. The envelope of the compressive stress-strain response of concreet04 is defined using the model proposed by Popovics [19].

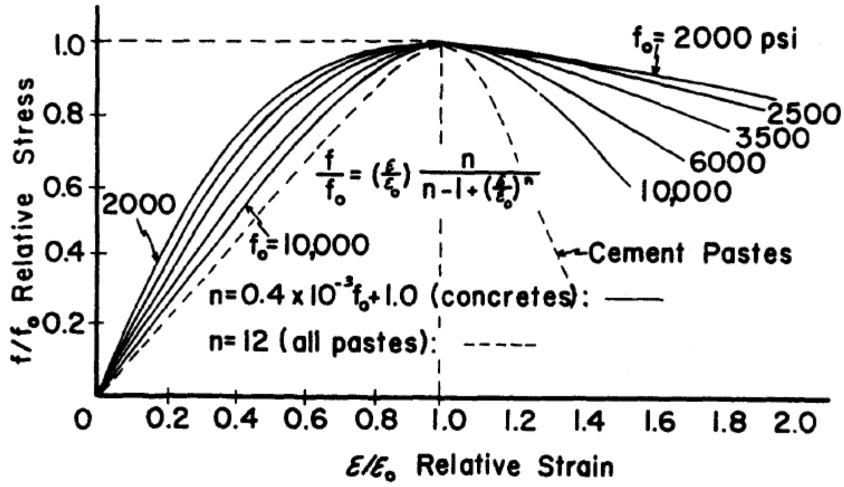

Figure 2.9 : Calculated relative stress-strain diagrams for normal-weight concretes of various compressive strengths and for cement paste, [19].

Concrete04 command needs the definition of characteristic properties of concrete such as compressive strength at 28 days, strain at maximum strength, strain at crushing strength, initial stiffness and optionally maximum tensile strength and ultimate tensile strain. Figure 2.10 shows an example for stress-strain history under cyclic loading generated using the concrete04 model.

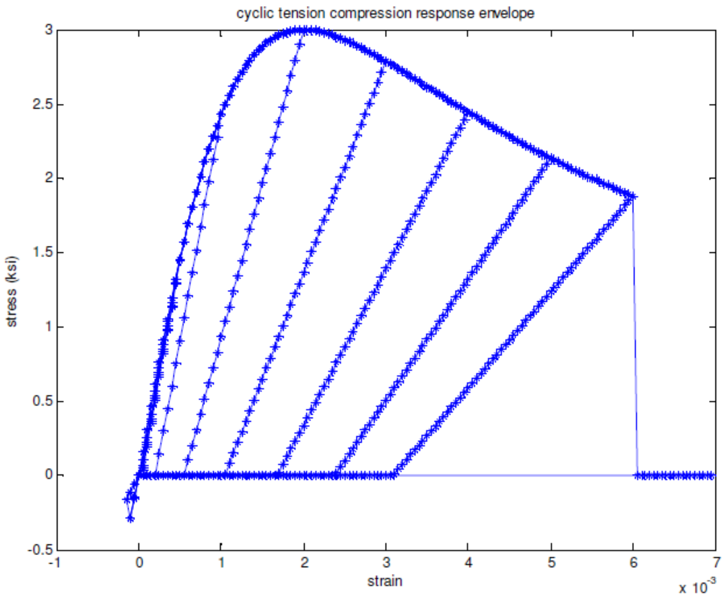

Figure 2.10 : An example cyclic tension-compression response envelope of concrete generated using the concrete04 model, [12].

Consequently, Concrete04 model represents strength degradation and faluire of concrete after the peak stress, however failure cannot be observed with concrete01 material model. Since, observation of failure of the element is required and tensile strength of the concrete is neglected, concrete04 is the most suitable material model for this study.

Generally, transversal reinforcements are implemented to RC elements in order to surround the longitudinal reinforcement. In spite of that transversal reinforcements, which could be sprials or hoops, significantly strengthen the concrete core of the section (Figure 2.11).

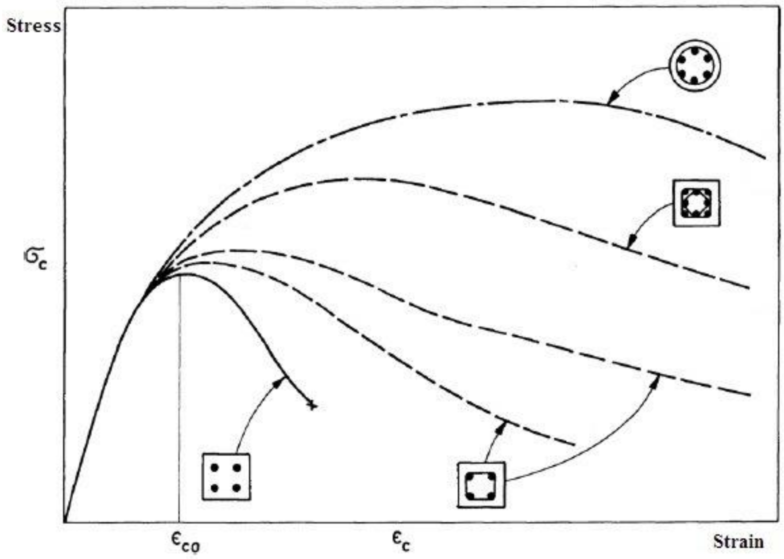

Figure 2.11 : A representation of stress-strain relation for RC sections with and without confinement.

Altough there are several studies for definition of confined concrete properties, three of the most popular confined concrete material models are discussed in this study. These are Sheikh-Üzümeri [13], Mander (Modified Kent-Park) [14] and Saatçioğlu-Razvi [15] confined concrete material models.

Sheikh and Üzümeri have suggested a complete stress-strain curve for confined concrete. The study comprises analytical modeling behavior of columns with confinements in terms of previously reported experimental results. Accordingly, the idea of effectively confined concrete area, that corresponds to concrete core applied for evaluation of strength of confined concrete. It is stated that, frequent placement of the stirrups and locating the longitudinal reinforcement effectively improve the strength and ductility of concrete, [13].

Saatcioglu and Razvi [15] expressed an analytical model in order to define stress-strain curve for concrete in 1992. A set of poorly confined and well-confined concrete input is tested to construct this analytical model. According to this concrete model, stress-strain curve starts with a positive slope parabolic arm and continues with a linear negative slope arm (Figure 2.12). The concept of evaluating lateral confinement pressure is the methodology of this study. Consequently, this work results in higher strength and ductility for confined concrete, [15].

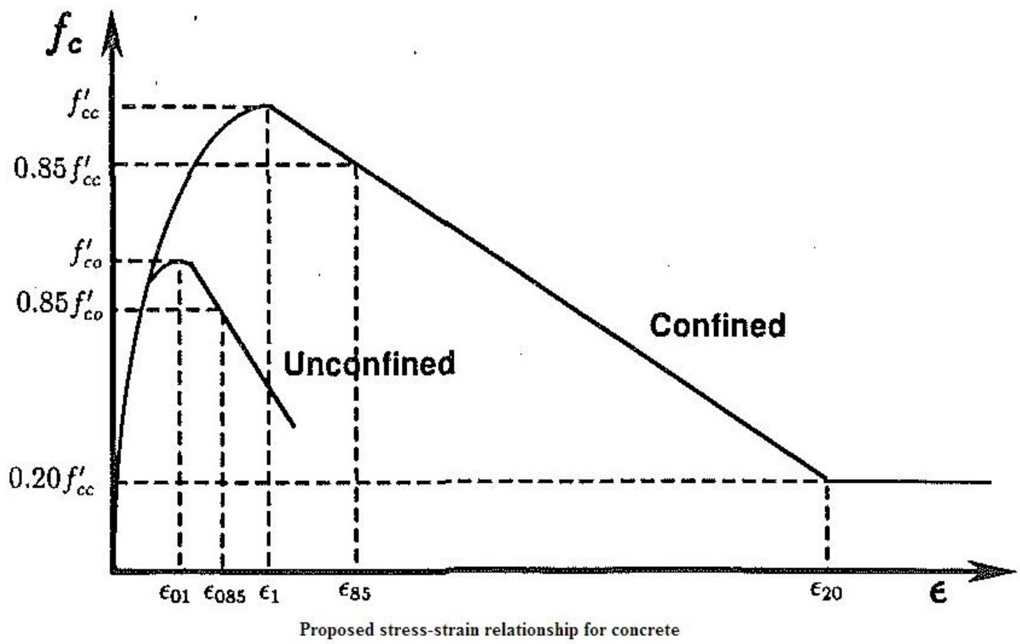

Figure 2.12 : Stress-strain curve of confined and unconfined concrete proposed by Saatcioglu and Razvi, [15].

Lowes et. al. [20] used Saatcioglu-Razvi concrete material model while modeling slender RC shear walls with Opensees within a NFS project. Concrete02 model, which has both tensile and compression response, has preferred in this work. Accordingly, Saatcioglu-Razvi model has a parabolic curve up to peak strength and then bilinear post-peak response, [20]. Unlike these previous studies, Concrete04 material command and Mander et. al. confined concrete material model are implemented for modeling concrete fibers in scope of this thesis study.

Additionally, Mander et. al. [14] proposed a stress-strain relationship under uniaxial compressive loading for tied concrete sections. One equation is developed for different types of confinements such as, spirals, circular hoops or rectangular hoops with or without supplementary crossties. The procedure is also applicable for cyclic loading cases. Distribution of longitudinal and transversal reinforcement effects effective lateral confining stress, which is used in order to consider impact of different types of reinforcement arrangements. An energy equalization method named energy balance approach is applied. Equalization of strain energy capacity of stirrups with strain energy accumulated in the concrete because of the transversal reinforcement leads to estimation of longitudinal compressive strain in the concrete that based on the first fracture of the stirrups, [14]. Since this method used in this study, a detailed explanation about Mander confined concrete material model is given as follows.

Figure 2.13 shows stress-strain relationship of confined and unconfined concrete and it is based on an equation suggested by Popovics [19].

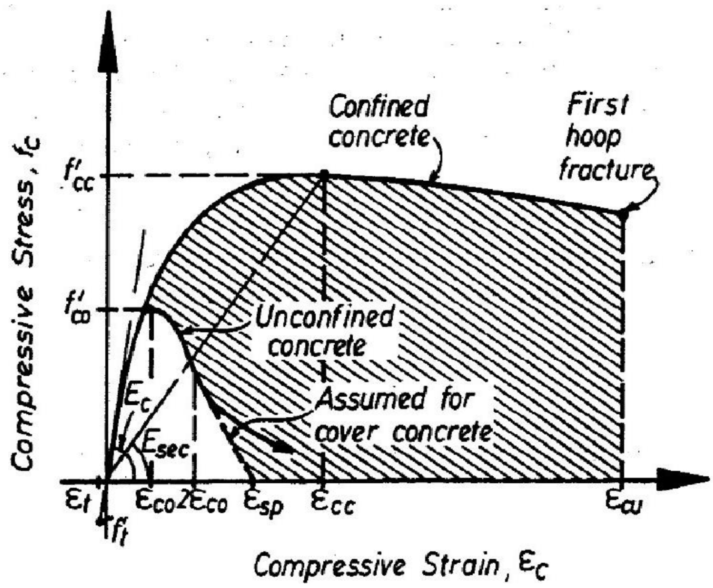

Figure 2.13 : Stress-strain model proposed for monotonic loading of confined and unconfined concrete [14]

It is stated that, a constitutive model involving a specified ultimate strength surface for multiaxial compressive stresses is used in Mander material model to determine confined concrete compressive strength (f'_{cc}), which is given below.

$$f'_{cc} = f'_{c0}\left(-1.254 + 2.254\sqrt{1 + \frac{7.94 f'_l}{f'_{c0}}} - 2\frac{f'_l}{f'_{c0}}\right) \quad \textbf{(2.1)}$$

Parameters that are required for calculation of compressive strength of confined concrete are explained below. Compressive strength of unconfined concrete (f'_{c0}) is defined by design codes in terms of concrete classes.

A similar approach to Sheikh and Üzümeri is used by Mander et. al. in order to determine the effective lateral confining pressure on the concrete section (f'_l). Effective lateral confining pressure is considered as follows.

$$f_l' = f_l k_e \tag{2.2}$$

In this equetion k_e is confinement effectiveness coefficient. It is used to enable the fact effectively confined concrete area (A_e) should be smaller than the area of the confined concrete (A_{cc}) which is described as area of the concrete within the center lines of the perimeter spiral or hoop. Consequently it leads to $A_e < A_{cc}$.

$$k_e = \frac{A_e}{A_{cc}} \tag{2.3}$$

In order to evaluate the area of the confined concrete core named as A_{cc} Equation **(2.4)** is defined. Subsequently, definition of the A_e which comes up to effectively confined concrete area is given in Equation **(2.6)**.

$$A_{cc} = A_c(1 - \rho_{cc}) \tag{2.4}$$

Area of core of section enclosed by centerlines of the perimeter hoop is shown as A_c and ρ_{cc} represents ratio of area of longitudinal reinforcement to area of core of section. So that the total area of longitudinal reinforcement (A_{sl}) need to be calculated.

$$\rho_{cc} = \frac{A_{sl}}{A_c} \tag{2.5}$$

In order to evaluate the area of effective confined concrete core at hoop level (A_e), total plan area of ineffectually confined core concrete at the level of the hoops (A_i) is required. Clear vertical spacing between hoop bars (s') and core dimensions to centerlines of perimeter hoop in x and y directions (b_c and d_c) are need to be identified.

$$A_e = (A_c - A_i)\left(1 - \frac{s'}{2b_c}\right)\left(1 - \frac{s'}{2d_c}\right) \tag{2.6}$$

As it is obvious from Equation **(2.7)** i th clear distance between adjacent longitudinal bars (w_i') must be calculated for determination of A_i. Figure 2.14 indicates the arching action that is assumed to occur between the levels of transverse rectangular hoop reinforcement. Arching action yields to develop the confining stress on the concrete core where the maximum transverse pressure from the confinement can be applied effectively. Additionally described parameters that are used to determine compressive strength of confined concrete are visually represented in this figure.

$$A_i = \sum_{i=1}^{n} \frac{(w_i')^2}{6} \tag{2.7}$$

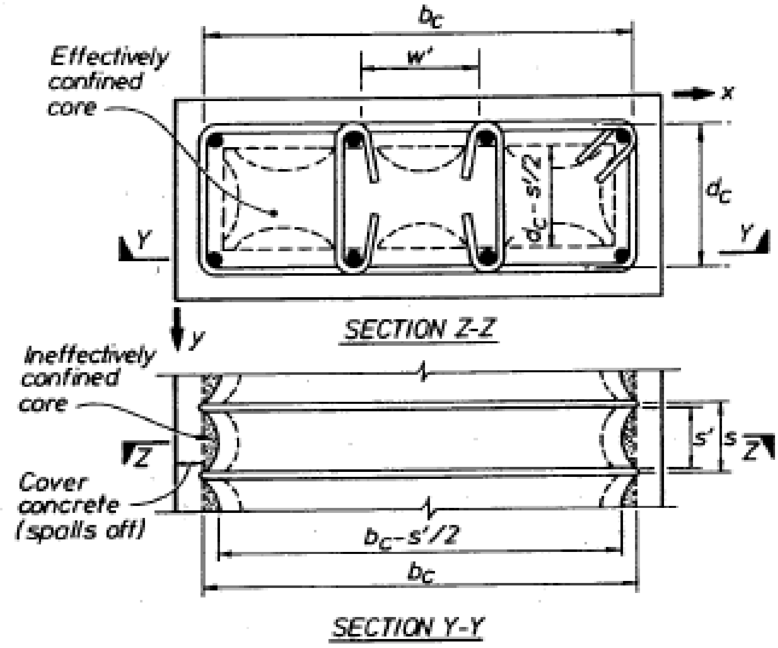

Figure 2.14 : Effectively confined core for rectangular hoop reinforcement, [14].

According to Equation **(2.2)**, f_l represents latreal pressure from the transverse reinforcement and it is assumed to be uniformly distributed over the surface of the concrete core. It is possible for rectangular reinforced concrete members to have different quantaties of transverse confining steel in the x and y directions. Accordingly, the lateral confining stress on the concrete (total transverse bar force divided by vertical area of confined concrete) is given in x direction as Equation **(2.8)** and in the y direction as Equation **(2.9)**. f_{yh} means yield strength of transverse reinforcement.

$$f_{lx} = \rho_x f_{yh} \tag{2.8}$$

$$f_{ly} = \rho_y f_{yh} \tag{2.9}$$

The proportion of the transversal reinforcement can be expressed as Equation **(2.10)** and **(2.11)** repectively for x and y directions. s defines center-to-center spacing of hoops and A_{sx} defines the total area of transverse bars running in the x direction, similarly A_{sy} is for y direction.

$$\rho_x = \frac{A_{sx}}{s \cdot d_c} \qquad \textbf{(2.10)}$$

$$\rho_y = \frac{A_{sy}}{s \cdot d_c} \qquad \textbf{(2.11)}$$

Finally according to Mander et. al strain of confined concrete at compressive strength (e_{cc}) and elastic modulus of confined concrete (E_c) are defined as follows.

$$e_{cc} = e_{c0}\left[1 + 5\left(\frac{f'_{cc}}{f'_{c0}} - 1\right)\right] \qquad \textbf{(2.12)}$$

$$E_c = 5000\sqrt{f'_{co}} \quad MPa \qquad \textbf{(2.13)}$$

Strain of confined concrete at ultimate stress symbolized as e_{ccu} and it can be obtained with Equation **(2.14)**. Where yield stress of the reinforcement is f_{yk} and e_{su} is the ultimate strain of it.

$$e_{ccu} = 0.004 + \frac{e_{su} \cdot f_{yk} \cdot \rho_y}{f'_{c0}} \qquad \textbf{(2.14)}$$

2.1.2 Material models for steel

Since the study is about steel-concrete composite structures with shear walls, both structural steel and reinforcing steel are o the carpet. This section contains information about reinforcing steel and stress-strain relationship for typical reinforcing steel can be seen in Figure 2.15.

Required reinforcement properties for design are usually given by design codes. Since this study based on Eurocode, contents of the Eurocode 2 about reinforcement steel is mentioned in this section. Additionally, Opensees commands used to define steel material objects are described.

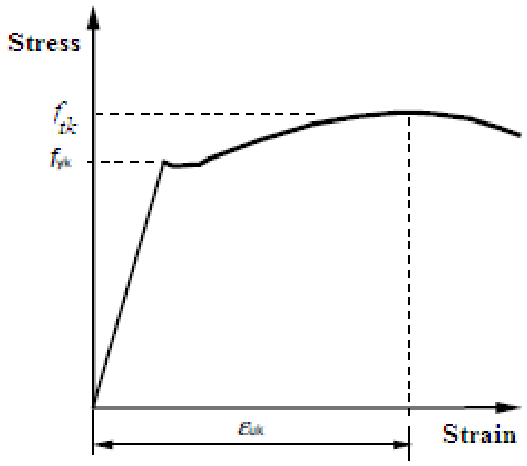

Figure 2.15 : Stress-strain relationship for typical reinforcing steel

Eurocode 2 contains the application rules for design and detailing only for a specified yield strength range, f_{yk} = 400 to 600 MPa. The yield strength f_{yk} and the tensile strength f_{tk} are defined respectively as the characteristic value of the yield load, and the characteristic maximum load in direct axial tension, each divided by the nominal cross sectional area.

Table 2.1 gives the properties of reinforcement suitable for use with Eurocode 2 and it is adapted from Eurocode 2 annex C, Table C.1., [17].

Table 2.1 : Properties of reinforcement according to Eurocode 2 [17].

Product form	Bars and de-coiled rods			Wire Fabrics			Requirement or quantile value (%)
Class	A	B	C	A	B	C	-
Characteristic yield strength f_{yk} (MPa)	400 to 600						5,0
Minimum value of k = $(f_t/f_y)_k$	≥1,05	≥1,08	≥1,15 <1,35	≥1,05	≥1,08	≥1,15 <1,35	10,0
Characteristic strain at max. force, ε_{uk} (%)	≥2,5	≥5,0	≥7,5	≥2,5	≥5,0	≥7,5	10,0
Bendability	Bend/Reband test			-			
Shear strength	-			0,3 A fyk (A is area of wire)			Minimum

Steel02 command builds uniaxial steel material object with isotropic strain hardening based on Giuffré-Menegotto-Pinto model in Opensees. Giuffré-Menegotto-Pinto proposed an equation for steel material under cyclic loading and it represents a curved trasition from straight-line asymptote with slope E_0 to another asymptote with slope E_1 (Figure 2.16). Initial stress σ_0 and strain ε_0 are at the point where the two asymptotes of the branch meet (point A in Figure 2.16), in like manner the last strain reversal ε_t and corresponding stress σ_t take place in point B in Figure 2.16. Ratio between slope E_1 and E_0 gives strain-hardeing ratio b and R is a parameter which effects the shape of the transition curve. ε_0, σ_0 and ε_t, σ_t should be redetermined after each strain reversal as shown in Figure 2.16, [21].

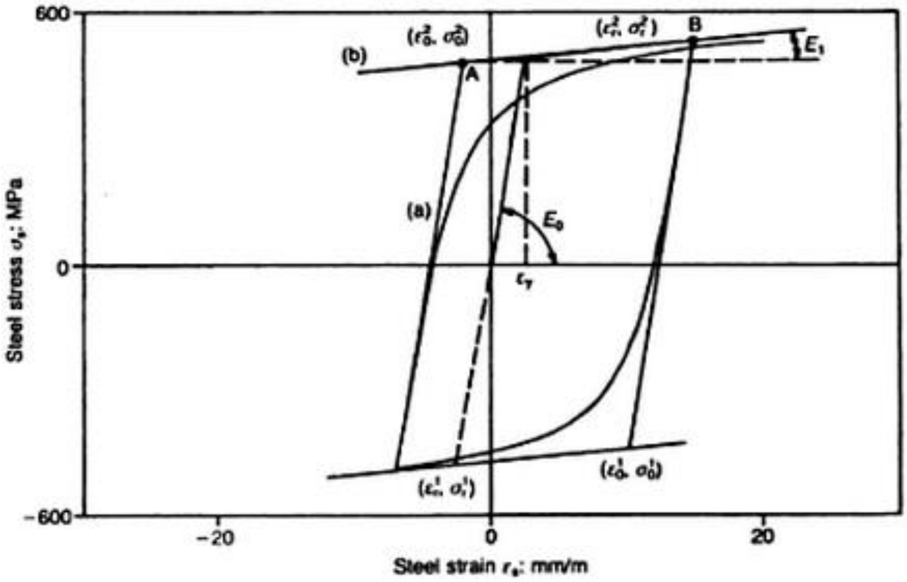

Figure 2.16 : Stress-strain relationship under cyclic loading for Giuffré-Menegotto-Pinto steel material model [21].

Accordingly, yield strength f_{yk}, initial elastic tangent E_0, strain-hardening ratio b and R parameter are required in order to construct a steel material object with Steel02 command. Material parameters of monotonic envelope and stress-strain curve for Steel02 are indicated in Figure 2.17.

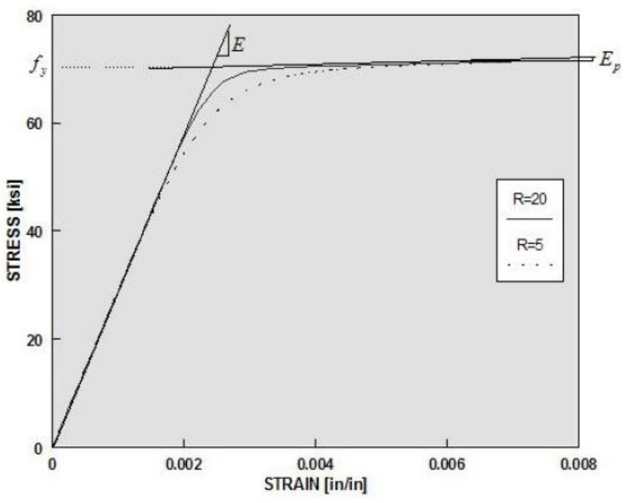

Figure 2.17 : Stress-strain relationship for Steel02 model, [12].

2.1.3 Material model for the effect of shear and shear strength

Shear strength is defined independently, and then it is assigned into section properties to combine with flexure and torsion capacity. The section assumed elastic in terms of shear behavior. Since shear walls are slender in this study elastic definition of shear is adequate.

Elastic material represents linear relationship between force and deformation. In 1676 Robert Hooke worked with springs and puroposed that, the relationship between stress and strain may be said to be linear for all materials. This contentful idealization and generalization applicable to all materials is known as Hooke's law at the present time, [22].

Elastic material model is implemented as uniaxial elastic material. This material model is used to represent shear capacity of wall section linearly (Figure 2.18). Definition of tangent, which correspond to shear modulus in this case, is sufficient.

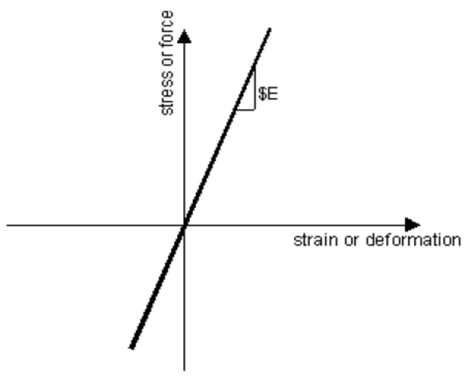

Figure 2.18 : Stress-strain relationship of elastic material model, [12].

Evaluation of shear modulus G_{co} is possible with Equation **(2.15)**, where υ poisson ratio and E_c is the elastic modulus of concrete material. The equation is adapted from Riley and Loren, [23].

$$G_{co} = \frac{E_c}{2 \cdot (1 + \upsilon)} \tag{2.15}$$

2.1.4 Material model for the effect of torsion and torsional capacity

Torsional capacity of the wall is implemented by using uniaxial material steel01. This material represents uniaxial bilinear material with kinematic hardening and optional isotropic hardening [12], (Figure 2.19). Torsional stiffness, strain-hardening ratio and torsional moment capacity is required for this material command. Torsional stiffness can be defined as $G_{c0}J$, where J represents polar moment of inertia.

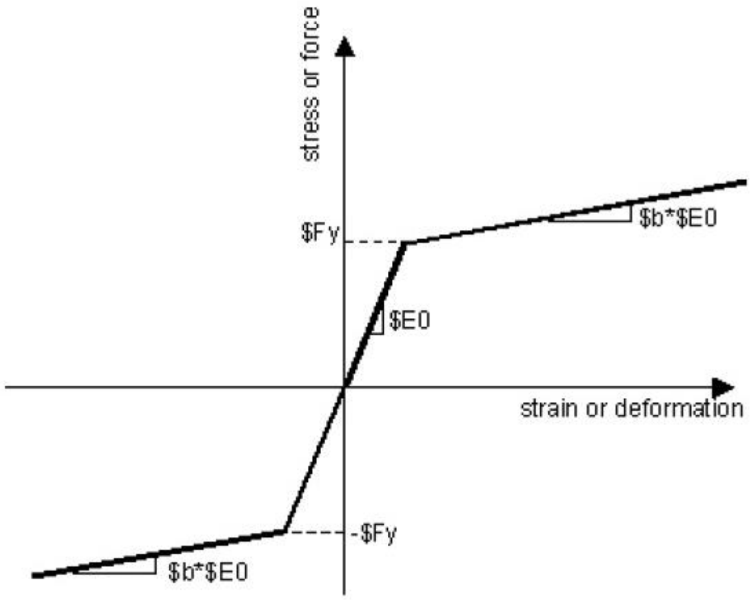

Figure 2.19 : Steel 01 material parameters of monotonic envelop [12].

Additionally, torsional moment capacity of the section M_T can be calculated as given in Equation **(2.16)**. Accordingly, maximum shear stress is τ_{max} and l_{max} represents length from further point to the center of the section, [23].

$$M_T = \frac{\tau_{max} \cdot J}{l_{max}} \tag{2.16}$$

It is possible to use Tresca crietion in order to evaluate maximum shear stress τ_{max}. Tresca crietion expresses that, yielding starts when the maximum shear stress in the material τ_{max} equals the maximum shear stress at yielding in a simple tension test τ_y. Therefore τ_{max} can be defined as follows, where σ_{max} and σ_{min} are the maximum and minimum principal stresses respectively, [24].

$$\tau_{max} = \frac{\sigma_{max} - \sigma_{min}}{2} \tag{2.17}$$

In this study τ_{max} can be evaluated based on compressive stress of concrete as explained in Equation **(2.18)**.

$$\tau_{max} = \frac{f_{c0}}{2} \tag{2.18}$$

2.1.5 Fiber beam-column elements: distributed plasticity

Taucer et. al. [25] performed the study named a fiber beam-column element for seismic response analysis of reinforced concrete structures as a part of larger study supported by California Department of Tranportation (CALTRANS) and National Scinece Foundation. In order to model RC elements that are exposed cycling loads, the authours purposes fiber beam-column element model, which gives accurate results and is computationally effective. The model represents distributed plasticity, [25].

For estimating stiffness strength and drift capacity that are significant participants of seismic performance approaches, beam-column elements results in perfectly in many circumstances and they are computatesionaly practical models. Other plasticity approaches are lumped plasticity type models and fiber shell model, which represents distributed plasticity similarly to beam-column element.

Plastic hinge model is an example for lumped plasticity type models. Construction of a lumped plasticity model is possible with definition of a zero length plastic hinge in forms of nonlinear springs. Besides, it usually does not work adequately for multi-story buldings in the other words for tall slender walls, because knowledge about location of inelastic actions is necessary. One plastic hinge generally occurs at the base of the wall but the difficulty is the secondary hinge, which is expected at futher up of the wall. Building simulation for each point with potential of yielding is needed to be performed in order to predict the location of the secondary hinge. That yields to increase the workload.

Fiber shell model is another approach to establish nonlinearity of the elements and it is an example for distributed plasticity type models. In contrast to lumped plasticity models, material nonlinearty is distributed trough the element and it can occur at any section of the element. Fiber shell model is usually preferred in case of private problems such as behavior examination since it provides attaining the accurate material response. Facility for simulation of inelastic flexure and shear exists according to the approach plane sections do not remain plane. On the other hand, increase of components of structure(s) or analysis for example multi-story structures or multiple ground motions cause significant increase of computational demand. Additonally it is not numerically powerful enough to satisfy requirements of multi dimensional continuum reinforced concrete models. Despite all capabilities, disadvantages of fiber shell model prompt the anlaysts to another approach.

Beam-column element model is a distributed plasticity model that leads to more accurate definition of inelastic behavior of RC elements than lumped plasticity models. It is also based on the assumption plane sections remain plane during the loading. Beam-column elements provide execellent results for slender shear walls that react predominantly in flexure, [20, 25].

In this study, lumped plasticity models are preferred for steel-concrete composite moment-frame members of the structure, but fiber beam-column element models are implemented in order to construct RC shear wall models. Implementation of these approaches and results of the case study are given in further sections.

2.1.5.1 Fiber section

Fiber beam-column element models composed of detailed geometry and material models to obtain reliable simulation of nonlinear behavior along the length of the element. The fiber model for reinforced concrete (RC) structures is developed by dividing each element into several sections along the member. The sections at each end of the element consists several subdivisions, which are fibers represents concrete and steel material. Figure 2.20 is a representation of this explanation.

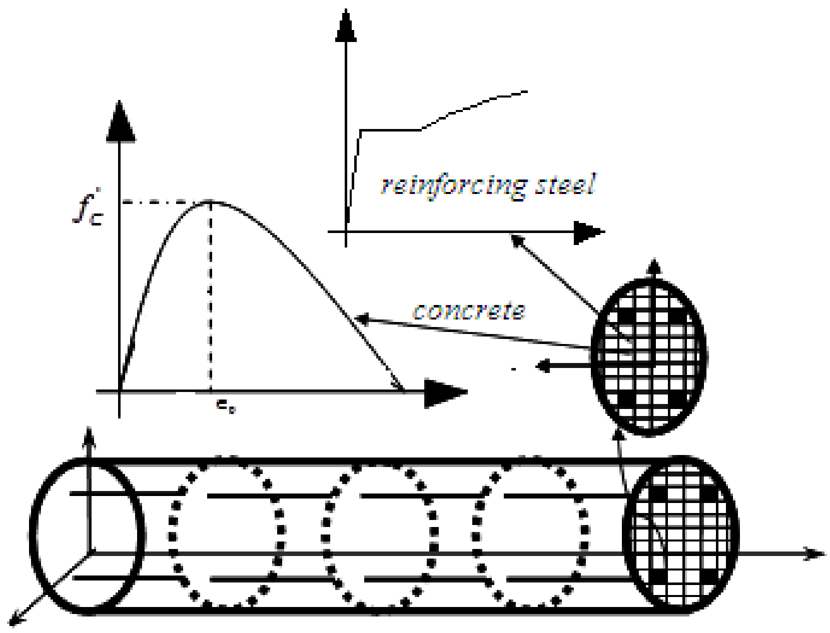

Figure 2.20 : An example for fiber beam-column element model.

The fiber section object comprises of fiber objects in Opensees. A fiber section has a general geometric configuration formed by subregions of simpler, regular shapes (e.g. quadrilateral, circular and triangular regions) called patches, (Figure 2.21). In addition, layers of reinforcement bars can be specified. The subcommands patch and layer are used to define the discretization of the section into fibers.

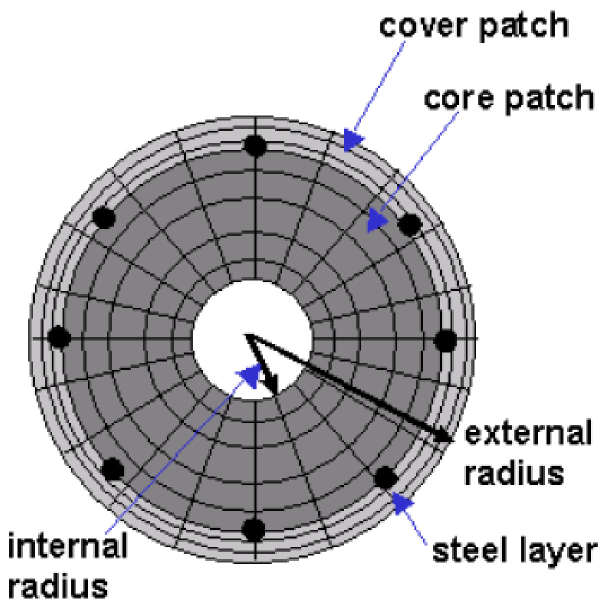

Figure 2.21 : An example for fiber section, [12].

2.1.5.2 Difference between forced-based and displacement-based beam column elements

The displacement-based approach follows classical finite element procedures. After the section deformations are interpolated from an approximate displacement field, element equilibrium relationship is built based on virtual displacement rules. Linear curvature distribution and constant axial deformation are applied along the length of the element in order to determine approximate nonlinear element response. Mesh refinement of the element is necessary to represent higher order distributions of deformations for displacement-based element. Addtionally, multiple elements are needed to be defined for a good simulation of actual curvature field, which is nonlinear. In case of modeling shear response description a plastic hinge is needed separately from the beam-column element.

Representation of both displacement-based and force-based approaches is shown in Figure 2.22.

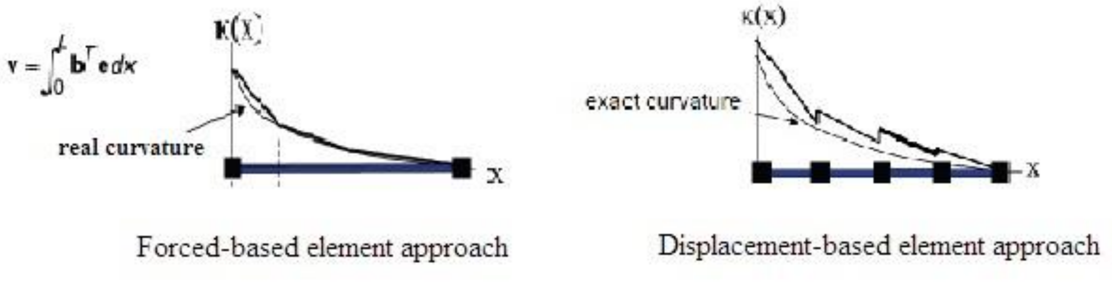

Figure 2.22 : Obtaining curvature of forced-based and displacement-based elements, [26].

The force-based approach depends on the availability of an exact equilibrium solution within the basic system of a beam-column element. Equilibrium between element and section forces is exact, which holds in the range of constitutive nonlinearity. Section forces, which are linear moment distribution, constant shear, and constant axial load along the length of the element, are determined from the basic forces by interpolation within the basic system. Interpolation comes from static equilibrium and provides constant axial force and linear distribution of bending moment in the absence of distributed element loads. Since Opensees is in a displacement based finite element analysis environment, forced-based beam column element requries intro-element solution to determine section strains and curvature. Principle of virtual force is used to formulate compatibility between section and element deformations. Addtionally accuracy can be incresead by increasing number of integration points or number of elements. Definition of shear behaviour additional to flexure is possible with section aggregator, in constrast to displacement-based element, (Figure2.23).

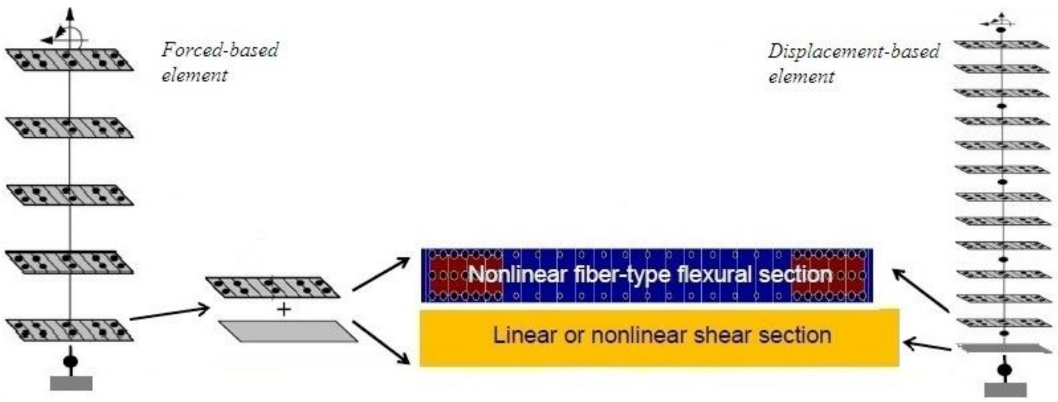

Figure 2.23 : Fiber type beam-column element, [20].

As a result, forced-based element and displacement-based element approaches are disparate methods so that application of them differs from each other. Although providing accurate results is possible only by increasing the number of elements in case of displacement-based element, increasing either the number of integration points or the number of elements improves accuracy of the solutions for forced-based element. In case of forced-based approach, both local and global quantities converge fast according to increase number of integration points. For displacement-based approach, higher derivatives converge slower to the exact solution and thus, accurate determination of local response quantities needs a finer finite element mesh than the accurate determination of global response quantities. Although it is computationally more expensive, forced-based element generally improves global and local response without mesh refinement. In order to achieve accurate local response of element number of integration points of a forced-based element has to be chosen such that integration weights at locations of plastic hinges match the plastic hinge lengths, [20, 26].

Lowes et. al. [20] has choosen fiber type forced-based beam-column element to model shear walls. In light of previous studies it is decided that forced-based element model is more suitable for simulation of shear walls of this study.

2.2 Modeling Steel-Concrete Composite Moment Frames

This study comprises assessment of steel-concrete composite sections additional to shear walls, since the three-dimentional (3D) model of a steel-concrete composite structure is in scope of the case study.

Steel concrete composite columns and beams are examined. Composite occurs in consequence of, circular steel sections filled with reinforced concrete columns and H-section beams act together with RC slab. Lumped plasticity model is choosen in order to substitute nonlinear behavior of composite components. Accordingly, it is assumed that plastic hinges occurs at the ends of the element and middle part remains linear elastic. All properties of nonlinear behavior are assigned into plastic hinge regions that take part at the ends of the elements.

Linear elastic part of the element simply can be defined with elastic beam-column element command. Characteristic properties of the composite section can be obtained in terms of Eurocode 2 [16]. On the other hand, bouc-wen and pinching material models adequately provide nonlinear behavior for plastic hinge regions. Definition of zero length elements is required in order to construct a plastic hinge region at the ends of the elements. In case of lumped plasticity of beam elements, bouc-wen and pinching material models is suitable and connection of these two material objects is possible with parallel material command. Bouc-wen material model alone is sufficient for plastic hinges of columns.

2.2.1 Elastic beam-column elements

When nonlinear behavior is repsented with lumped plasticity models, mid-span of the element is considered as linear elastic. Opensees provides elastic beam-column element command that enables to construct elastic beam-column object. Required information to build an elastic beam-column object are cross-sectional area, Young's modulus and shear modulus of the element and torsional moment of inertia, second moment of area in both directions of cross section.

Liner elastic element properties of composite beams and columns are calculated according to Eurocode 4 [27], which is the European design code for composite steel and concrete structures. A representation of composite beam is shown in Figure 2.24. Elastic (Young’s) modulus of the beams and beam-column connection joints are assumed equal to the elastic modulus of structural steel material. Additionally elastic modulus of composite columns, which are represented in Figure 2.25, is calculated in terms of Eurcode 4 Section 6.7.3.3, [27].

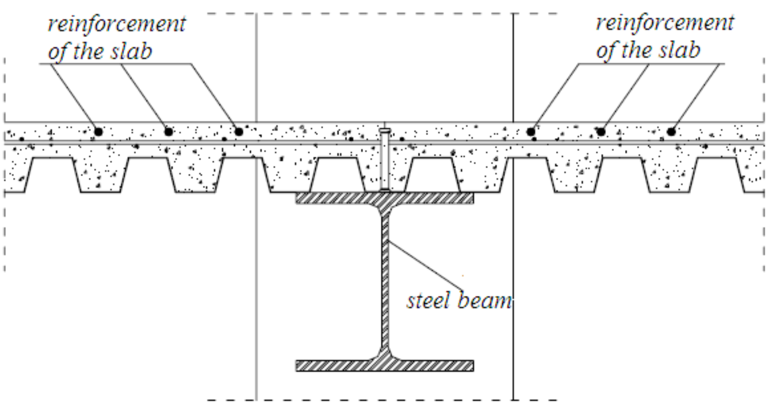

Figure 2.24 : A representation for composite beams.

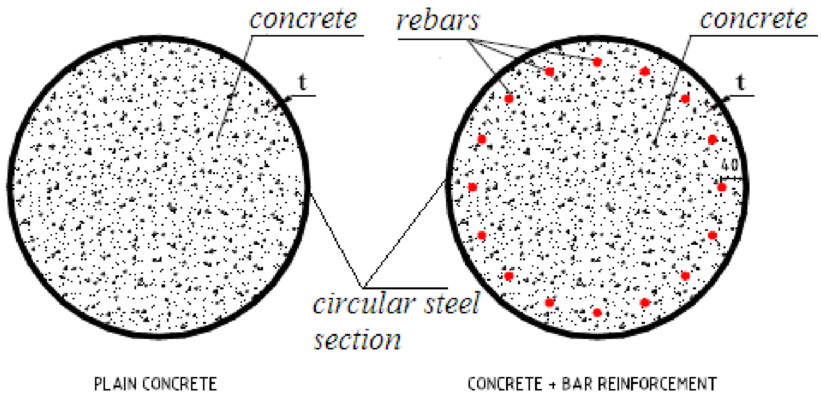

Figure 2.25 : A representation for composite columns.

It is stated that characteristic value of the effective flexural stiffness $(EI)_{eff}$ of a cross section of a composite column should be calculated from Equation **(2.19)**, where K_e is a correction factor that should be taken as 0.6. Additionally, I_a, I_c, and I_s are the second moments of area of the structural steel section, the un-cracked concrete section and the reinforcement for the bending plane being considered.

$$(EI)_{eff} = E_a I_a + E_s I_s + K_e E_{cm} I_c \quad \textbf{(2.19)}$$

2.2.2 Modeling of lumped plasticity

The inelastic action of RC components concentrates at the ends of the beams and columns under seismic loads. Therefore, a procedure, which composes a definition of zero length plastic hinges in the form of nonlinear springs located at the ends of the frames, used to be common. These models comprise various springs that are connected in series or parallel according to the formulation, [25].

Zero-length element command is used to create a zero-length element between two nodes that have the same geometric coordinates (Figure 2.26). This zero-length element enables the analyst to locate the plastic hinge. Multiple uniaxial material objects are needed to be defined to represent the force-deformation relationship for the element between the nodes.

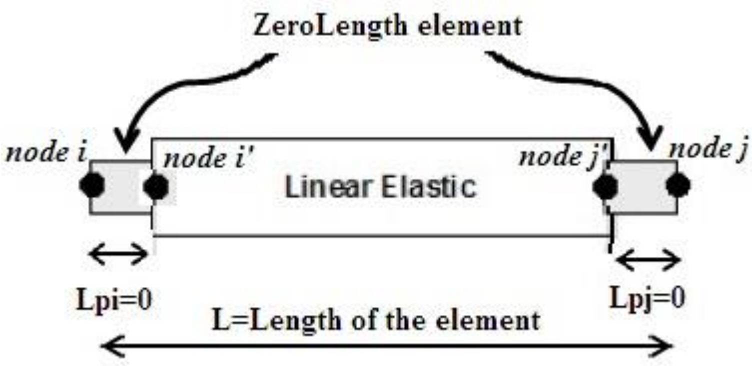

Figure 2.26 : Representation of ZeroLength element.

Bouc-Wen and Pinching material models are assigned to the plastic hinge (zero-length element) region for definition of nonlinear behavior. An examination about Bouc-Wen material model is performed.

Bouc (1967) proposed a sophisticated, smoothly changing hysteresis model for a single-degree-of-freedom (SDOF) mechanical system that is exposed to forced vibration. Wen derived Bouc's hysteretic constitutive law and developed an approximate solution procedure for random vibration analysis in terms of equivalent linearization method by using the mechanical model shown in Figure 2.27 in 1980. Baber and Wen (1981) improved the model to take into account the strength and stiffness degradation as a function of hysteretic energy dissipation and implemented it to a multiple-degree-of-freedom (MDOF) system. Baber and Noori (1985, 1986) further improved the modified Bouc model by incorporating pinching while maintaining it in a form compatible with Baber and Wen, and Wen's equivalent linearization solution, [28]. The final model, with Baber and Noori's [29] single-element pinching model, is preferred to build a boucwen material model by Opensees.

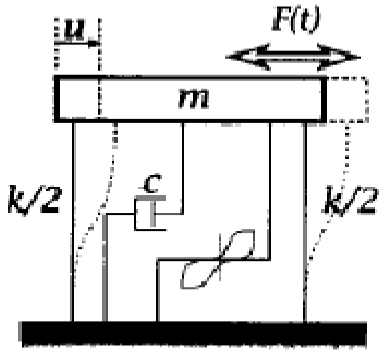

Figure 2.27 : Schematic model of hysteretic SDOF system, [27].

UniaxialMaterial BoucWen command is used to construct a uniaxial Bouc-Wen smooth hysteretic material object. This material model is an extension of the original Bouc-Wen model that includes stiffness and strength degradation according to Baber and Noori [29] as explained above. Figure 2.28 is an example for stress-strain curve of Bouc-Wen material model.

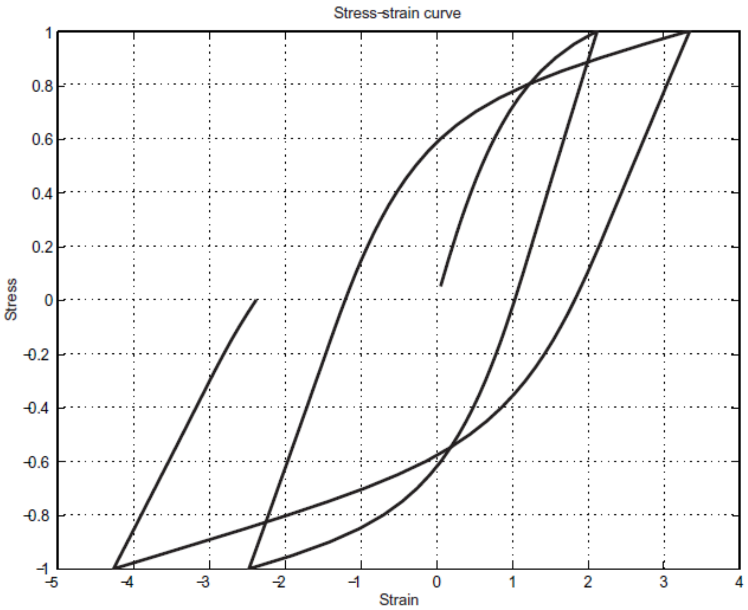

Figure 2.28 : Stress-strain curve for one-member truss with degrading Bouc-Wen material, [30].

Pinching4 command constructs a uniaxial material that represents a ‘pinched’ load-deformation response and exhibits degradation under cyclic loading. Cyclic degradation of strength and stiffness occurs in three ways: unloading stiffness degradation, reloading stiffness degradation, strength degradation (Figure 2.29).

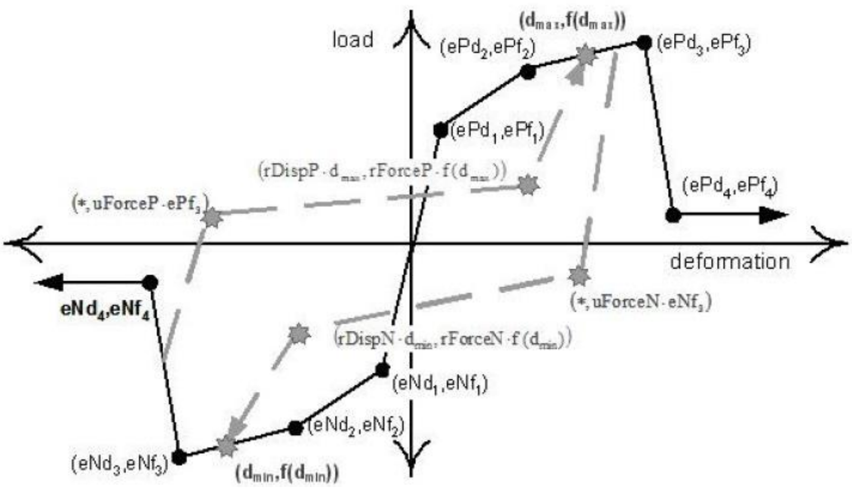

Figure 2.29 : Definition of pinchin4 uniaxial material model, [12].

Parallel material command builds a parallel material object made up of an arbitrary number of previously constructed uniaxial material objects. It composes of nonlinear springs that are connected in parallel to eachother as shown in Figure 2.30. In this study this command is used to connect bouc-wen material object with pinching4 material object in order to identify inelastic behavior of beams at plastic hinges.

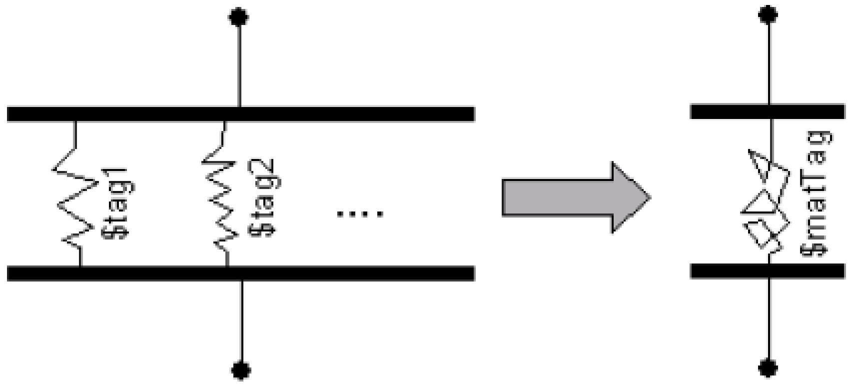

Figure 2.30 : Graphically represented parallel material, [12].

3. METHODS FOR PERFORMANCE ASSESSMENT OF BUILDINGS

Quantative level of the real seismic performance related with the damage of a structure exposed to a specified ground motion is a common research topic. This assessment can be performed either experimentally or analytically. This study comprises analytical seismic performance assessment, wherein a comprehensive modelling of the structure together with methods of structural analysis to provide elobrated information about seismic performance of structures is used. Nonlinear static (pushover) analysis or nonlinear dynamic (time-history) analysis are usually used methods for performance evaluation. Both pushover and time-history analysis methods are explained in this section.

3.1 Performance Assessment With Nonlinear Static Analysis Per Eurocode 8

Eurocode 8 [10] is a specification that is for the design and construction of buildings and structural engineering works in seismic regions. Its purpose is to ensure that in the event of earthquakes; human lives are protected, damage is limited and that important structures for civil protection remain in service.

Additonally, description of the pushover analysis is given in Eurococde 8. It is stated that pushover analysis is a non-linear static analysis carried out under conditions of constant gravity loads and monotonically increasing horizontal loads. It can be applied to verify the structural performance of newly designed and of existing buildings for the following purposes; to verify or revise the overstrength ratio values, to estimate the expected plastic mechanisms and the distribution of damage, to assess the structural performance of existing or retrofitted buildings and as an alternative to the design based on linear-elastic analysis. In the last case, the target displacement should be used as the basis of the design.

Consequently, Eurocode 8 involves a performance evaluation procedure by using nonlinear static (pushover) analysis. This study concern about that the procedure provides determination of target displacement. The target displacement can be defined as the seismic demand derived from the elastic response spectrum in terms of the displacement of an equivalent single-degree-of-freedom system. Furthermore, this procedure is based on the N2 method, which is proposed by Fajfar and Gaspersic, [3].

N2 method, which is an interpreted procedure in order to analyze nonlinear seismic damage of planar building structures, had been developed and presented. Both existing and newly design structures can be evaluated with this method. When predominant mode of the structure is the first mode, procedure most probably results in good prediction of global seismic demand. Generally, estimation at the local level such as demand in terms of deformation, dissipated energy, and damage indices are suitable for practical purposes. This procedure is applicable for different ground motions and structural parameters and it allows to examine the influence of these parameters on structure response. In case of significant higher mode effects, some demand parameters calculated with N2 method may be underestimated, [3].

The target displacement is determined from the elastic response spectrum. An example for a MDOF system and its elastic response spectrum is represented in Figure 3.1. The capacity curve, which represents the relation between base shear force and control node displacement, is determined in accordance with pushover analysis. Visual representation of obtaining pushover curve for a MDOF system is shown in Figure 3.2. Determination of target displacement according to Eurocode-8 is explained step by step.

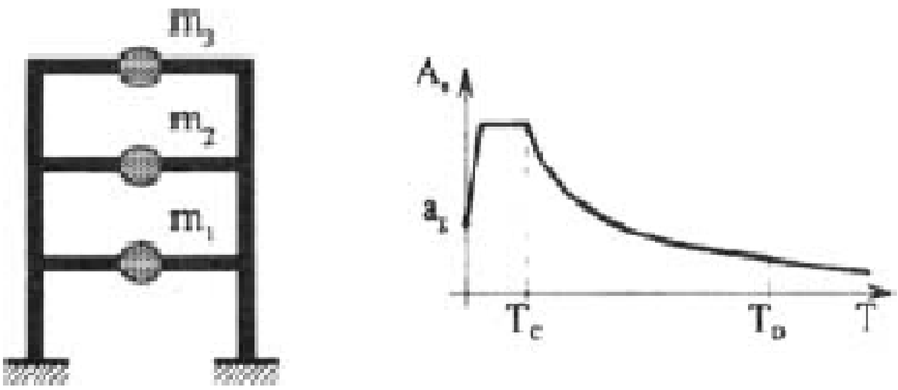

Figure 3.1 : Input data for pushover, [3].

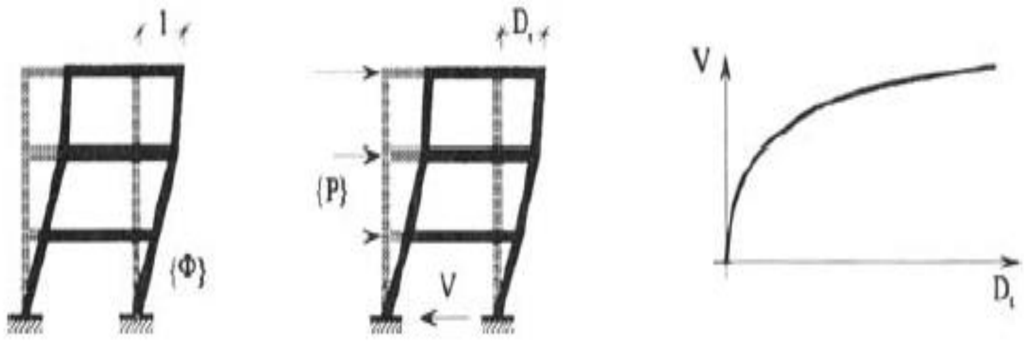

Figure 3.2 : Represetation for evaluation of pushover (capacity) curve [3].

First step is transformation to an equivalent single degree of freedom (SDOF) system, (Figure 3.3). Several variants have been proposed for the transformation of a planar MDOF system to an equivalent SDOF system. Fajfar used and explained one of these procedures as follows. The variant of the transformation that is used by Fajfar and accordingly stated in Eurocode-8 [10] was derived by assuming a time-independent displacement shape $\{\Phi_n\}$ (normalized to the top displacement $\Phi_n = 1$) and a vertical distribution of lateral resistance $\{P\} = [M]\{\Phi\}$, where $[M]$ is a diagonal mass matrix. Furthermore, it was required that the original response spectra could be used (i.e. that the transformation of the spectral amplitudes is not needed).

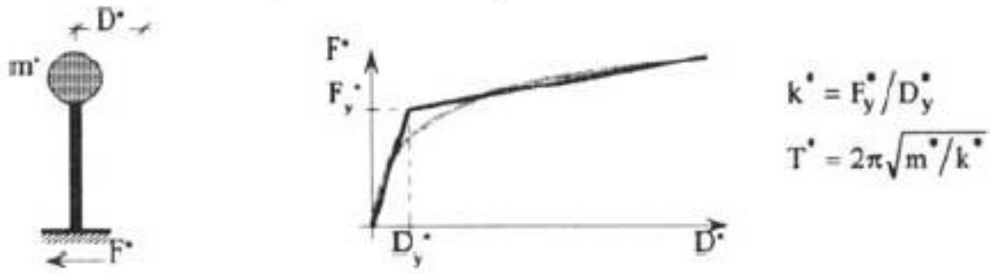

Figure 3.3 : Transformation from MDOF sytem to SDOF system.

The resulting transformation can be written in the form:

$$R^* = c_0\, R \tag{3.1}$$

where R^* represents the quantities in the equivalent SDOF system such as force F^* displacement d^* and hysteretic energy E_H^*; and R represents the corresponding quantities in the MDOF system such as base shear F_b, top displacement d_n, and hysteretic energy E_H. Constant c_0 is defined as shown in Equation **(3.2).**

$$c_0 = \frac{\{\Phi\}^T [M] \{\Phi\}}{\{\Phi\}^T [M] 1} = \frac{\sum m_i \Phi_i^2}{\sum m_i \Phi_i} \quad \textbf{(3.2)}$$

In this equation m_i is the concentrated mass at the i^{th} storey. The value in the denominator represents the mass of the equivalent SDOF system (see Equation **(3.4)**). Numerical experiments have shown that the results are relatively insensitive to small or moderate changes in $\{\Phi\}$. Consequently, a rough estimate of deformation shape $\{\Phi\}$ can be made. For the pushover analysis the lateral load distribution $\{P\} = [M]\{\Phi\}$ should be used, [3].

Accordingly, transformation of a MDOF system to SDOF in order to evaluate target displacement is described in Eurocode 8 [10] as follows. Relation between normalized lateral forces $\bar{F}_i$ and normalized displacements Φ_i is assumed as shown in Equation **(3.3)**. Displacements are normalized in such a way that $\Phi_n = 1$, where n is the control node (usually, n denotes the roof level). Consequently, $\bar{F}_n = m_n$.

$$\bar{F}_i = m_i \Phi_i \quad \textbf{(3.3)}$$

The mass of an equivalent SDOF system m^* is determined same as explained above and the Equation (**3.4**) shows the formula. Accordingly, transformation factor Γ can be computed as shown in Equation (**3.5).**

$$m^* = \sum m_i \Phi_i \quad \textbf{(3.4)}$$

$$\Gamma = \frac{m^*}{\sum m_i \Phi_i^2} = \frac{\sum \bar{F}_i}{\sum \left(\frac{\bar{F}_i^2}{m_i} \right)} \quad \textbf{(3.5)}$$

The force F^* and displacement d^* of the equivalent SDOF system are evaluated by using transformation factor Γ. The equations for determination of force F^* and displacement d^* are given in Equations **(3.6)** and **(3.7)**, where F_b and d_n are, respectively, the base shear force and the control node displacement of the MDOF system.

$$F^* = \frac{F_b}{\Gamma} \quad \textbf{(3.6)}$$

$$d^* = \frac{d_n}{\Gamma} \tag{3.7}$$

Subsequently, the idealized elasto-perfectly plastic force-displacement relationship is needed to be determined. It is assumed that the yield force F_y^*, which represents also the ultimate strength of the idealized system, is equal to the base shear force at the formation of the plastic mechanism. Stiffness of the idealized system is determined in such a way that the areas under the actual and the idealized force – deformation curves are equal, (Figure 3.4).

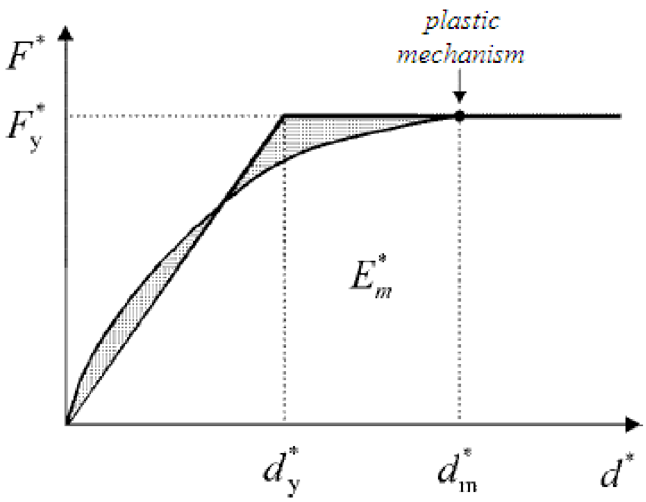

Figure 3.4 : Determination of the idealized elasto-perfectly plastic force-displacement relationship, [10].

Based on this assumption, the yield displacement of the idealized SDOF system d_y^* can be calculated as stated in Equation **(3.8)**, where E_m^* is the actual deformation energy up to the formation of the plastic mechanism.

$$d_y^* = 2\left(d_m^* - \frac{E_m^*}{F_y^*}\right) \tag{3.8}$$

Third step of this procedure is determination of period of idealized equivalent SDOF system. Equation **(3.9)** represents calculation for the period of the idealized equivalent SDOF system (T^*).

$$T^* = 2\pi\sqrt{\frac{m^* d_y^*}{F_y^*}} \tag{3.9}$$

The target displacement of the structure with period T* and unlimited elastic behavior is given in Equation **(3.10)**, where $S_e(T^*)$ is the elastic acceleration response spectrum at the period T*.

$$d_{et}^* = S_e(T^*)\left[\frac{T^*}{2\pi}\right]^2 \qquad \textbf{(3.10)}$$

For the determination of the target displacement d_t^* for structures in the short-period range and for structures in the medium and long-period ranges different expressions should be used as indicated below. The corner period between the short and medium period range is T_C.

- In case of short period range, which means $T^* < T_C$, two cases are possible.

  - First case is elastic response case that occurs due to

$$F_y^*/_{m^*} \geq S_e(T^*) \qquad \textbf{(3.11)}$$

Accordingly, the target displacement d_t^* can be assumed as follows,

$$d_t^* = d_{et}^* \qquad \textbf{(3.12)}$$

  - The other case is nonlinear response which is caused by:

$$F_y^*/_{m^*} < S_e(T^*) \qquad \textbf{(3.13)}$$

Therefore, the target displacement d_t^* can be calculated with Equation **(3.14)**, where q_u is the ratio between the acceleration in the structure with unlimited elastic behaviour $S_e(T^*)$ and in the structure with limited strength $F_y^*/_{m^*}$.

$$d_t^* = \frac{d_{et}^*}{q_u}\left(1 + (q_u - 1)\frac{T_C}{T^*}\right) \geq d_{et}^* \qquad \textbf{(3.14)}$$

$$q_u = \frac{S_e(T^*)m^*}{F_y^*} \qquad \textbf{(3.15)}$$

- On the other hand, in case of medium or long period range, which means $T^* \geq T_C$, target displacement can be assumed equal as Equation **(3.16)**. However, d_t^* should not exceed $3d_{et}^*$.

$$d_t^* = d_{et}^* \tag{3.16}$$

The relation between different quantities is shown in Figure 3.5. The figures are plotted in acceleration - displacement format. Period T* is represented by the radial line from the origin of the coordinate system to the point at the elastic response spectrum defined by coordinates $d^* = S_e(T^*)\left(T^*/_{2\pi}\right)^2$ and $S_e(T^*)$.

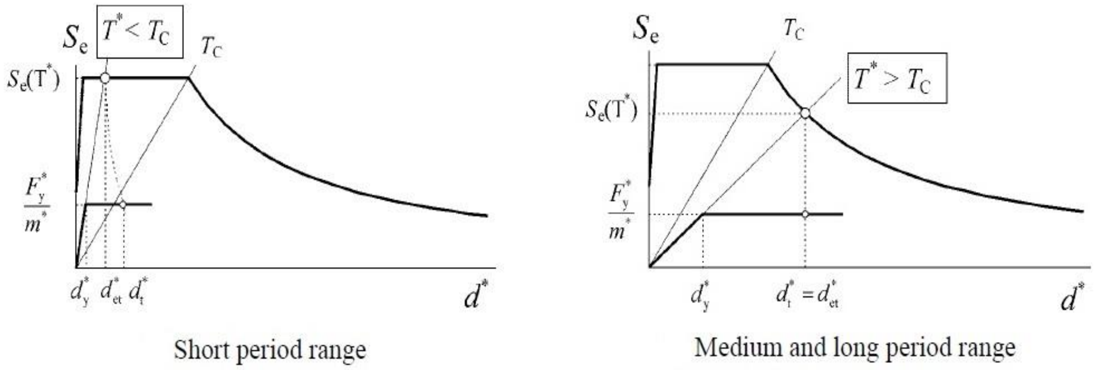

Figure 3.5 : Determination of the target displacement for the equivalent SDOF system [10].

Finally, determination of the target displacement for the MDOF system can be obtained due to target displacement of SDOF system. Required equiation is given as Equation **(3.17)**. The target displacement corresponds to the control node, [10].

$$d_t = \Gamma d_t^* \tag{3.17}$$

3.2 Performance Assessment With Nonlinear Dynamic Analysis

Nonlinear dynamic analysis can be performed with exposing a combination of ground motion records to the structural model. Thus, it provides accurate results. It is possible to represent the ground motion in terms of ground acceleration time-histories and related quantities (velocity and displacement). Applied ground accelerations (accelograms) can be recorded or artificial accelograms. Addionally, time step d_{time}, duration of the ground motion T_{max} and maximum peak ground acceleration (pga) are important paramters of these accelograms.

The equilibrium for evaluation of dynamic response of multi degree of freedom (MDOF) systems with time-history analysis is given below. There m represents mass matrix, c is damping coefficient and f_s is elastic force or inelastic resisting force. u represents displacement vector so that, $\dot{u}$ and $\ddot{u}$ equals to respectively velocity and acceleration. Exitation vector is defined as $p(t)$, [31].

$$m\ddot{u} + c\dot{u} + f_s(u, \dot{u}) = p(t) \quad \textbf{(3.18)}$$

In non-linear dynamic analysis, the non-linear properties of the structure are considered as part of a time domain analysis. Accordingly, material nonlinearty and geometrical nolinearty (P-Delta) is taken into account in the material model.

A procedure for dynamic analysis is inclueded in Eurocode 8. The main objectives of this procedure are represented here. It is stated that, when a spatial model of the structure is required, the seismic motion shall consist of three simultaneously acting accelerograms. Depending on the nature of the application and on the information actually available, the description of the seismic motion may be made by using artificial accelerograms and recorded or simulated accelerograms. Since this study is performed only with artificial accelograms, rules of Eurcode 8 for artificial accelograms are presented.

Artificial accelerograms shall be generated so as to match the elastic response spectra and for 5% viscous damping. The duration of the accelerograms shall be consistent with the magnitude and the other relevant features of the seismic event underlying the establishment of design ground acceleration a_g. When site-specific data are not available, the minimum duration T_S of the stationary part of the accelerograms should be equal to $10\ s$. The suite of artificial accelerograms should observe the following rules;

- A minimum of three accelerograms should be used.
- The mean of the zero period spectral response acceleration values (calculated from the individual time histories) should not be smaller than the value of $a_g \cdot S$, where S represents soil factor, for the site in question.

- In the range of periods between $0.2\,T_1$ and $2\,T_1$, where T_1 is the fundamental period of the structure in the direction where the accelerogram will be applied; no value of the mean 5% damping elastic spectrum, calculated from all time histories, should be less than 90% of the corresponding value of the 5% damping elastic response spectrum.

Three artificial accelograms, which are corresponding to elastic response spectra, are obtained with software SIMQKE. It is proposed by Massachusetts Institute of Technology, [32].

4. MODEL BUILDING FOR CASE STUDY

This part of the thesis is carried out as a continuation of the project ATTEL [33], which is both an analytical and experimental study and conducted in University of Trento, Italy. The project ATTEL comprises assessment of high strength steel (HSS) and steel-concrete composite circular hollow sections (CHS) for columns and connections under earthquake and fire loads. Analytical study had been performed for two-dimensional (2D) moment resisting frame, for columns and for connections.

Although the Project ATTEL proposed to develop new design criteria to extend using HSS and steel-concrete composite filled tubes (CFT), this study is not concerned with the design of the structure. This study evaluates the seismic performance of the structure that has already been designed.

Analyses of two-dimensional (2D) shear walls and three dimensional (3D) structure that are exposed to earthquake loads are in the scope of this study. Modeling and analysis of shear walls are performed firstly. Then shear wall model is combined with 3D model of the structure. This section contains explanation of analyses of 2D shear wall and performance assessment of 3D building at the shear wall direction. This assessment is performed according to Eurocode 8.

4.1 Structural System of the Building

This section contains detailed information about the structure that is subject to case study of the thesis. Geometrical information, modeling of steel-concrete composite frames and properties and modeling of shear walls are explained.

The sturcure has considerable structural properties, that high strength steel is used for columns and columns are circular hollow sections filled with reinforced conrete. Structural information about the 3D building is provided from the Msc thesis of Fassin, since the modeling and analysis for 2D moment frame of the structure is performed within thesis of Fassin, [34].

The structure is a five-story building; each story has 3.5 meters of story height. Dimensions of building are 32m x 32m. There are 4 spans in each direction, that means a square mesh of primary beams with 8 m (Figure 4.1). The secondary beams are placed two in each mesh and with 2.67 m far from the primary beams. Lateral load resisting system is moment frames with steel-concrete composite columns in one direction (Y direction), in the other direction (X direction) frames with reinforced concrete shear walls.

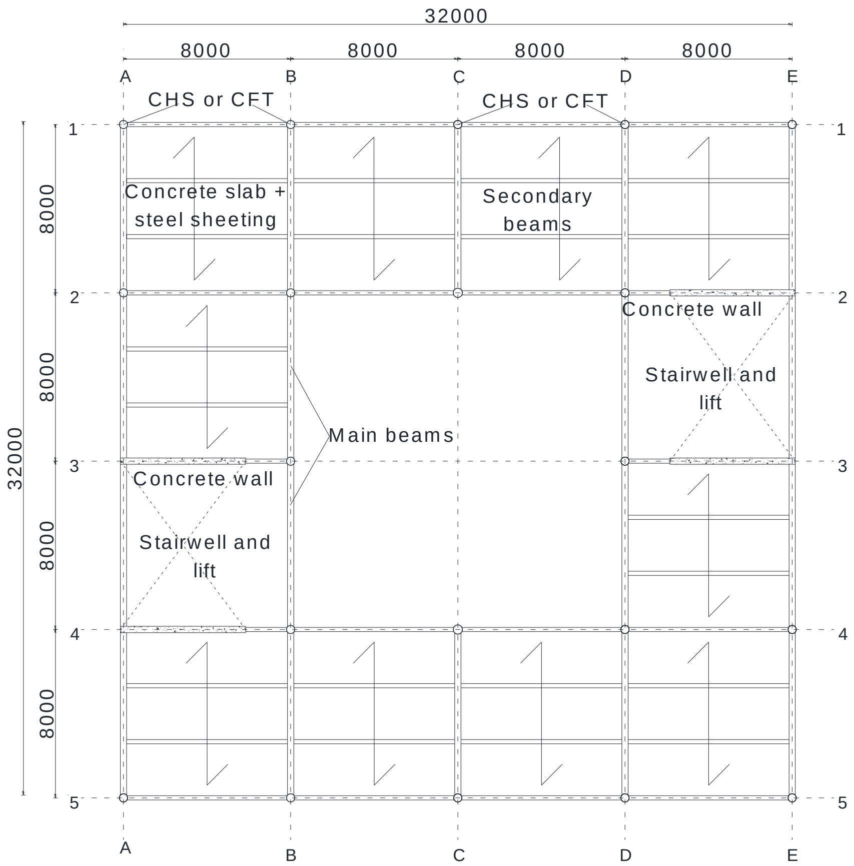

Figure 4.1 : Plan view of the ground floor.

The stairwells are located between two shear walls. This type of design is done as prevention in case of fire or earthquake. There are four equal shear walls in the building. Modeling and analysis of the shear wall has done separetely from 3D building to check the behaviour of the shear wall. After that, the shear wall model is entagrated to Opensees model of 3D building.

As it is seen in Figure 4.2, beams that are located between axes 2-2 and 4-4 are larger than other primary beams, since they are passing trough the open space. These beams have 16 m span and HEB 650 type of beams with S355 class of steel are used there. Primarly beams are HEB 280 and HEB 200 is preferred for secondary beams. Steel class of HEB 280 is choosen as S275.

Accordingly, length of the primary beams is 8 m and area of them is 6041.11 mm^2. CFT columns have 3.5 m height and 99314.67 mm^2 area. The beam-column connections, in other words joints are assumed 0.515 m long with 6041.11 mm^2 area, which is equal to area of beams. Detailed drawings of the structure are represented in Appendix A.

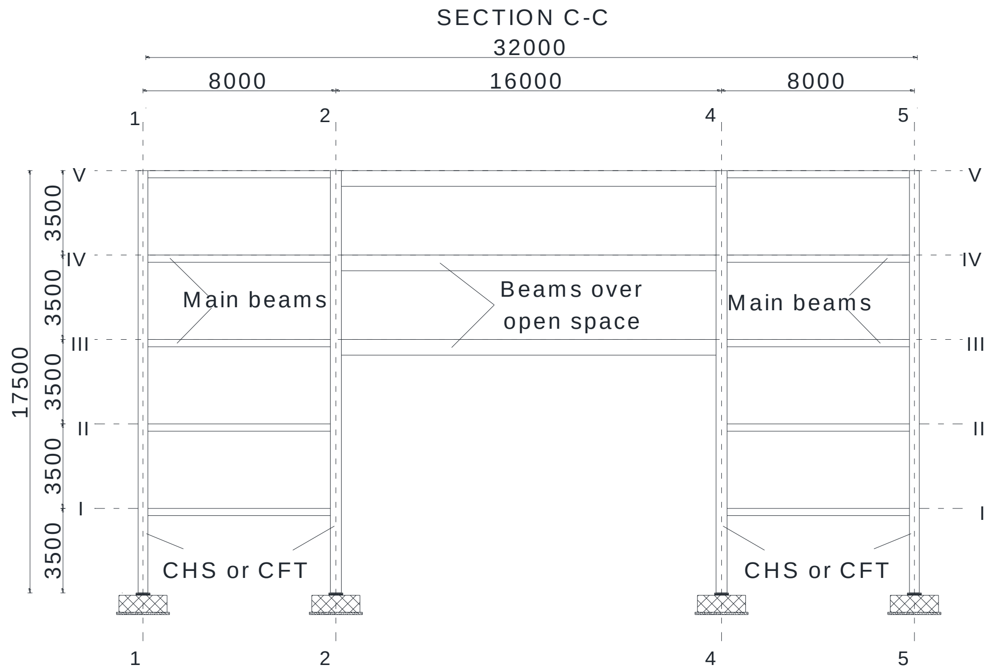

Figure 4.2 : Sectional view of axis C-C.

The beams are connected to the concrete slab, so that they are assumed as composite members. The slab has 110 mm total thickness, consisting of the steel sheeting with 1 mm thickness and 55 mm height. Hence, there is 55 mm reinforced concrete. Reinforcement is minimum required reinforcement, which equals to rebars with 10 mm diameter and 100 mm intervals. This slab is designed with assumption that it works together with the beams through the connectors Nelson (a type of connector) applied on top of the beam flange. Figure 4.3 represents a section of the composite slab. Detalied illustrations of the composite slab and beams are shown in Appendix A.

Columns are composed of composite filled tubes. Steel circular sections have 406 mm diameter and 12 mm wall thickness.

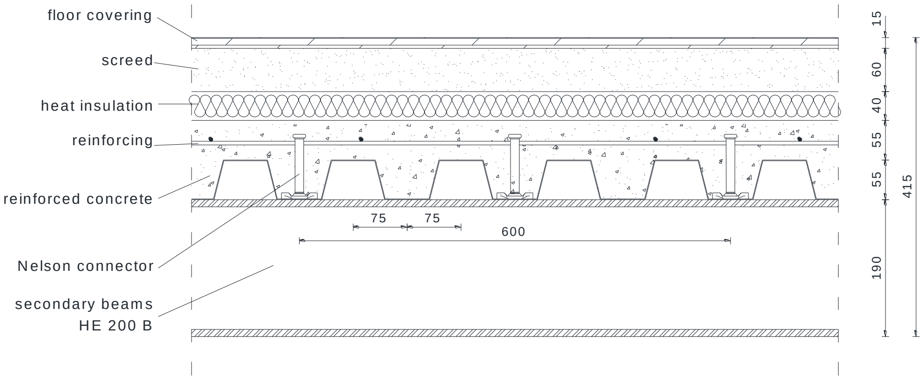

Figure 4.3 : Sectional view of composite slab.

Dimensions of shear walls are 6m x 0.30m with 17.5m height, which is the height of the structure. According to these dimensions, shear walls are slender reinforced concrete shear walls. As follows, height (h_w) to length (l_w) ratio is greater than 2.0, [17].

$$h_w/_{l_w} = {}^{17.5m}/_{6.0m} = 2.916 > 2.0 \tag{4.1}$$

There are four equal shear walls, which are located at the same direction of the building. Consequently, only one type of shear wall has been modeled. Geometrical representation of the shear wall is given in Figure 4.4.

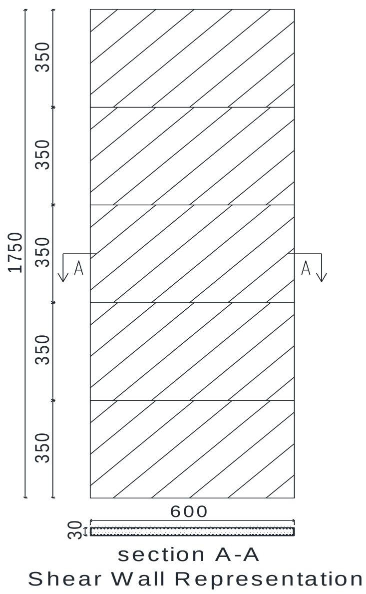

Figure 4.4 : A representation of shear wall.

Detailed definition of geometrical properties of RC shear wall is required in order to build confined concrete material and fiber section. Core dimensions to centerlines of perimeter hoop in x and y directions are $b_c = 1.21\, m$ and $d_c = 0.25\, m$. Reinforcement size differs at each level of the wall. Detailed drawing and table of quantities for reinforcement details of shear wall are given in appendix A.

For the ground floor, where confined concrete is used, diameter of transverse reinforcement is $d_{tr} = 8\, mm$ that comes up to $\emptyset\, 8$ and diameter of longitudinal reinforcement is $d_l = 22\, mm$, which comes up to $\emptyset\, 22$. Figure 4.5 represents ground floor section.

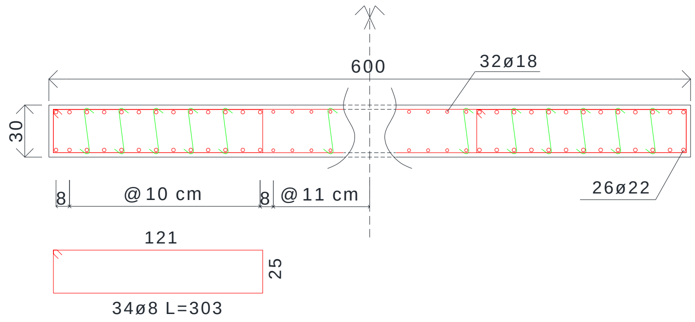

Figure 4.5 : Reinforcement details of ground floor shear wall section.

Since reinforced concrete and steel materials are collaborated in design of this building, it can be named as a composite building. In this sense, columns are circular hollow sections filled with reinforced concrete. Beams are steel sections connected with connectors to reinforced concrete slabs. Sectional stiffness of these composite columns are evaluated according to Equation **(2.19)**. On the other hand shear walls are reinforced concrete components.

Ordinary structural steel is used for beams. Primary beams HEB280 and secondary beams HEB200 has steel class S275 and main large beams (beams with 16 m span) are HEB650 and has steel class S355. The plates are also S355. Tubes that are used for columns are formed with high strength steel (HSS) class S590. Type of bolts that are used in connections is 10.9.

Steel sheeting is used in order to locate concrete slab on the steel beams. Class of steel sheeting is CR 250. Steel beams are connected with shear connectors from the upper flange to the steel sheeting. Shear connector type is Nelson 450.

Reinforced concrete elements have two material components, as it is known; concrete and reinforcing steel. Similar to explanations given before, concrete material definition is divided into two, confined and unconfined concrete. Concrete material is assumed unconfined for composite components. However, confined concrete part of shear walls is taken into account.

The reinforcing steel class is BC450 and mechanical properties that are identified according to the Eurocode 2 and stress-strain relationship of reinforcing steel is represented in Figure 4.6. Characteristic yielding strength f_{yk} of BC450 is $450\ MPa$. Elastic modulus E, which is defined as the ratio of tensile stress to tensile strain, is $200 \times 10^3\ MPa$. So that yielding strain e_{sy} can be calculated with f_{yk}/E that results in 0.00225. Ultimate strength f_u and corresponding strain e_{su} are respectively given as $517.5\ MPa$ and 0.075.

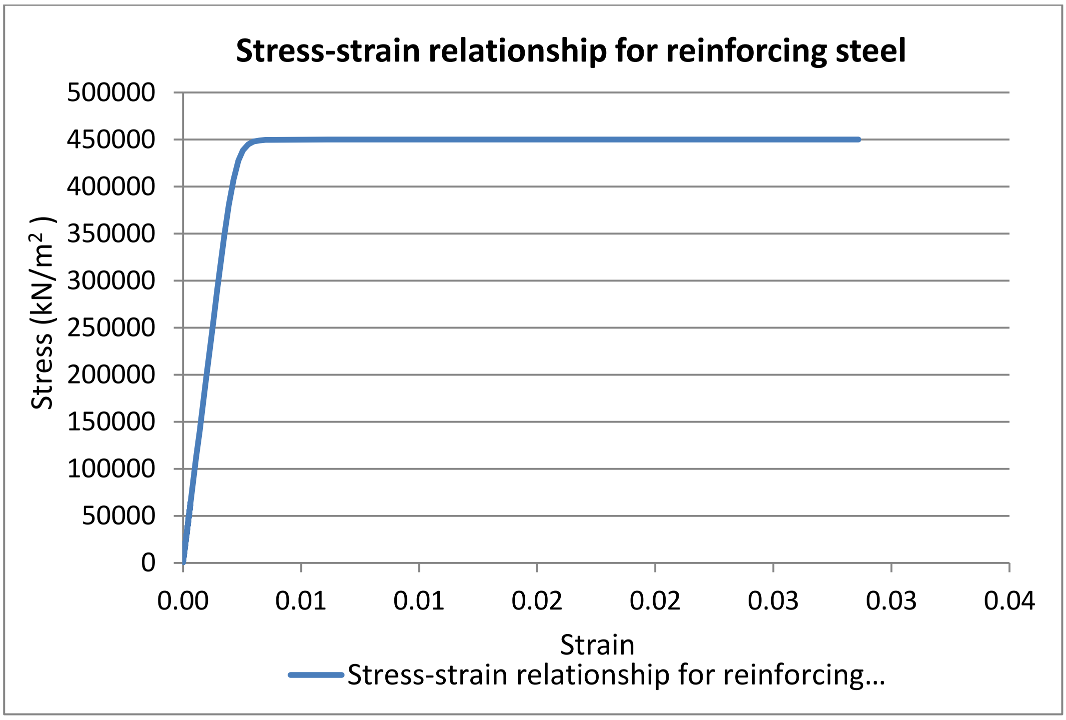

Figure 4.6 : Stress-strain relationship for reinforcing steel.

Unconfined concrete is the concrete without transversal reinforcements. This type of concrete has the characteristic properties of the concrete that is given by design codes. In this project shear walls have transversal reinforcement at all floors, but extra hoops are located at edge of the ground floor section (Figure 4.7). There is transversal reinforcement between longitudinal ones and cover concrete but there are not extra hoops, at other parts and other floors of the wall. In addition, the shear wall section is wide. Therefore, concrete properties of these parts are assumed as unconfined concrete.

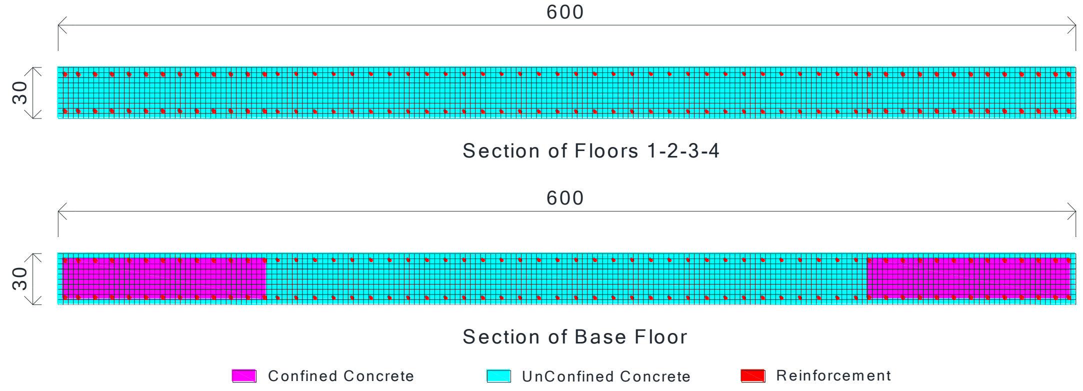

Figure 4.7 : Representation of fibers of sections.

Used concrete class is C30/37. Mechanical properties of unconfined concrete are applied in terms of Eurocode 2. Characteristic compressive strength f'_{c0} and corresponding strain e_{c0} for concrete class C30/37 are repectively 30 MPa and 0.02. Strain at ultimate strength e_{cu} for the same concrete class is 0.035.

Mostly reinforced concrete elements have spirals or hoops, which surround the longitudinal reinforcement. Even though these transversal reinforcements are used to surround longitudinal rebars, they considerably increase strength of concrete that remains inside transversal reinforcement. Mechanical properties of confined concrete, the concrete that remains inside transversal reinforcement, has determined by using Mander material model. Calculations for mechanical properties of confined concrete are explained and results are compared with results of Opensees.

Mander confined concrete model has elaborated previously. Equation to evaluation of compressive strength of confined concrete was given in Equation **(2.1)**. Calculations for mechanical properties of confined concrete defined in shear walls of the study are given in this section. Accordingly, required parameters for calculation of compressive strength of confined concrete are given below. Compressive strength unconfined concrete f'_{c0} and yield strength of transverse reinforcement f_{yh} are initially needed. f'_{c0} is defined above and f_{yh} is equal to yield strength of the reinforcing steel f_{yk}, which is 450 MPa for reinforcing steel class BC450 according to Eurocode 2.

Ratio of area of longitudinal reinforcement to area of core of section ρ_{cc} is one of the required parameters. According to Equation **(2.5)**, area of core of section enclosed by centerlines of the perimeter hoop A_c and total area of longitudinal reinforcement A_{sl} are needed for calculation of ρ_{cc}. A_c is calculated as follows:

$$A_c = b_c \cdot d_c = 1.21\, m \cdot 0.25\, m = 0.3025\, m^2 \tag{4.2}$$

Total area of longitudinal reinforcement is calculated for confined part of the section. There are 26 $\emptyset$ 22 at the edge regions of the wall at ground floor and total area A_{sl} is given below.

$$A_{sl} = 26 \cdot \frac{22^2\pi}{4} \cdot 10^{-6} = 0.00988\, m^2 \tag{4.3}$$

Accordingly, ratio of area of longitudinal reinforcement to area of core of section ρ_{cc} is given in Equation **(4.4)**.

$$\rho_{cc} = \frac{A_{sl}}{A_c} = \frac{0.00988\, m^2}{0.3025\, m^2} = 0.0326 \tag{4.4}$$

Considering Equation **(2.4)**, area of concrete core A_{cc} is calculated as follows:

$$A_{cc} = A_c(1 - \rho_{cc}) = 0.3025 \cdot (1 - 0.0326) = 0.2926\, m^2 \tag{4.5}$$

In order to obtain confinement effectiveness coefficient (for rectangular hoops) k_e, area of effective confined concrete core at hoop level A_e is required in addtion to A_{cc}. Steps to calculate A_e are shown in Equations **(2.6)** and **(2.7)**. So that, total plan area of ineffectually confined core concrete at the level of the hoops A_i is calculated due to Figure 4.5. Where w_i' (which stands for i th clear distance between adjacent longitudinal bars) starts with 8 mm and continues as 10 mm.

$$A_i = \sum_{i=1}^{n} \frac{(w_i')^2}{6} = \frac{(0.008)^2}{6} + 11 \cdot \frac{(0.01)^2}{6} = 1.94 \cdot 10^{-4} \tag{4.6}$$

Clear vertical spacing between hoop bars s' is sepcified in order to implement to Equation **(2.6)**. Representation of s' and s can be seen in Figure 4.8. s is vertically center to center spacing of hoops and it is 10 mm for ground floor section of the shear wall.

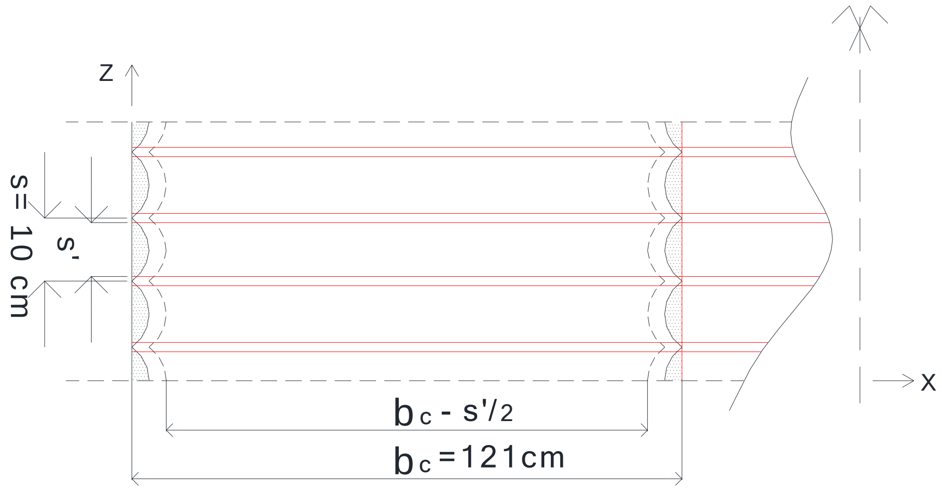

Figure 4.8 : A vertical section of RC shear wall at ground floor.

Thus, clear vertical spacing between hoop bars is obtained as $s' = s - d_{tr} = 0.1\ m - 0.008\ m = 0.092\ m$.

$$A_e = (0.3025 - 1.94 \cdot 10^{-4}) \left(1 - \frac{0.092}{2 \cdot 1.21}\right) \left(1 - \frac{0.092}{2 \cdot 0.25}\right) = 0.222 \quad \textbf{(4.7)}$$

Confinement effectiveness coefficient k_e is calculated due to parameters defined above for providing the fact $A_e < A_{cc}$.

$$k_e = \frac{A_e}{A_{cc}} = \frac{0.222\ m^2}{0.2926\ m^2} = 0.759 \quad \textbf{(4.8)}$$

Since compressive strength of confined concrete is evaluated for strong direction of the shear wall, the lateral confining stress on the concrete is obtained for x direction f_{lx} in terms of Equation **(2.8)**. Therefore, ratio of the transverse confining steel volume to the volume of confined concrete core at x direction ρ_x is obtained according to Equation **(2.10)**, where A_{sx} is the total area of transverse bars running in the x direction.

$$A_{sx} = 2 \cdot \frac{8^2 \cdot \pi}{4} \cdot 10^{-6} = 1 \cdot 10^{-4} m^2 \quad \textbf{(4.9)}$$

$$\rho_x = \frac{A_{sx}}{s \cdot d_c} = \frac{1 \cdot 10^{-4}}{0.1 \cdot 0.25} = 0.004 \quad \textbf{(4.10)}$$

All parameters for calculation of effective lateral confining stress on the concrete in the x direction f_{lx} are calculated, and it is exposed as follows according to Equation **(2.8)**:

$$f_{lx} = \rho_x \cdot f_{yh} = 0.004 \cdot 450000 = 1800 \ {}^{kN}\!/_{m^2} \qquad \textbf{(4.11)}$$

Herein transition from lateral confining stress f_{lx} to effective lateral confining pressure at x direction on the concrete section f_l' was described in Equation **(2.2)** and the result is given in Equation **(4.12)**.

$$f_l' = k_e f_{lx} = 0.759 \cdot 0.004 \cdot 450000 = 1366.2 \ {}^{kN}\!/_{m^2} \qquad \textbf{(4.12)}$$

Finally, all required components for calculation of compressive strength of confined concrete are obtained. Consequently f_{cc}' is given below according to Equation **(2.1)**. All these parameters of Mander confined concrete material model are defined in Opensees script. When the results of Opensees compressive strength of confined concrete calculations are compared with the result found out in Equation **(4.13)**, 0.012% difference is obtained and it is a tolerable error.

$$f_{cc}' = 30000\left(-1.254 + 2.254\sqrt{1 + \frac{7.94 \cdot 1366.2}{30000}} - 2\frac{1366.2}{30000}\right) \qquad \textbf{(4.13)}$$

$$f_{cc}' = 38551.407 \ {}^{kN}\!/_{m^2}$$

Additionally strain of confined concrete at compressive strength (e_{cc}) and elastic modulus of confined concrete (E_c) can be defined according to Mander et. al. as given in equations respectively **(2.12)** and **(2.13)**. For this shear wall section, they are given below.

$$e_{cc} = 0.002\left[1 + 5\left(\frac{38551.407}{30000} - 1\right)\right] = 0.00485 \qquad \textbf{(4.14)}$$

$$E_c = 5000\sqrt{30} \cdot 1000 = 27386127.88 \ {}^{kN}\!/_{m^2} \qquad \textbf{(4.15)}$$

Strain of confined concrete at ultimate stress e_{ccu} is calculated in terms of **(2.14)** and result is as follows:

$$e_{ccu} = 0.004 + \frac{0.075 \cdot 450000 \cdot 0.004}{30000} = 0.0085 \qquad \textbf{(4.16)}$$

Opensees gives the same results with the calculations above. Opensees results for elastic modulus $E_c = 27386127.875 \ {}^{kN}\!/_{m^2}$ and strain results at compressive strength and ultimate strength of concrete are respectively $e_{cc} = 0.00485$ and

$e_{ccu} = 0.0085$. As a result, Opensees data gives accurate results. Stress strain relationships for confined and unconfined concrete fibers are illustrated in Figure 4.9 due to Opensees pushover analysis results. Negative values represent compressive.

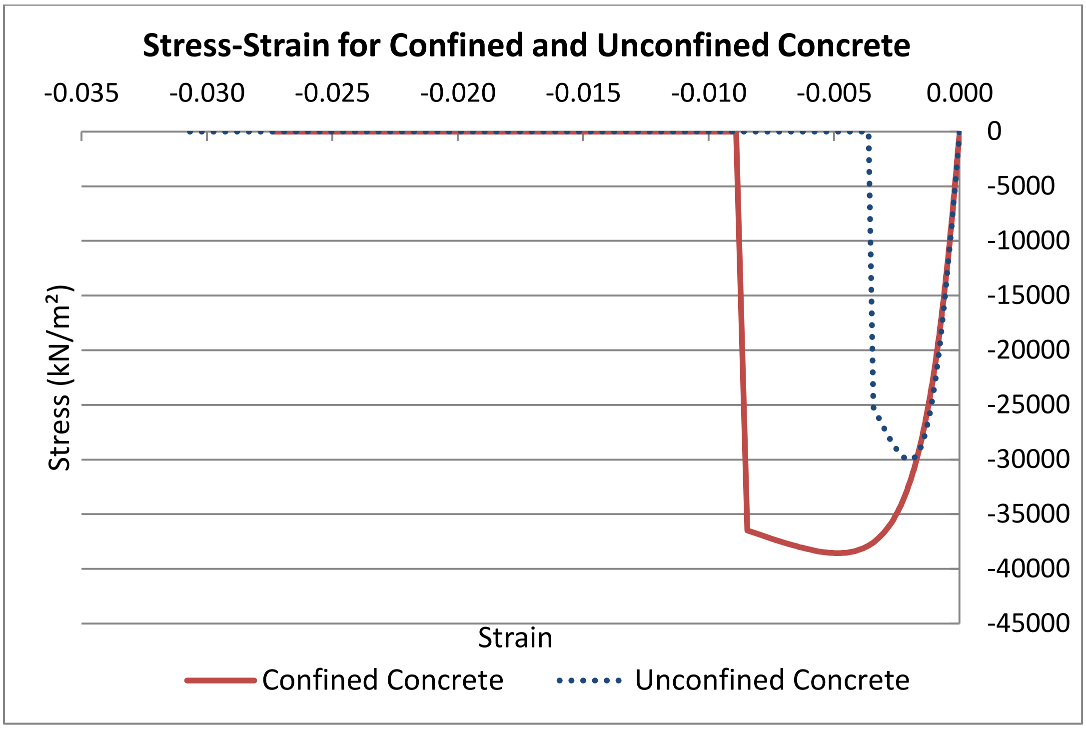

Figure 4.9 : Comparison between confined and unconfined stress-strain relationship.

Shear strength and torsional capacity of shear wall section is implemented with various material models. Definition of these properties in Opensees is represented futher, but calculations of shear strength and torsional capacity exist below.

Since the shear wall is slender as shown in Equation **(4.1)**, a flexural collapse is expected. In this case, shear is assumed linear-elastic. Elastic material model is implemented with uniaxial elastic material command in Opensees. According to Equation **(2.15)**, shear modulus of shear wall section G_{co} is calculated and poisson ratio υ is taken as 0.25.

$$G_{co} = \frac{27386127.88}{2 \cdot (1 + 0.25)} = 10954451.15\ {}^{kN}/{}_{m^2} \tag{4.17}$$

Shear section stiffness can be defined as gross section stiffness or reduced section stiffness for elastic models. Reduced section stiffness is preferred in this study. It is assumed that, 0.1 of gross section area is the effective area for the shear. Gross section area A_g is obtained as; $A_g = 0.3m \cdot 6m = 1.8\, m^2$. Accordingly shear capacity V is calculated as given below and implemented as tangent ($E) in uniaxial elastic material model (Figure 2.18).

$$V = 0.1 \cdot G_{co} \cdot A_g = 0.1 \cdot 10954451.15 \cdot 1.8 = 1971801.207\, kN \tag{4.18}$$

Torsional capacity of the section is necessary for 3D model of shear wall. There are not any torsional effects İn 2D model under lateral loading, so that torsional capacity of the wall is implemented only to the 3D model. Tresca criterion is used to calculate maximum shear stress τ_{max} due to Equation **(2.18)**. Torsional moment capacity M_T is defined as strength of material, torsional stiffness $G_{c0}J$ is defined as initial elastic tangent and strain-hardening ratio b is defined as 0.01 (Figure 2.19).

$$\tau_{max} = \frac{f'_{c0}}{2} = \frac{30000}{2} = 15000\, {}^{kN}\!/_{m^2} \tag{4.19}$$

Firstly, polar moment of inertia for rectangular secions J can be obtained with the formula; $J = l_w \cdot d_w^3/3$ which equals to $6 \cdot 0.3^3/3 = 0.66\, m^4$. Subsequently torsional stiffness is obtained as follows:

$$G_{c0}J = 10954451.15 \cdot 0.66 = 7229937.759\, kNm^2 \tag{4.20}$$

Length from further point to the center of the section l_{max} for the shear wall section that has $6\, m$ width, is obtained as; $l_{max} = b/2 = 3m$. Due to Equation **(2.16)**, torsional moment capacity M_T is evaluated below.

$$M_T = \frac{\tau_{max} \cdot J}{l_{max}} = \frac{15000 \cdot 0.66}{3} = 3300\, kNm \tag{4.21}$$

4.2 Analytical Models of the Moment Frames and Shear Walls

Firstly, 2D moment frames are built. Components are modeled as elastic and nonlinearty of the elements are defined with lumped plasticity models.

Elastic beam-column element definition is applied for columns and beams. At the ends of the elements a plastic hinge region is defined with zero length element and nonlinearty is implemented to these regions. Bouc-wen material and pinching material models are used in order to define nonlinearity.

Nonlinearty of columns is expressed only with Bouc-wen model, but both Bouc-wen and pinching models are applied for nonlinearty of beams. Combination of bouc-wen and pinching objects is provided with parallel material command, [34].

Transformation of 2D frames to 3D structure is performed and properties of the frames do not change. Torsional properties are defined in addition to 2D modeling. Shear walls are implemented to 3D model as the last step of modeling.

Initially a 2D shear wall model is built separately from the building model, in Opensees. Thus, behavior of the shear wall model is checked before integrating to the 3D building model. In this model one element defined for each floor, this means there are totally five elements in 2D shear wall model. The wall is fixed at the base and it is assumed as cantilever in case of 2D modeling. Loads are applied uniformly to nodes, which are defined as one node at each floor.

Additionally geometric nonlinearity is defined by using P-Delta command that represents P-Delta effect. P-Delta command is used to construct the P-Delta coordinate transformation object, which performs a linear geometric transformation of beam stiffness and resisting force from the basic system to the global coordinate system, considering second-order P-Delta effects, [12].

Material properties are implemented by using uniaxial material model. Uniaxial material model assumes that plane sections remain plane and perpendicular to the neutral axis. In addition, the material models cover nonlinear force and deformation relationship of element sections which is called material nonlinearity.

A preliminary study is performed about concrete material models to find the compatible material model for this study. Two types of concrete materials, which are concrete 01 and concrete 04 material objects, are applied. Stress-strain response of these materials are examined and compared, (Figure 4.10). Detailed information about concrete 01 and concrete04 material models are given in Chapter 2.

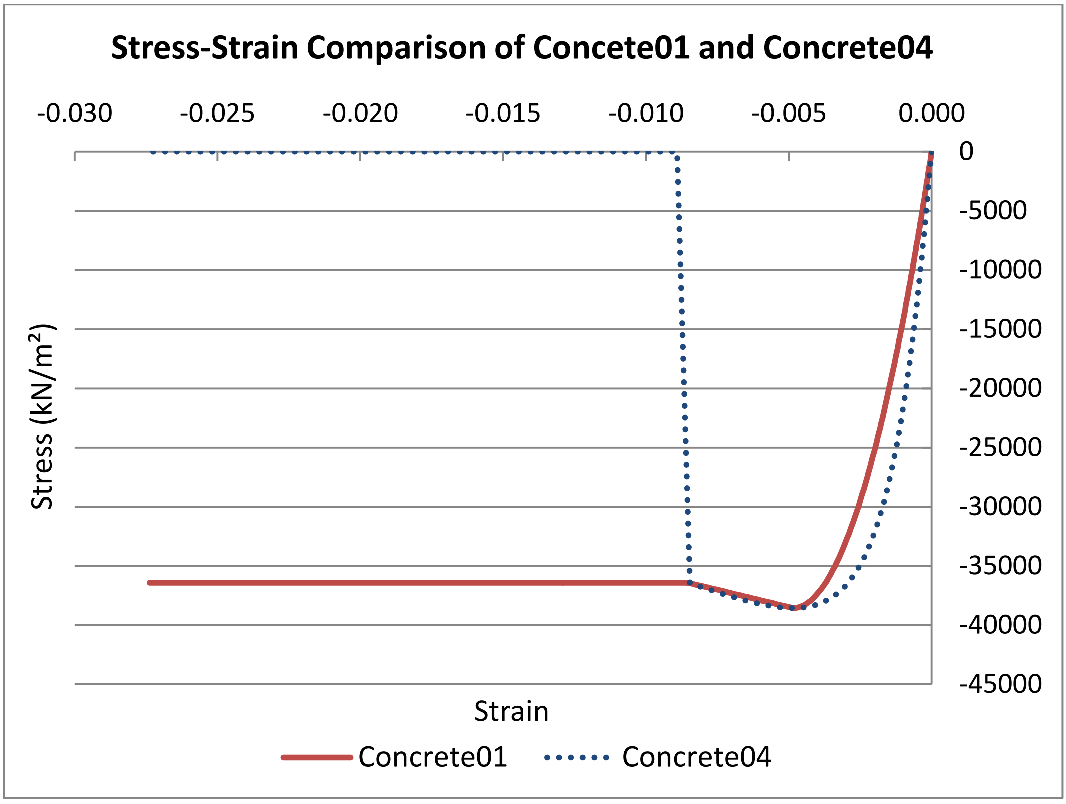

Figure 4.10 : Comparison of stress-strain curves of concrete01 and concrete04 material models for confined concrete fibers.

Kent-Scott-Park Model of the concrete material is implemented as uniaxial material concrete01 in Opensees. Concrete01 material gives behavior of concrete material with degraded linear stiffness according to the work of Karsan-Jirsa. It does not perform tensile strength as shown at Figure 2.4. Popovics material model of concrete is implemented as uniaxial material concrete04. This material model performs tensile strength with exponential decay [12]. In Kent-Scott-Park model, deformation of concrete material increases at constant load after the failure. This behavior causes difficulties to find out crushing strength of the shear wall. Besides in Popovics model after failure of concrete material, strength decreases sharply until zero. By using concrete04 material model failure of shear wall can be observed (Figure 4.11). Therefore, Popovic material model, which is implemented as uniaxial material concrete04, fulfills requirements of this study. Stress-strain relationship for concrete04 material can be seen in Appendix C.

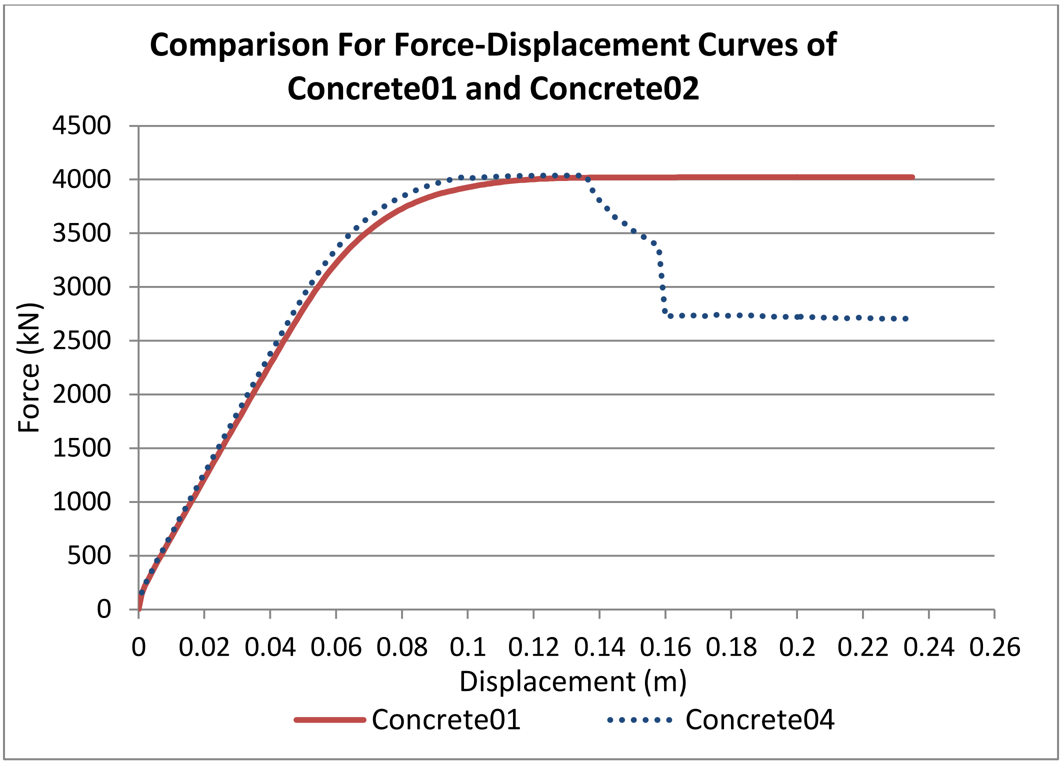

Figure 4.11 : Comparison of pushover-curves for shear walls with concrete 01 and concrete04 material models.

Although definition of tensile strength of concrete is possible by using concrete04 material objects, it is neglected for both confined and unconfined concrete in this study.

Giuffré-Menegotto-Pinto Model is used to define behavior of reinforcing steel. This model constitutes strain hardening at post yielding and works under cyclic loading. Giuffré-Menegotto-Pinto Model can be implemented with isotropic strain hardening as uniaxial material steel02.

Charactreistic properties of reinforcing steel are explained in Section 4.1. Additionally, values that control the transition from elastic to plastic branch and strain hardening value are required parameters for steel02 material model. Strain hardening b is assumed as zero. Other values are defined according to the suggestions given in Opensees command manual, for instance transition parameters are implemented as $R_0 = 15$, $cR_1 = 0.925$ and $cR_2 = 0.15$.

Shear behavior of the wall is assumed as elastic and uniaxial elastic material command is used to construct the shear material. Shear capacity V, which is obtained as $1971801.207\ kN$, applied as tangent ($E) of uniaxial elastic material model.

Torsional strength of the section is implemented with steel01 material command. Subsequently torsional stiffness $G_{c0}J$, which is equal to 10954451.15 kN/m^2, is defined as initial elastic tangent, strain-hardening ratio b is defined as 0.01 and torsional moment capacity M_T is implemented instead of yielding strength.

Fiber model is used to define shear wall section in Opensees. Fibers are smaller regions of the section for which the material stress-strain response is integrated to give resultant behavior, [12]. Each fiber represents the material in that position of the section. Representation of section is shown in Figure 4.7.

Section is subdivided into 240 regions in y direction, 12 regions in z direction for concrete material definition. Since the transversal reinforcement at edges of the section is located only at ground floor, confined concrete material properties is implemented only at ground floor sections at edges of the section (Figure 4.7). Reinforcement steel material properties are implemented with layer straight object at the exact locations of reinforcements.

Shear strength and torsional capacity of the section are defined separately from section definition and combined to the model using section aggregator command. Section aggregator combines material objects into a single section force-deformation model. Shear capacity of section that is defined with elastic material object is combined with flexural section, by section aggregator object both for 2D and 3D model of shear wall (Figure 4.12). Torsional capacity of section that is defined with steel01 material object is combined with flexural and shear section by section aggregator object for only 3D model of shear wall (Figure 4.13).

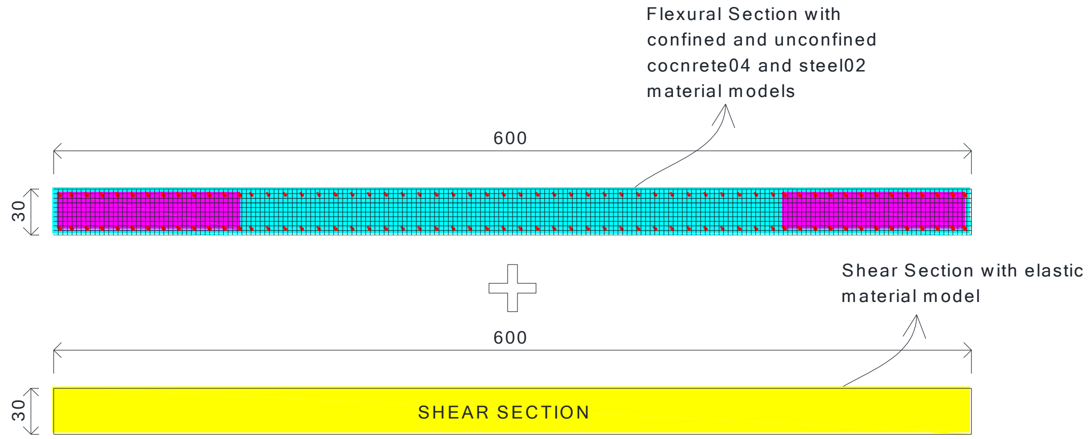

Figure 4.12 : Representation of section aggregator for 2D model.

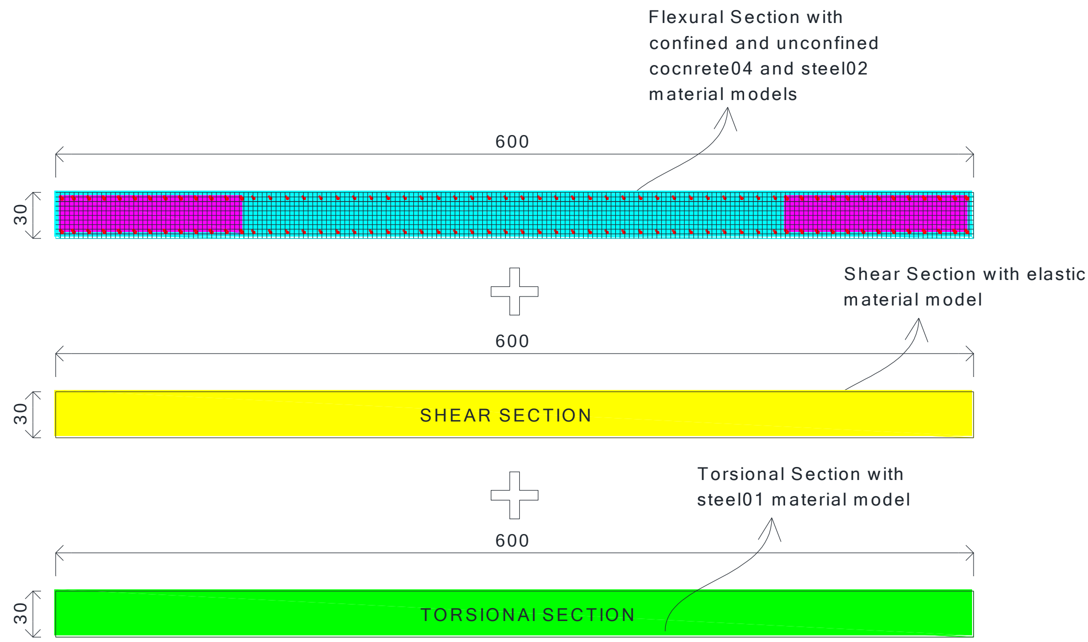

Figure 4.13 : Representation of section aggregator for 3D model.

Decision of how to model the shear wall is made according to examination given in Section 2.1.5. With refrence to this section lumped plasticity model needs knowledge or assumption of location and extent of plastic hinge. Additionally in this model nonlinear behavior occurs only at the plastic hinge region, other parts of the element remain elastic.

Distributed plasticity model does not need plastic hinge assumptions. Additionally distributed plasticity definition gives perfect results for slender shear wall modeling, [35]. Nonlinear beam-column element object, which considers spread of plasticity along the element, is implemented in order to build shear wall model with distributed plasticity.

Beam column element can be defined as forced based element or distributed based element. However, definition of these elements is different from each other. In order to increase the accuracy of the solution, number of elements or number of integration points could be increased for forced based element. On the other hand, only increasing number of elements gives more accurate results for distributed based element model. Forced based element converges faster according to increase of number of integration points. Additionally distributed based element needs finer fiber mesh for local response than global response. However, forced based element does not require mesh refinement for computation of global and local response, [26].

Finally, shear wall element that is defined with distributed plasticity is built by using force based nonlinear beam-column element object. One element is defined for each floor and five integration points are defined for each element (Figure 4.14).

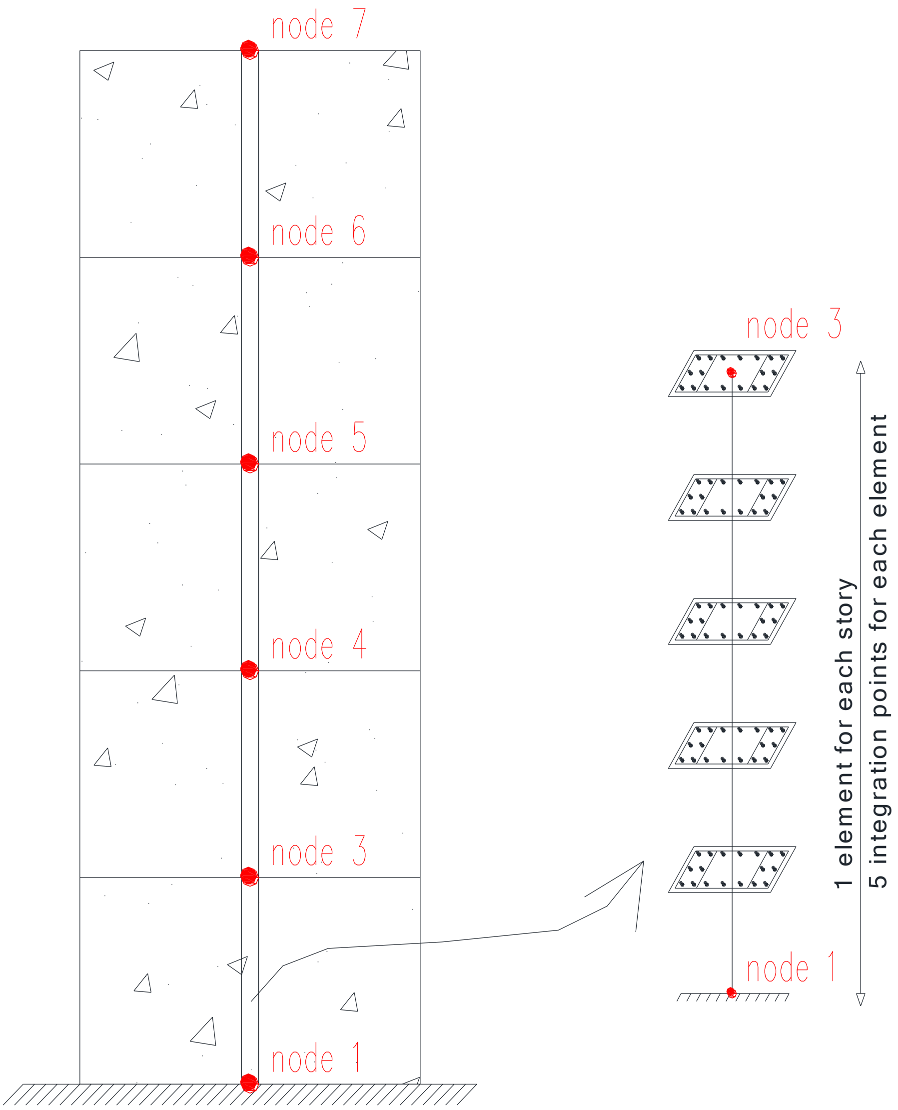

Figure 4.14 : Representation of forced-based beam-column element model.

4.3 Analyses Of The Shear Wall and Building

Analyses of 2D shear wall model are performed initially and analyses of 3D building model are followed them. Three types of analyses, which are moment-curvatre, monotonic nonlinear and cyclic nonlinear analyses, are perfomed. On the other hand, 3D structure is exposed to different analyses from the shear wall such as modal, monotonic pushover and time-history analyses.

4.3.1 Analysis of the shear wall

A set of analysis is performed in order to control the input data and behavior of used commands for shear wall. These analyses are respectively gravity, moment-curvature, pushover and cyclic nonlinear (ECCS) [36] analyses.

Gravity analysis is a static linear analysis and gravity loads are generally independent from the type of analysis. Gravity analysis is performed for both 2D shear wall model and 3D building model. Gravity loading, analysis and results of analysis for shear wall are discussed in this section.

Weight of the shear wall is assumed as gravity load of the shear wall. Density γ is assumed 2.5 ton/m^3 for reinforced concrete material. Accordingly shear wall mass for each floor is calculated (Figure 4.15) and loading is shown in Figure 4.16. Node numbers also can be seen in these figures. Masses at nodes 3, 4, 5 and 6 is represented as m_1 and calculated in Equation **(4.22)**, with considration of story height h_s that is equal to 3.5 m. Addionally, m_2 represents mass at node 7 and it is assumed to be equal to half of m_1. So that, $m_2 = m_1/2 = 7.875\ ton$.

$$m_1 = 1.8 \cdot 2.5 \cdot 3.5 = 15.75\ ton \quad \textbf{(4.22)}$$

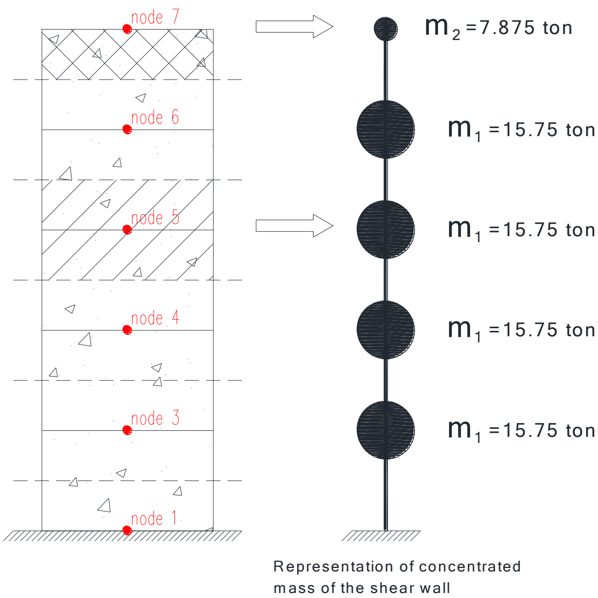

Figure 4.15 : Mass distribution of shear wall.

Gravity loads and load distribution is applied based on concentrated mass definition. Axial (gravity) loads at nodes 3,4,5 and 6 can be named as P_1. Since acceleration of gravity g is $9.806\ m/s^2$, P_1 is equal to $m_1 \cdot g$ and it results in; $P_1 = 15.75 \cdot 9.806 = 154.4445\ kN$. Accordingly P_2 is equal to $m_2 \cdot g$ and it is $77.222\ kN$ Gravity load distribution is represented in Figure 4.16.

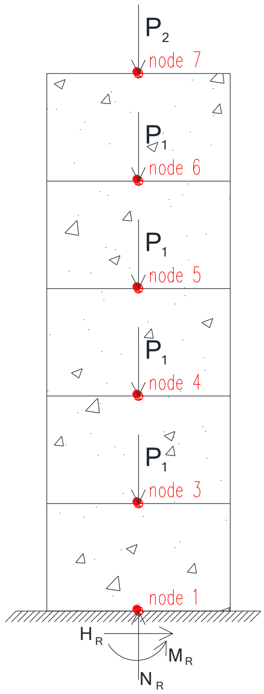

Figure 4.16 : Gravity loading of shear wall.

Three support reactions could occur at the base of 2D shear wall model since fixed support is defined at node1. Only axial loads are implemented during the gravity analysis, so that horizontal support (shear) reaction and moment reaction is expected to be zero. Additionally vertical support reaction should be equal to total axial loading.

$$N_R = 4 \cdot P_1 + P_2 = 4 \cdot 154.4445 + 77.222 = 695\ kN \qquad \textbf{(4.23)}$$

Finally gravity analysis results are checked whether meets the expectations. Vertical support reaction N_R is obtained $695\ kN$, which is same as calculated value. Horizontal support reaction and moment reaction are obtained as respectively $-7.212 \times 10^{-29} kN$ and $-5.174 \times 10^{-14}\ kNm$ which are almost zero. Finally, gravity analysis results confirm that Opensees data is correct.

Moment-curvature analysis is performed in order to evaluate moment capacity of shear wall section at the ground floor. This analysis is a two dimensional (2D) and a cross-sectional analysis. Therefore, a zero-length element is defined with the fiber section.

It is the ground floor section of the shear wall shown in Figure 4.7. Two nodes (Node1 and Node2) are defined at coordinate (0, 0, 0) in order to build zero length element. Node1 is restrained in all directions and Node2 is restrained only in direction y. Loads are applied at Node2. Visual definition of loading and moment-curvature analysis is shown in Figure 4.17.

Total gravity load of the shear wall is applied as an axial load during the analysis and gravity analysis is performed initially. Later curvature is taken into account as the control parameter. Curvature is increased step by step until the maximum curvature of the section. As a result moment-curvature of the element with zero thickness is obtained.

Finally moment curvature analysis is a cross-sectional analysis that is not concerned about the properties of the element, like height, definition or support conditions of the element, except the cross-sectional properties. Results of this analysis are compared with calculated moment capacity of the shear wall section. Calculations and analysis results are given further under the analysis results section.

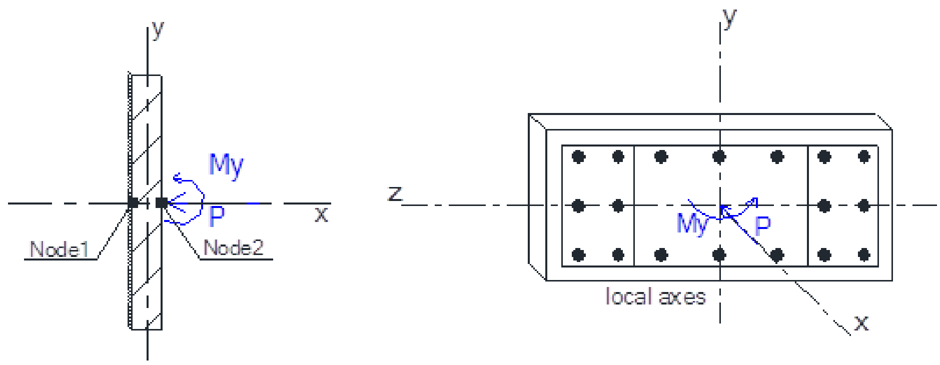

Figure 4.17 : Representation of loadig for moment-curvature analysis.

4.3.1.1 Static monotonic nonlinear (pushover) analysis

Nonlinear static analysis is analysis of a structure using a specified load pattern, where loading is started from zero, and increased up to a stated displacement. Initially gravity loads and then lateral forces are applied. Lateral forces should be increased systematically until the failure of the structure. In this study displacement is applied instead of horizontal force. Load pattern is shown in Figure 4.18. Displacement increment is assumed 1 mm for each step. This analysis is performed to investigate the relation between base shear force and roof displacement of the structure. Generally, displacement of the node, which is at the mass center of the roof, is taken as roof displacement of the structure. As a result of this analysis pushover curve (the curve where base shear force versus roof displacement) is obtained.

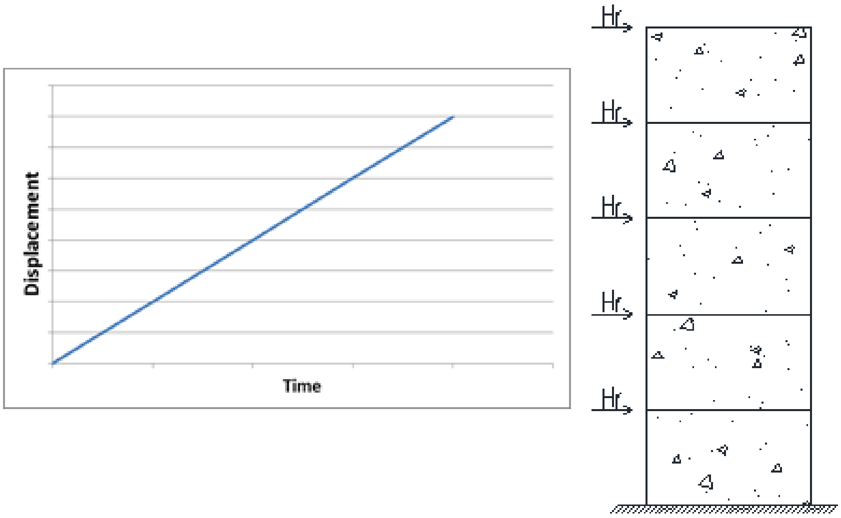

Figure 4.18 : Representation of static monotonic loading.

4.3.1.2 Static cyclic nonlinear (ECCS) analysis

Cyclic nonlinear analysis is performed in order to evaluate the hysteretic behavior of shear wall. ECCS procedure is implemented for cyclic loading, [36]. According to ECCS [36] procedure loading depends on increase of displacement. Characteristic of increase of displacements is given step by step. Steps are given below.

One cycle in the	$-e_y/4$	$+e_y/4$	interval
One cycle in the	$-e_y/2$	$+e_y/2$	interval
One cycle in the	$-3e_y/4$	$+3e_y/4$	interval
Three cycles in the	$-e_y$	$+e_y$	interval
Three cycles in the	$-2e_y$	$+2e_y$	interval
Three cycles in the	$-4e_y$	$+4e_y$	interval
Three cycles in the	$-6e_y$	$+6e_y$	interval
Three cycles in the	$-8e_y$	$+8e_y$	interval

Yielding displacement (e_y) is obtained according to pushover curve due to methodology that is defined in ECCS procedure (Figures 4.19 and 4.20). A regular behavior of shear wall is expected under regular loading.

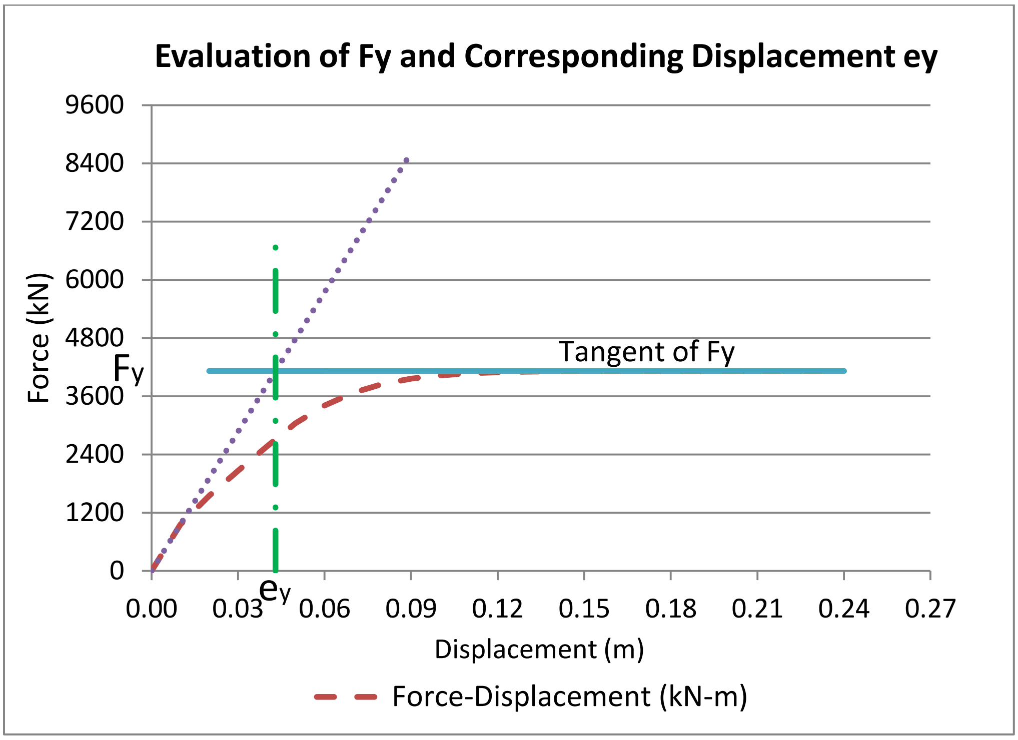

Figure 4.19 : Evaluation of yielding displacement (e_y).

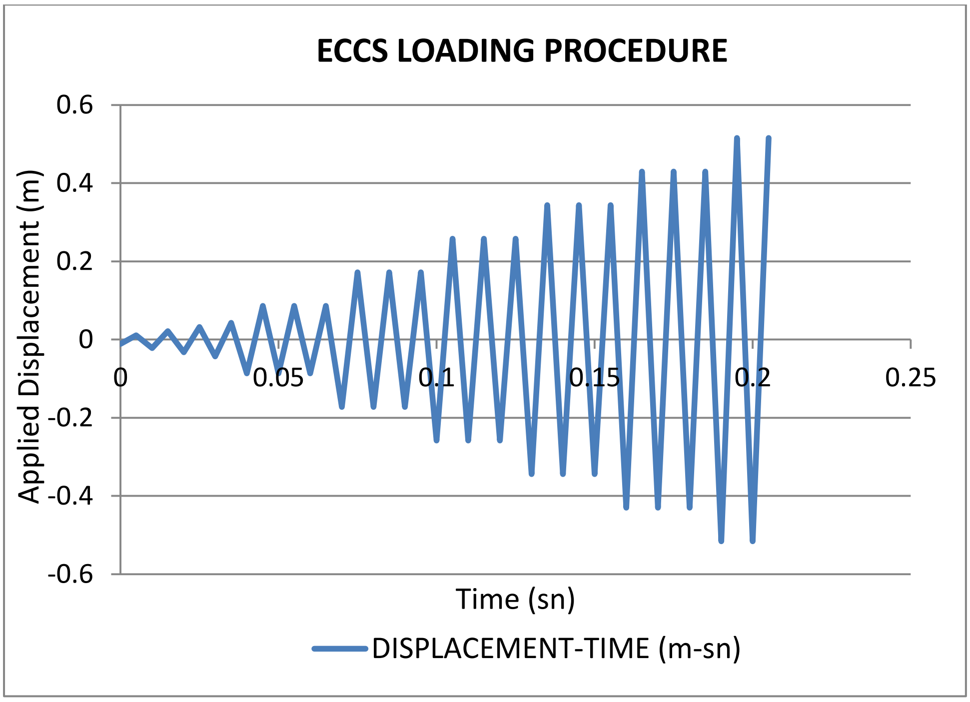

Figure 4.20 : ECCS loading procedure.

4.3.2 Analyses of the building

Analyses for 3D structure are performed in order to evaluate performance level of 3D structure. Both non-linear static analysis and nonlinear dynamic analysis are performed and displacement demans according to these analysis are compared. Three type of analysis are performed, which are nonlinear static (pushover), modal and nonlinear dynamic analyses.

Information about pushover analysis is given in Section 4.3.1. Load pattern and assumptions, which are given in that section, are applied for 3D building model too. This analysis is performed for 3D building model in order to obtain nonlinear behavior the structure and to evaluate seismic performance of the building according to Eurocode 8.

Modal analysis is performed in order to evaluate vibration characteristics of the structure, which is needed for assessment of seismic performance of the structure according to Eurocode 8. Mode shapes and natural frequencies are obtained.

Time-history analysis of 3D building is performed in order to evaluate dynamic response of the structure under seismic loading. Displacement demand of the structure is obtained as a result of time-history analysis. Three artificial accelerograms, which are matching with the response spectrum, are imposed as loading of dynamic analysis. Maximum peak ground acceleration (pga) is 2.82823 m/s^2 as stated in the accelerograms. Accelograms are shown in Appendix B. Scale factor is assumed 1.0; otherwise, the accelerograms would not match with the response spectrum.

Dynamic analysis parameters are assumed as follows; time step d_{time} as $0.01\ s$ and duration T_{max} as $25\ s$. Additionally ground motion is applied in shear wall direction. In this study main purpose of the nonlinear dynamic analysis is comparison of demand displacement and target displacement of the structure. Results of dynamic analysis and comparison of displacements are given in further sections.

4.4 Analyses Results

Analyses results generally fulfill expectations. It is proved that shear wall model works in good manner, pushover curve and strength level is as expected and time-history analaysis provides the maximum top displacements of the structure. In this context, detailed explanations about analysis results are presented.

4.4.1 Moment-curvature analysis results of shear wall

Moment capacity of ground floor section of the shear wall is calculated. This section contents calculations of moment capacity of shear wall section for the ground floor. Result of calculations gives an idea about moment capacity of shear wall. Additionally a comparison between the results of Opensees analysis and moment capacity calculations is performed.

Moment-curvature analysis is perfomed for ground floor section of shear wall in Opensees. Results are shown in Figure 4.21. Moment capacity M_{MC} of the ground floor section is $41773\ kNm$ and corresponding curvature φ is $0.007\ 1/m$ with reference to these results.

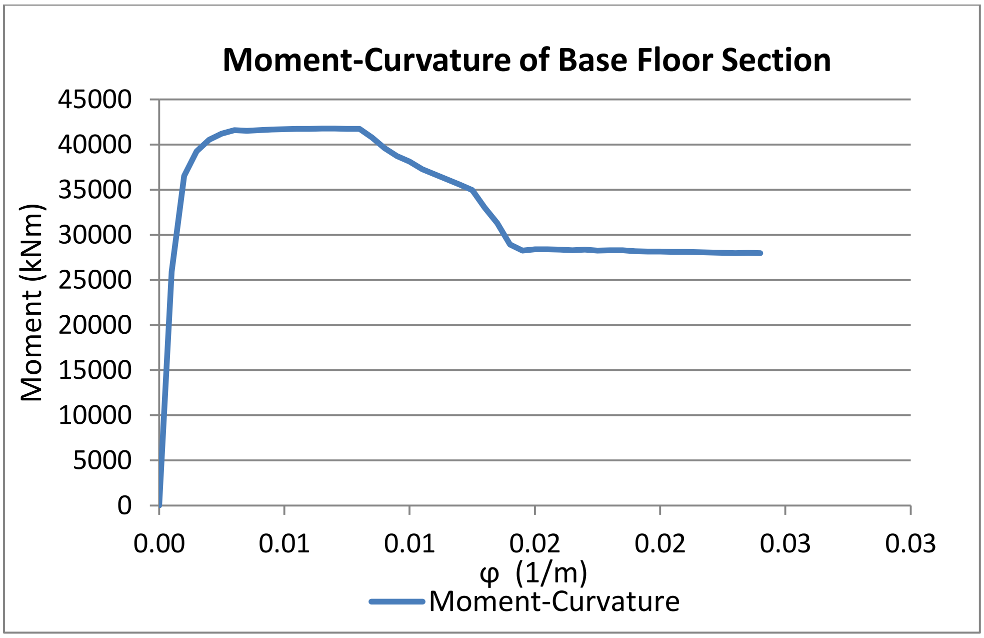

Figure 4.21 : Moment-curvature of shear wall section.

Moment capacity calculations of shear wall section are performed with a civil engineering software, Gelfi [37]. This software has been developed by Piero Gelfi [37] for civil engineering problems. Properties of shear wall section were given previously. Moment capacity calculations are performed only for the section of base level of the shear wall. Total gravity load of the shear wall N_0, which equals to $695\ kN$, is applied to the section as initial axial load. As a result, moment capacity of the shear wall M_{Gelfi} is obtained as $41264\ kNm$ (Figure 4.22).

$$M_{Gelfi} = 41264\ kNm \tag{4.24}$$

Finally, difference between Gelfi calculations and moment-curvature analysis results is $1.22\ \%$ (Equation **(4.28)**), that is an acceptable error. These results are also compared with pushover analysis results.

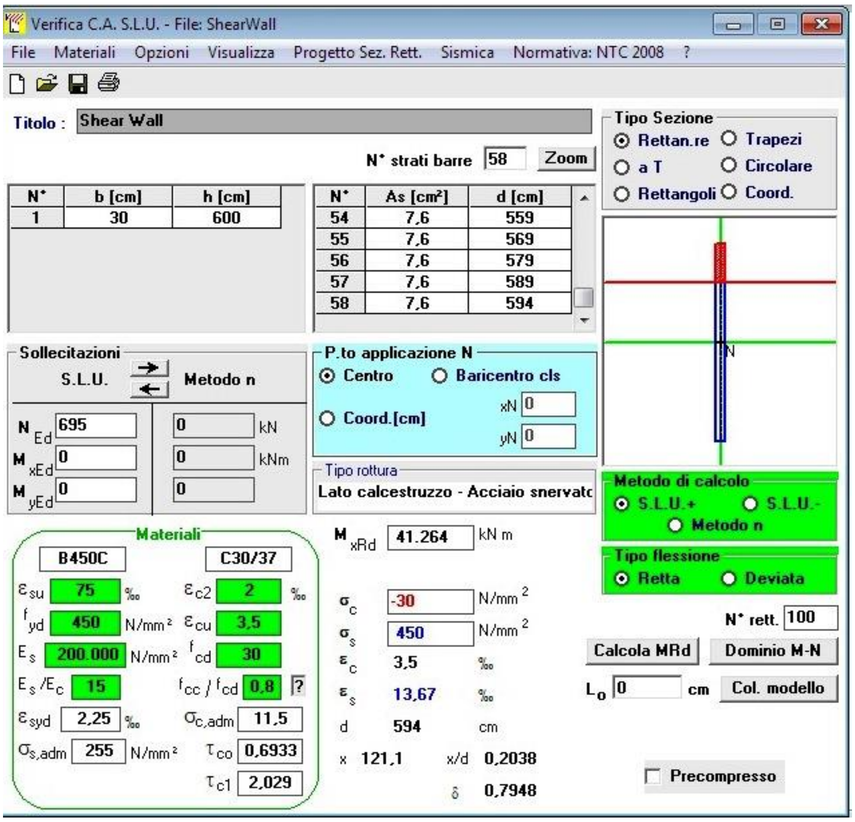

Figure 4.22 : Moment capacity calculations of shear wall section.

4.4.2 Pushover analysis results of shear wall

Pushover analysis enables to evaluate nonlinear behavior of the shear wall. Pushover (capacity) curve of the shear wall is given in Figure 4.23. According to this curve, behavior of the wall is linear until the first cracking. Then slope of the curve changes. In the third part of the curve, non-linear behavior is observed. The wall reaches maximum shear capacity in third part of the curve for this load pattern. Afterwards about $33\ \%$ of strength reduction is observed, which means failure of the shear wall. Calculations of strength loss are given below. Shear capacity and corresponding displacement of the shear wall under this load pattern are obtained respectively as $P_{max} = 4037.43\ kN$ and $d_{Pmax} = 12.9\ cm$. Crushing strength of the section $P_{crushing}$ is $2716.88\ kN$. Strength loss is calulated as follows due to this values.

$$\frac{P_{max} - P_{crushing}}{P_{max}} \cdot 100 = \frac{4037.43 - 2716.88}{4037.43} \cdot 100 = 32.7\ \% \qquad \textbf{(4.25)}$$

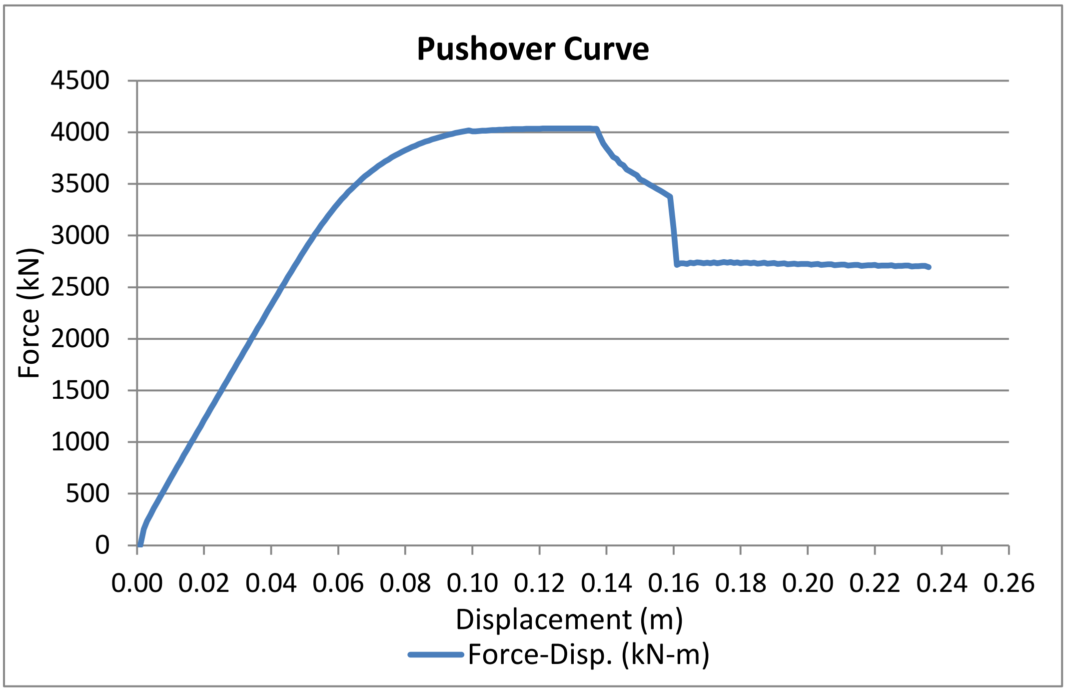

Figure 4.23 : Pushover (capacity) curve.

Shear reaction changes according to loads and load pattern, even so capacity curve shows maximum shear reaction of the structure. Besides that base moment reaction always gives the moment capacity of the structure. Base moment reaction of the shear wall section for pushover analysis is investigated. Nonlinear behavior is observed in moment diagram too (Figure 4.24). As a result, moment capacity of shear wall section M_{max} is $42436.1\ kNm$ according to pushover analysis. Comparison of moment capacity results of moment-curvature analysis, pushover analysis and Gelfi calculations are given below.

$$\frac{M_{max} - M_{MC}}{M_{max}} \cdot 100 = \frac{42436.1 - 41773}{42436.1} \cdot 100 = 0.15\ \% \qquad \textbf{(4.26)}$$

Difference between moment capacity obtained with moment curvature analysis of ground floor section and moment capacity, which is result of pushover analysis is calculated as 0.15 % in terms of Equation **(4.26)**.

$$\frac{M_{max} - M_{Gelfi}}{M_{max}} \cdot 100 = \frac{42436.1 - 41264}{42436.1} \cdot 100 = 2.76\ \% \qquad \textbf{(4.27)}$$

Equation **(4.27)** shows calculation difference of moment capacity according to Gelfi software and moment capacity, which is result of pushover analysis and it comes up to 2.76 % .

$$\frac{M_{MC} - M_{Gelfi}}{M_{MC}} \cdot 100 = \frac{41773 - 41264}{41773} \cdot 100 = 1.22\ \% \qquad \textbf{(4.28)}$$

Moment capacity obtained with moment curvature analysis and moment capacity according to Gelfi software for ground floor section are not same and variance is calculated as 1.22 % as shown in Equation **(4.28)**.

Gelfi calculations and moment curvature analysis are cross sectional analysis. On the other hand pushover is a structural analysis. Therefore 2-3 % difference is expected between these analysis results and results supports this expectation.

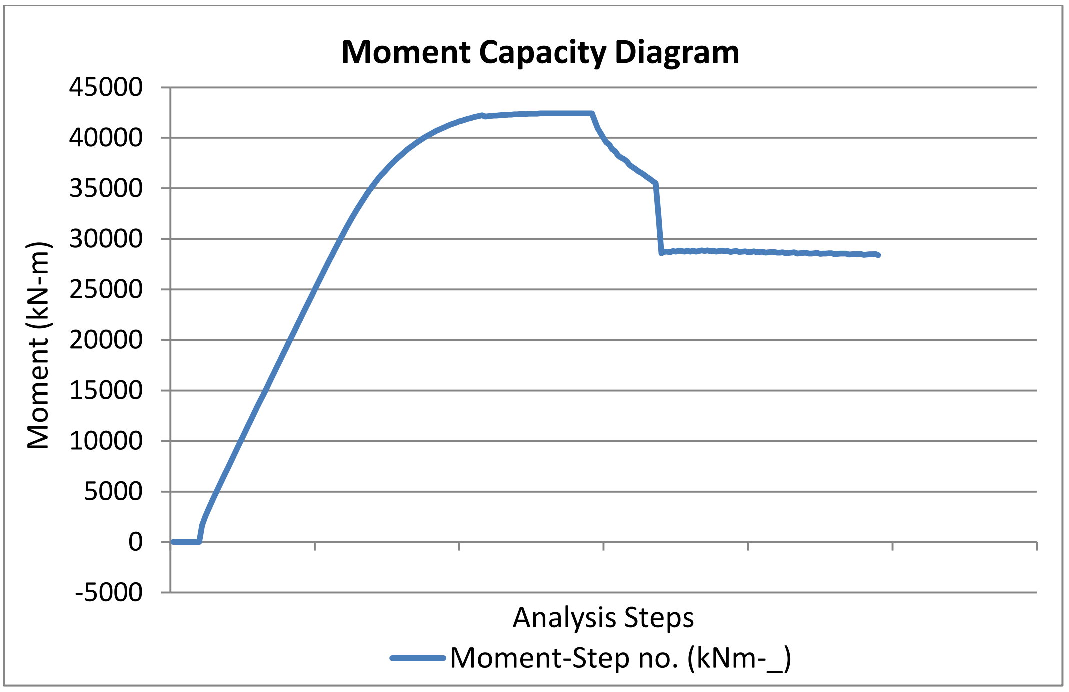

Figure 4.24 : Moment capacity diagram according to pushover analysis.

4.4.3 Cyclic nonlinear analysis results of shear wall

Hysteretic behavior of shear wall is evaluated as a result of cyclic analysis. Force-displacement curve is shown in Figure 4.25. A regular behavior is obtained as expected. However, increment of strength is observed on force-displacement curve. First increment occurs, after the first yielding cycle, which is at the yielding displacement (e_y) interval (Figure 4.25). Assessment of stress-strain relations of fibers under ECCS loading is performed in order to explain these increments of force.

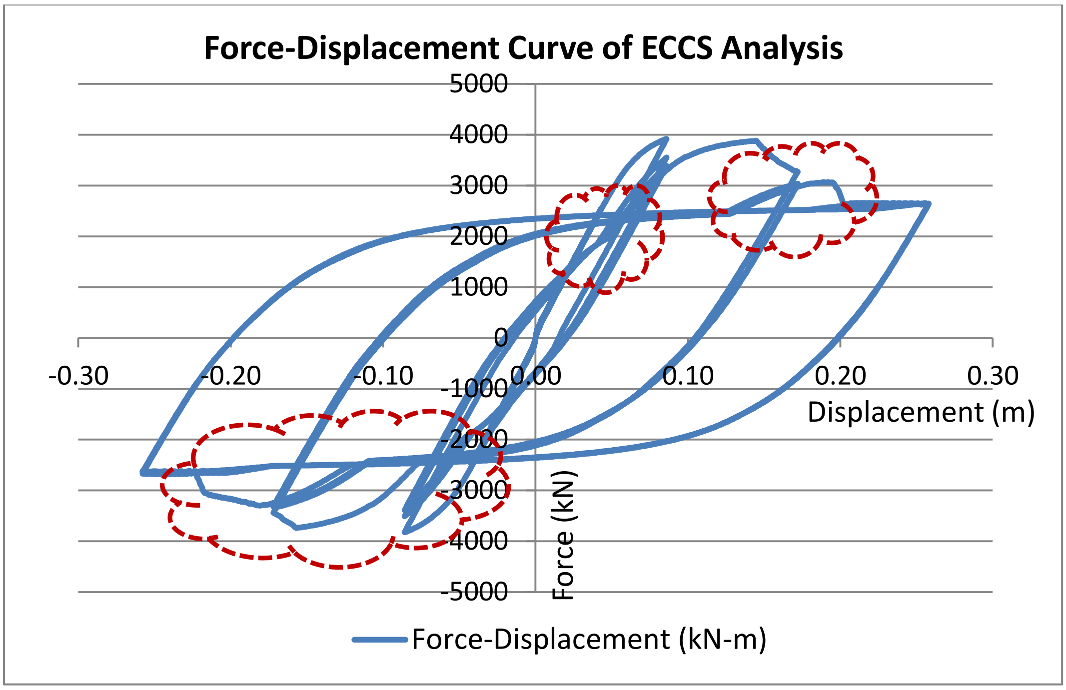

Figure 4.25 : Force-displacement curve of shear wall under ECCS loading.

Stress-strain relationships of concrete fibers are examined for ground floor section of shear wall wherein maximum moment occurs. Moreover, confined concrete fibers are located only in ground floor. Figure 4.26 is a representation of ground floor section and names of concrete fibers which are examined.

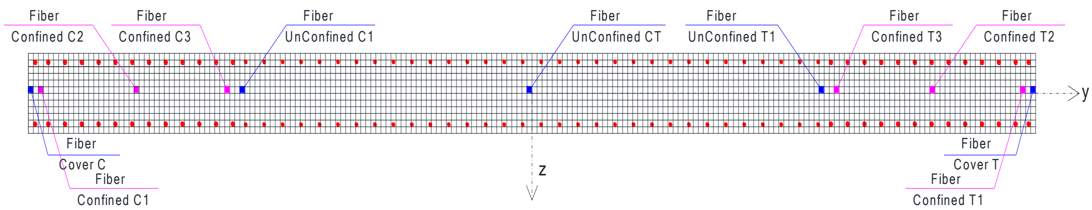

Figure 4.26 : Representation of fiber names.

Stress-strain diagrams of fibers are shown in Figures 4.27 and 4.28. Material model of concrete is uniaxial material concrete04, with zero tension strength. Accordingly, stress of concrete fibers is zero under tension effect. Minus sign represents compression. Stresses of confined and unconfined concrete fibers reach respectively 38000 kN/m^2 and 30000 kN/m^2, which are the maximum strength of these fibers.

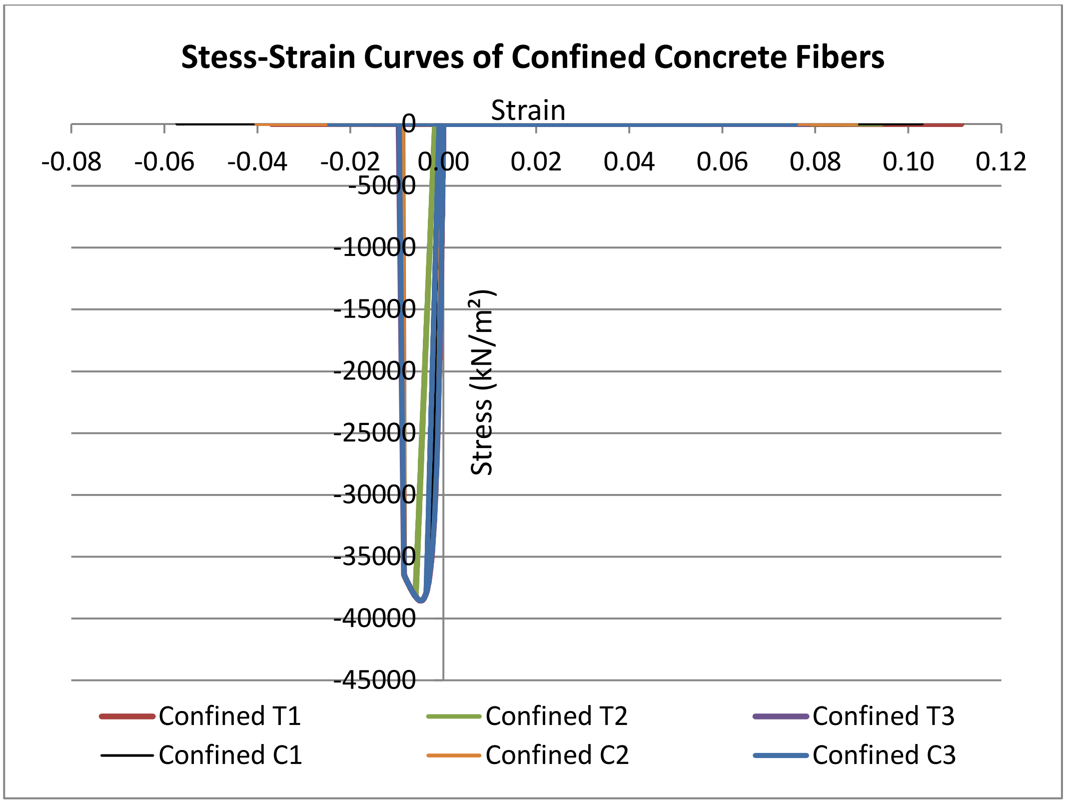

Figure 4.27 : Stress-strain relationship of confined concrete fibers.

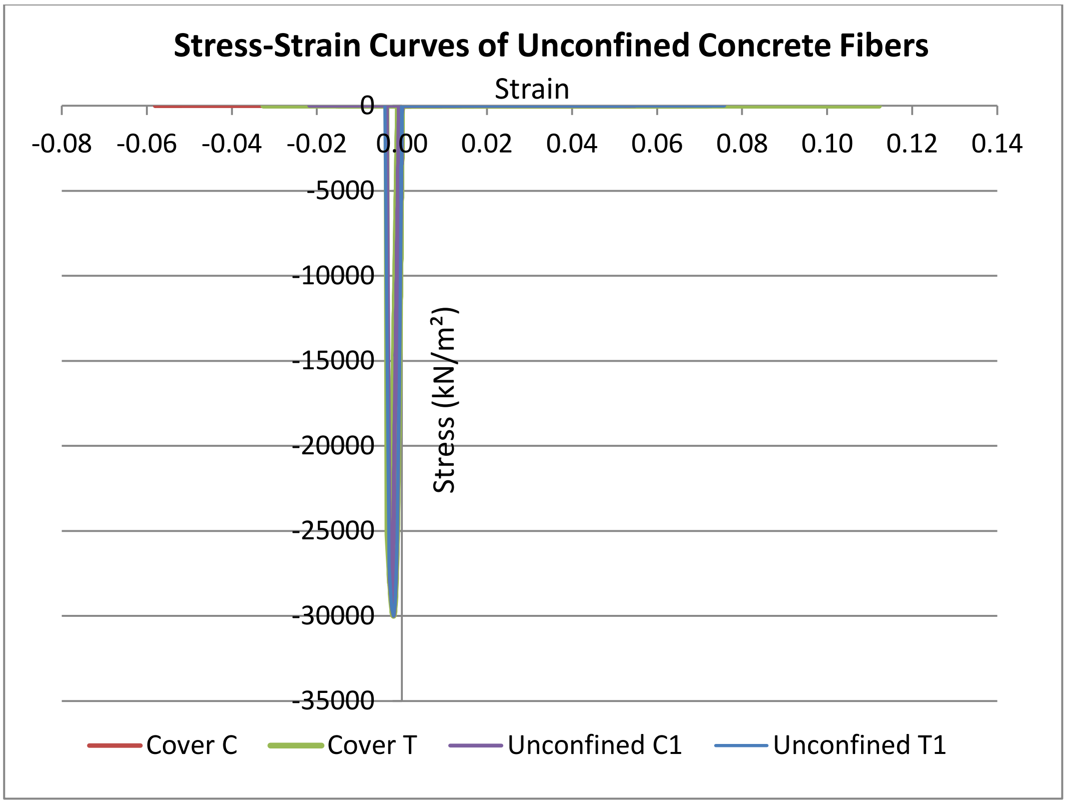

Figure 4.28 : Stress-strain relationship of unconfined concrete fibers.

In order to evaluate failure of concrete fibers stress vs. analysis step curve is plotted (Figures 4.29 and 4.30). Accordingly, fibers, which are nearest to the edge of the section reach the maximum strength initially, and failure occurs in those fibers before others. Failure is observed in that stress of the fiber remains zero despite loading. On the left side of the section, fiber Confined C1 reaches maximum strength and fails primarily. Failure of Confined C1 is seen at 1966th step of the analysis. After that Confined C2 reaches maximum strength and fails at 1983th step of the analysis. Subsequently failure of Confined C3 occurs at 4086th step of the analysis. Although Unconfined C1 is located farther than Confined C3 from edge of section, failure of Unconfined C1 occurs a few steps (4081st step) before failure of Confined C3, because compressive strength of confined concrete is more than compressive strength of unconfined concrete. Similar behavior exists on the right side of the shear wall section (Figure 4.30). As a result, failure process of fibers shows that effective length of the section, which means the total length of fibers that has load-bearing capacity, decreases step by step. This means length of level arm is decreasing. This decrease of level arm causes increase of shear force, since the moment capacity of the section is constant.

Finally, in the first steps of loading, stress is maximum on the edge fibers of the shear wall section, where y is 300 cm or -300 cm. In this case level arm of moment can be assumed as whole width of the wall section which is 600 cm and maximum. Along with the increase of loading, failure occurs on the edge fibers. For each failure that fiber becomes useless and the fiber next to it has the maximum stress. This means level arm is shortening at each failure. Consequently shear reaction increases due to level arm, since moment capacity of the wall section is stationary. This is the reason of strength increment that is shown in Figure 4.25.

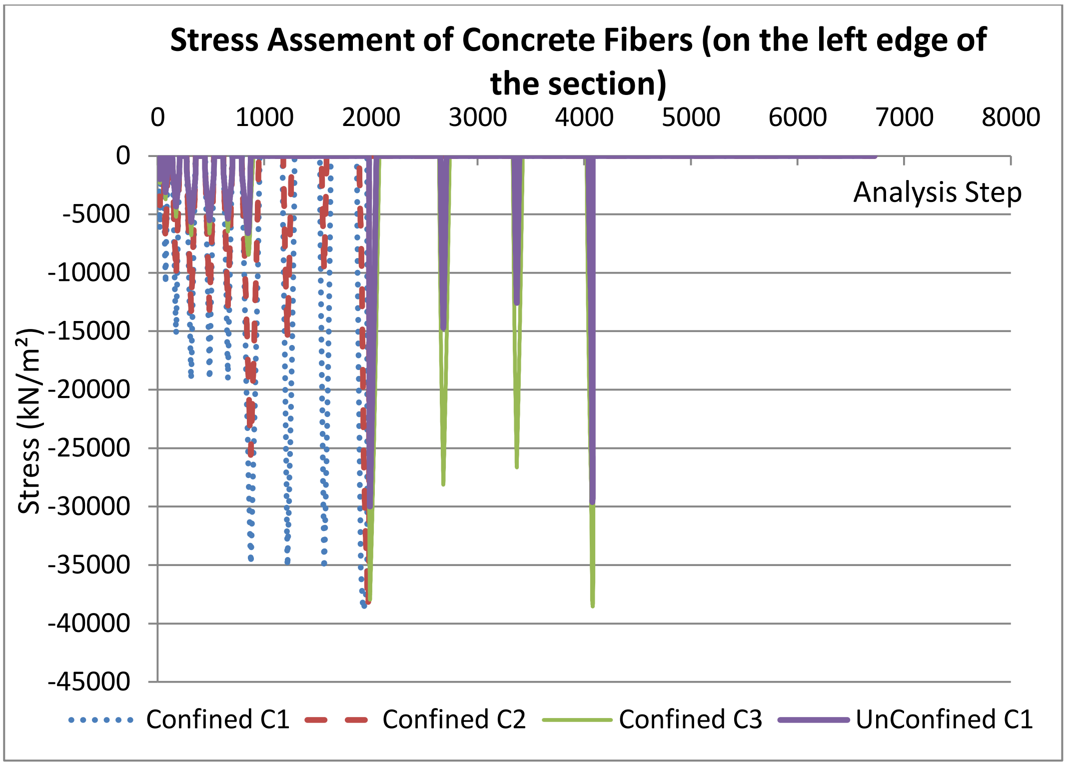

Figure 4.29 : Stress-strain assesment of confined concrete fibers on the left edge of the section.

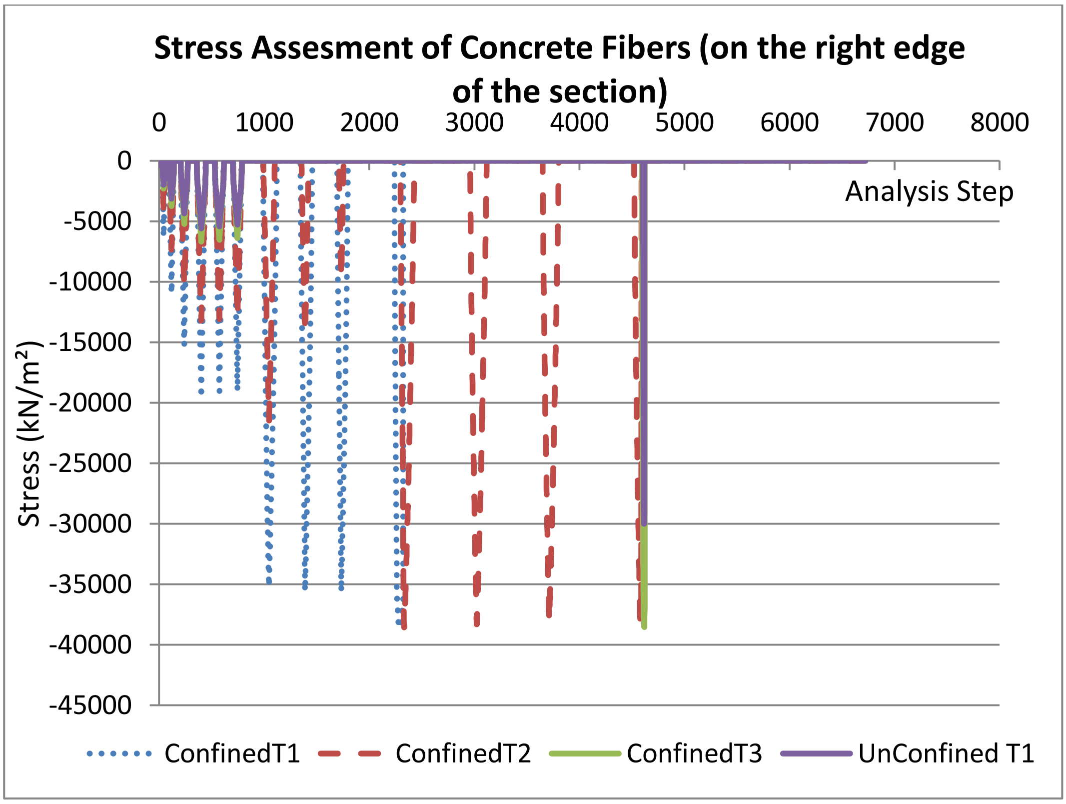

Figure 4.30 : Stress-strain assesment of confined concrete fibers on the right edge of the section.

4.4.4 Pushover analysis results of the building

Pushover analysis of the building is performed and pushover curve is shown in Figure 4.31. Additionally, moment resistant frames and shear walls are examined separately. Figure 4.32 shows comparison of shear capacity between frames and shear walls. According to the results shear capacity (F_{max}) and corresponding displacement (d_{Fmax}) of the structure are respectively $16258.64\ kN$ and $13.7\ cm$.

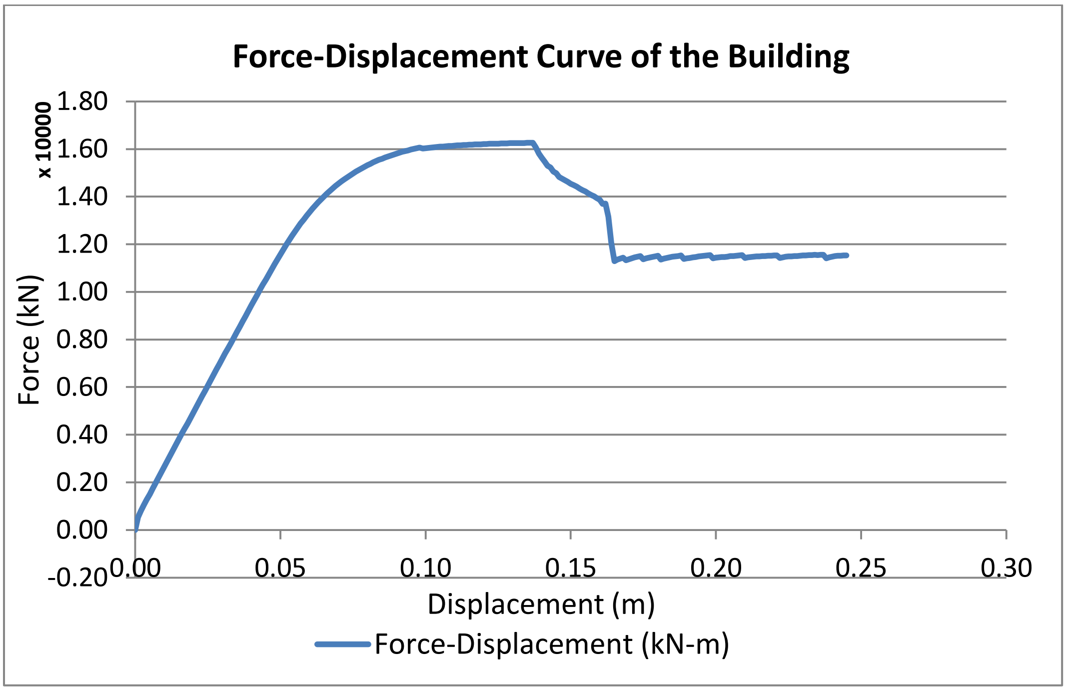

Figure 4.31 : Pushover curve of 3D structure model.

Strength loss of the structure should be evaluated in order to decide whether the failure of the entire structure is occurred or the structure still has bearing capacity. Ultimate strength of the structure $F_{ultimate}$ is computed as $11293.36\ kN$ (Figure 4.31). Subsequently strength reduction of the structure can be obtained as follow:

$$\frac{(F_{max-}F_{ultimate})}{F_{max}} \cdot 100 = 30.543\ \% \qquad \textbf{(4.29)}$$

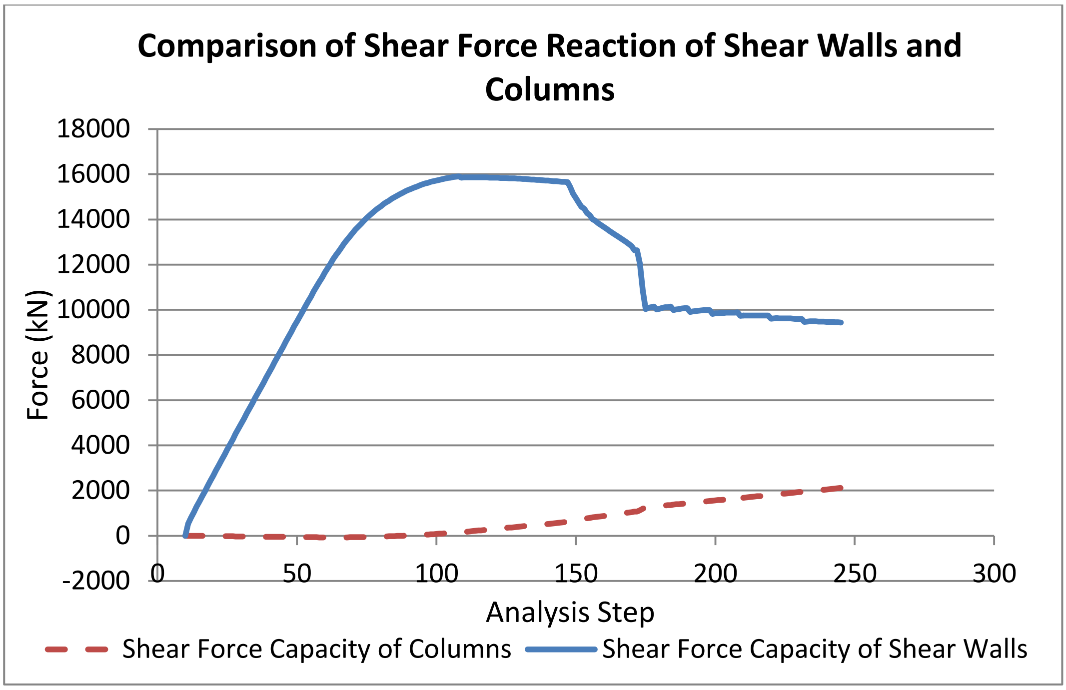

Figure 4.32 : Pushover curves of shear walls and columns.

Figures 4.33 and 4.34 are about the moment capacities. Moment capacity of the structure can be seen in Figure 4.33. Figure 4.34 represents comparison of moment capacities of the shear walls and the frames. Behavior is similar to the pushover curve and meets with the expectations. Moment capacity of the structure is $170456.82\ kNm$. It is considered that failure of the structure occurs when the shear walls collapse.

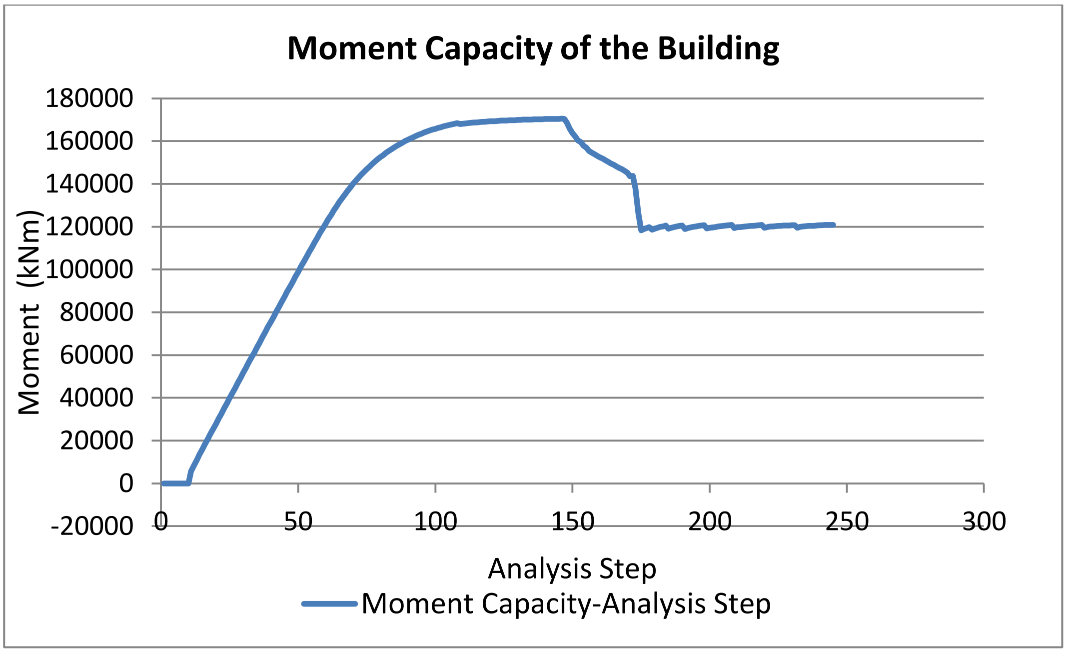

Figure 4.33 : Moment reaction of 3D structure model.

After the failure of shear walls, shear force reaction of the frames increases. However, with the failure of the shear walls, about 30 % of strength loss occurs for whole structure. As a result, failure of shear walls means failure of the structure.

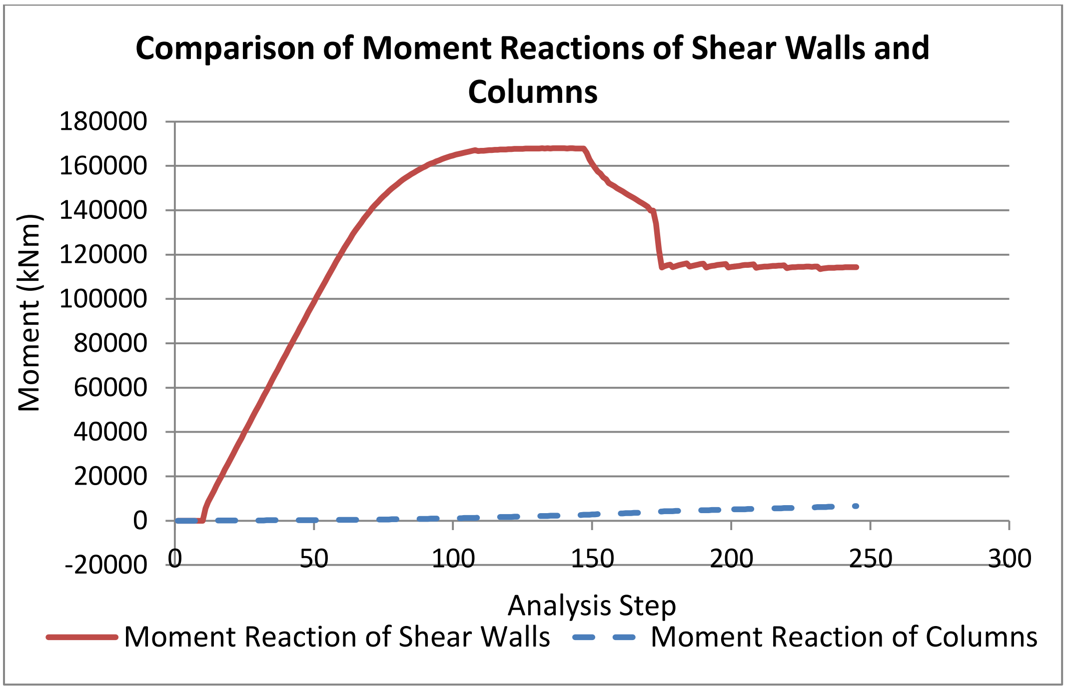

Figure 4.34 : Moment reactions of shear walls and columns.

4.4.5 Modal analysis results of the building

Eigenvalue analysis is performed in five modes. These five mode shapes are obtained as shown in Table 4.1. 4th mode shape, which is the predominant mode shape in shear wall direction, is shown in Appendix C.

Table 4.1 : Moadal analysis results of 3D structure.

Node	1st Mode		2nd Mode		3rd Mode		4th Mode		5th Mode	
	X (10^{-13})	Y (10^{-2})	X (10^{-12})	Y (10^{-2})	X (10^{-12})	Y (10^{-2})	X (10^{-2})	Y (10^{-12})	X (10^{-13})	Y (10^{-2})
7	7.55	-1.80	-5.43	-2.42	-3.52	2.15	2.24	1.67	6.24	2.10
6	4.79	-1.58	-3.83	-1.77	-2.52	0.61	1.62	2.24	5.41	-0.71
5	2.52	-1.24	-2.35	-1.14	-1.60	-0.96	1.02	3.80	4.25	-1.09
4	0.98	-0.77	-1.12	-0.57	-0.81	-1.15	0.51	5.25	2.74	0.95
3	0.18	-0.29	-0.29	-0.16	-0.24	-0.86	0.14	1.91	1.07	1.36
1	0.00	0.00	0.00	0.00	0.00	0.00	0.00	0.00	0.00	0.00

In this study, analyses are performed parallel to shear wall direction, in order to analyze effects of shear walls. First three mode shapes and fifth mode shape are effective in Y direction, which is direction of moment resisting frames. However fourth mode shape gives the mode shape of X direction, which is parallel direction to the shear walls. Fourth mode shape can be used for performance evaluation of the structure at X direction. Periods of the structure are given in Table 4.2.

Table 4.2 : Periods of the building.

Period No	Period T (sec)
1	2.453
2	1.042
3	0.682
4	0.444
5	0.339

4.4.6 Time-history analysis results of the building

Lateral displacements of each floor are obtained with nonlinear time history analysis method for each of three acclerograms. Roof displacement records are represented in Appendix C, Figures C4, C5 and C6. Maximum displacements of each floor are shown in Table 4.3.

Table 4.3 : Maximum displacements.

Floor No	Acc_a	Acc_b	Acc_c
	Maximum displacements (mm)		
Base	0	0	0
1	2.3418	1.9601	1.9801
2	8.2616	7.0243	7.0506
3	16.574	14.265	14.336
4	26.297	22.845	23.045
5	36.459	31.903	32.303

Maximum absolute roof displacements of the structure due to accelerograms a, b and c are respectively 3.65 cm 3.19 cm and 3.23 cm. Average of the maximum roof displacements are calculated in order to compare with the target displacement that is explained in next section (Table 4.4).

Table 4.4 : Max. displacements for top of the building according to time-history analysis.

Roof displacement of the structure acc. to time-history.		
Accelogram	Max. absolute displacement (cm)	Average displacement (cm)
a	3.65	
b	3.19	3.36
c	3.23	

4.5 Target displacement of the building according to Eurocode 8

Seismic performance assessment can be performed with both linear and nonlinear analyses. In this study nonlinear assessment is carried out based on either nonlinear static (pushover) or nonlinear dynamic analyses (time history). Even though nonlinear dynamic analysis is a powerful method for seismic performance assessment of structures, pushover analysis is mostly preferred method. Nonlinear dynamic analysis is a more complex method since it requires a set of suitable ground motion entries that needs a comprehensive study, and the calculations are time consuming. As a result, pushover analysis is a simple option for practical design applications.

Eurocode 8 [10] provides an approach for seismic performance assessment with nonlinear static analysis method. Target displacement is calculated in agreement with this method. Accordingly the target displacement is defined as the seismic demand derived from the elastic response spectrum. Pushover curve of the structure is obtained and represented previously. Force-displacement curve of the building is transformed to an equivalent single degree of freedom (SDOF) system. Subsequently, period of the idealized equivalent SDOF system is determined and finally target displacement is calculated.

Mass of the structure is calculated according to mass of the structural members and it is assumed that mass is concentrated at the center of the each floor, (Table 4.5). Normalized forces and displacements, accordingly normalized modes are required with respect to Eurocode 8, Annex B [10]. Modes are normalized with assumption of $\Phi_n = 1$, where n is the control node of the displacement

Table 4.5 : Mass distribution to the floors for 3D structure model.

Mass of 3D structure	
Floor No.	M_i(ton)
5	623.7908
4	1591.067
3	1591.067
2	1406.244
1	1406.244
Base	0

In this study control node is the node at the center of the roof. Normalization is shown in Table 4.6. Additionally relation between normalized force and displacement is given in Equation **(3.3)**. These calculations are performed in terms of explanations that are given in Section 3.1.

Table 4.6 : Normalization of predominant (4^{th}) mode shape.

Column A	Column B	Column C
Floor No.	Φ_4(4th mode in X direction)	Normalization of modes
5	0.0224	1
4	0.0162	0.7234
3	0.0103	0.4581
2	0.0051	0.2276
1	0.0014	0.0632
Base	0	0

A transformation factor is calculated in order to transform results of the structural system, which is multi degree of freedom system (MDOF), to an equivalent single degree of freedom (SDOF) system. The transformation factor is calculated with respect to Equations **(3.4)** and **(3.5)**. Calculation of transformation factor, which is given below, related to concentrated masses and normalized mode shape. They are shown respectively in Tables 4.5 and 4.6.

$$\Gamma = \frac{m^*}{\sum m_i \Phi_i^2} = \frac{2912.668\ ton}{1868.728\ ton} = 1.5586 \qquad \textbf{(4.30)}$$

Maximum force and corresponding displacement of equivalent SDOF system is evaluated with Γ according to Equations **(3.6)** and **(3.7)**. Calculations are as follow:

$$F^* = \frac{F_b}{\Gamma} \qquad F_y^* = 10432.733\ kN \qquad \textbf{(4.31)}$$

$$d^* = \frac{d_n}{\Gamma} \qquad d_m^* = 0.0873\ m \qquad \textbf{(4.32)}$$

Evaluation of maximum force and corresponding displacement of equivalent SDOF system yield to obtain force-displacement curve of equivalent SDOF system. It can be seen in Figure 4.35.

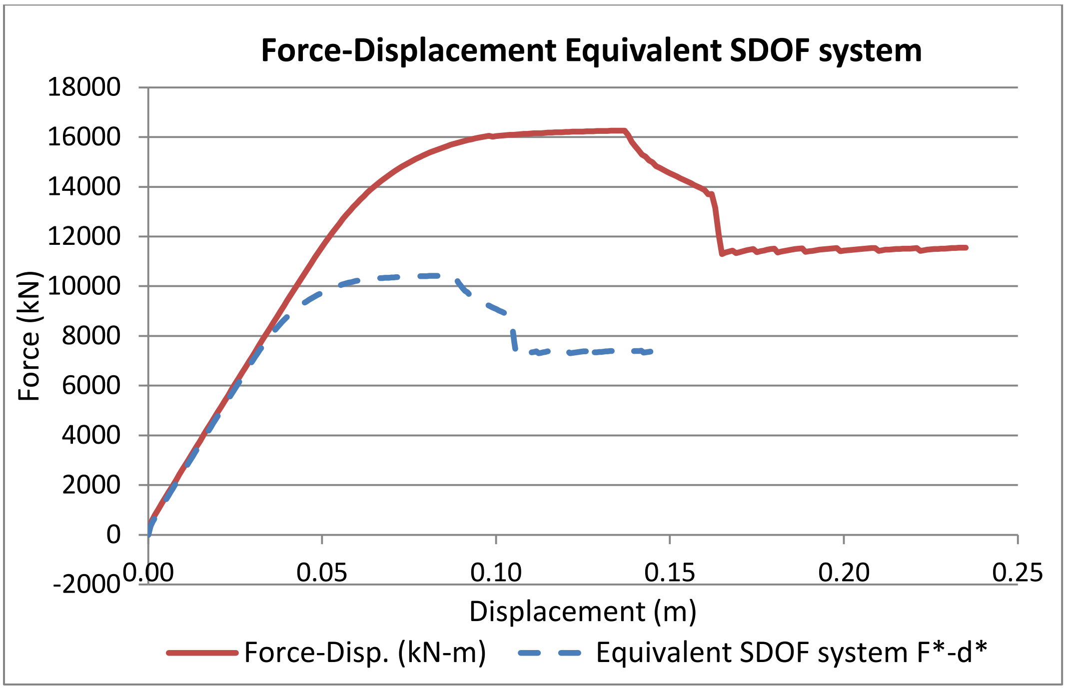

Figure 4.35 : Force displacement curve of equivalent SDOF system.

An idealized elasto-perfectly plastic force-displacement curve is determined with respect to previously explained equivalent energy procedure. Yielding force of equivalent SDOF system F_y^* is also the ultimate strength of idealized system. Idealization is performed by equalizing the areas under the actual and idealized force-displacement curves (Figure 3.4). Equation **(3.8)** contains formula to obtain d_y^*. Consequently, the yield displacement of idealized SDOF system d_y^* can be calculated as follows,

$$d_y^* = 2\left(d_m^* - \frac{E_m^*}{F_y^*}\right) = 0.0471\ m \qquad \textbf{(4.33)}$$

Herein E_m^* is computed as $664.44\ kN\ m$. Idealized curve and area of E_m^* is shown in Figure 4.36. The period of idealized equivalent SDOF system T^*, where d_y^* is $0.0471\ m$, is determined due to Equation **(3.9)** as $0.721\ s$.

Calculation of the target displacement of the structure (d_{et}^*) with unlimited elastic behavior and period T^*, was shown in Equation **(3.10)**. However, it is possible to obtain d_{et}^* with an illustration of acceleration response spectrum to displacement reponse spectrum relationship and its interaction with the idealized equivalent SDOF system. Elastic response spectra and acceleration-displacement response spectrum of this structure can be seen Appendix B.

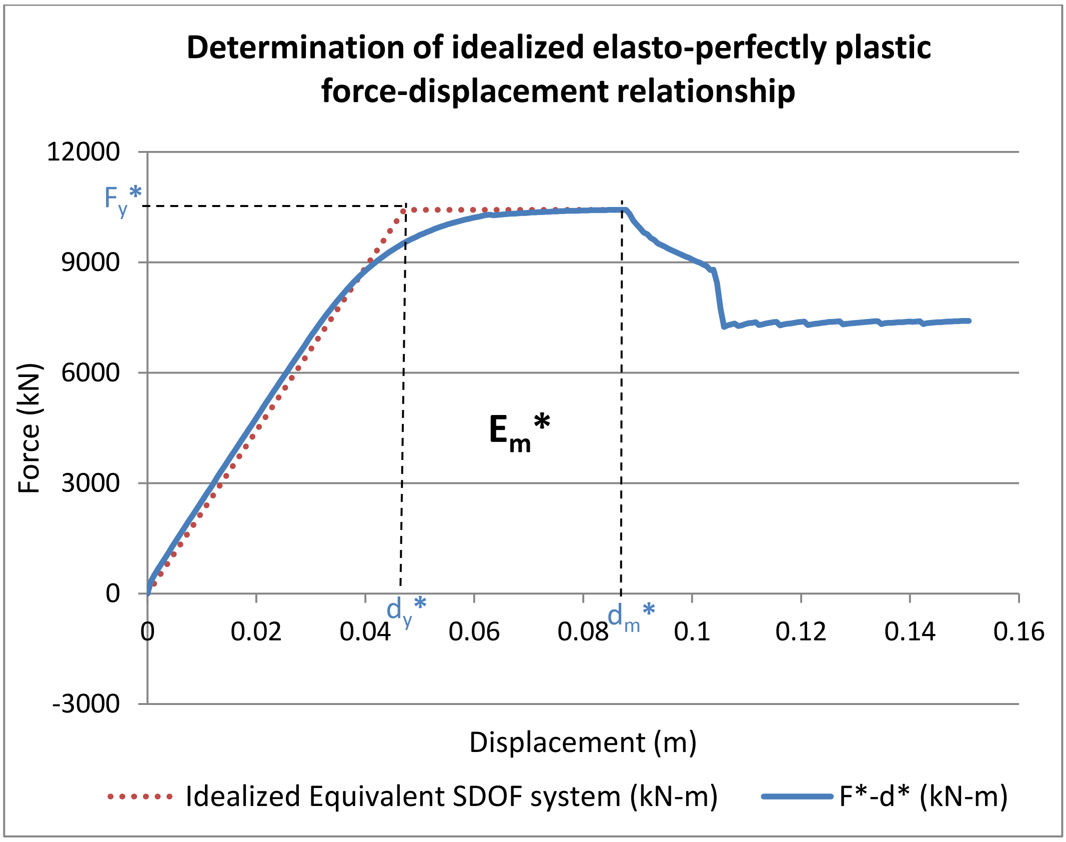

Figure 4.36 : Determination of idealized elasto-perfectly force-displacement relationship.

The target displacement of the SDOF system d_t^* is evaluated depending on period and period range of the structure. Accordingly different expressions should be used for structures in short range and for structures in medium-long period ranges. This expressions are given previously in Section 3.1. T_C is the corner period that determines the boundary between short period range and medium or long period ranges of the structure. As stated in elastic response spectra (Appendix B) T_C is 0.588 seconds. In this case T^* is greater than T_C, which means idealized equivalent SDOF system is in medium-long period range.

The structure satisfies the condition $T^* > T_C$. Therefore it is assumed that target displacement of idealized equivalent SDOF system d_t^* is equal to the target displacement of the structure with unlimited elastic behavior and period T^* (d_{et}^*) according to Equation **(3.16)**. Determination of d_t^* is performed as represented in Figure 4.37. Target displacement of the equivalent SDOF system d_t^*, which is equal to d_{et}^* is obtained as $8.69\,cm$. The target displacement of MDOF system is evaluated by multiplying d_t^* to transformation factor Γ (Equation **(3.17)**).

$$d_t = d_t^*\Gamma = 13.534\,cm \qquad \textbf{(4.34)}$$

As a result, target displacement of the structure d_t is evaluated as $13.534\,cm$ according to Eurocode 8 Annex B, [10].

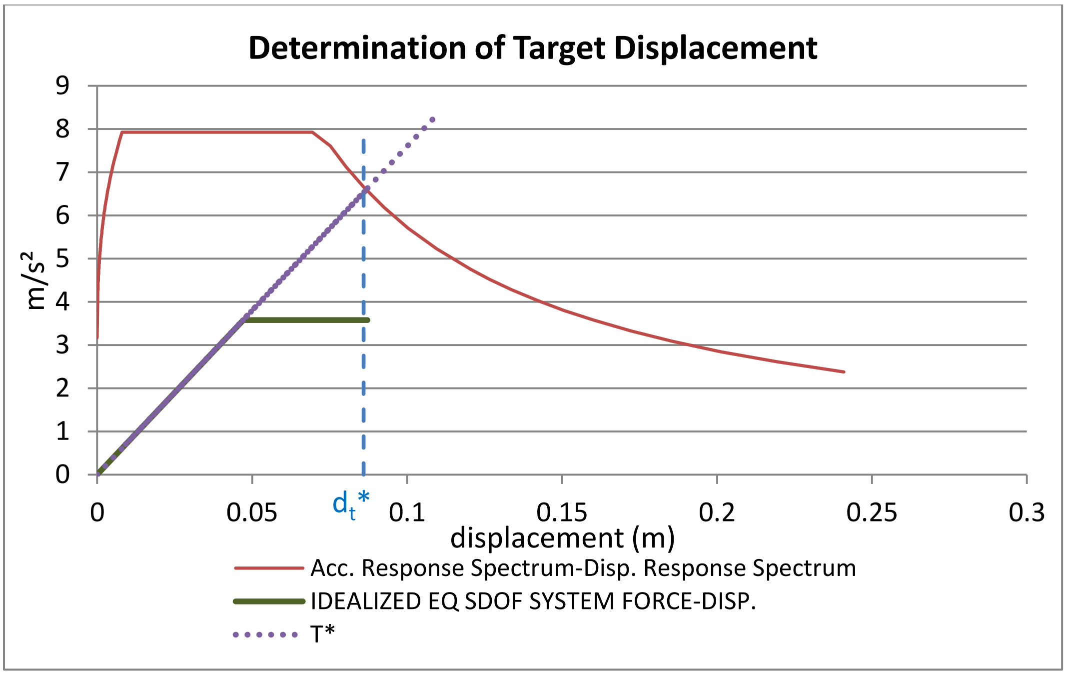

Figure 4.37 : Determination of target displacement.

Finally, the displacements are obtained according to time history analysis with spectra compatible artificial accelerograms (Table 4.4) and target displacement of the structure is also obtained according to Eurocode 8. As a result, average displacement of three artificial accelerograms is 3.36 cm and target displacement is 13.534 cm. Consequently, average displacement of time history analysis is considerably smaller than the target displacement. It is posibble to deduce that the structure is extremely rigid in the shear wall direction (Table 4.7).

Table 4.7 : Comparison of displacements

Roof disp. of 3D structure for time-history analysis			Comparison of d_t and d_d
Accelogram	Max. absolute displacement (cm)	Average displacement, d_d (cm)	
a	3.65		$d_d < d_t$
b	3.19	3.36	$3.36 < 13.534$
c	3.23		(cm)

5. CONCLUSIONS AND RECOMMENDATIONS

This study is conducted in order to obtain target displacement of the structure. Target displacement is the displacement that structure should not exceed under given seismic hazard level. The studied structure is a 3D model of a steel-concrete composite building with reinforced concrete shear walls. Furthermore, this study consists the assessment of the seismic performance evaluation with respect to nonlinear static (pushover) analysis procedure that is included in Eurocode 8. This procedure is offered as a simpler method and alternative to nonlinear dynamic (time-history) analysis. Performance level of the structure is obtained with comparison of the target displacement and demand displacement according to time history analysis. All these analysis are perfomed in the strong directions of the shear walls, so that, conclusions are about this direction of the structure. Displacements are obtained according to time history analysis with spectra compatible artificial accelerograms. Target displacement of the structure is also obtained according to Eurocode 8.

In the scope of this research, previously examined and proposed methods are utilized for a simple modeling of RC shear walls that provides reliable results. The shear wall is modeled and analyzed using Opensees. In this context, conclusions are given below.

- Opensees software is used in order to model and perform analysis and it can be concluded that it is a powerful tool for sophisticated analyses like time-history analysis. It is practical, since it allows modeling in different levels of the structure such as, element level, section level or fiber level.
- In case of modeling slender reinforced-concrete shear walls, nonlinear beam-column element that provides distributed plasticity gives perfect response. Since the analysis results satisfy the expectations, it can be inferenced that beam-columm element modeling is practicle and gives accurate results.
- There are two types of modeling for beam-column element; forced based and displacement based. Forced based beam column modeling gives accurate

results with one element and five sections. Accordingly, it is highly suitable for modeling slender RC shear walls, since the displacement based element needs a great number of element and sections for accuracy.

- Static cyclic analysis is also performed for the shear wall with the purpose of testing the behavior of the shear wall model. ECCS procedure is applied since the loading is regular according to it, so that a regular response is expected. However, strength increments are observed in some parts of the force-dislpacement curve. After an assessment, it is revealed that, failure of the fibers at the edge of the section decreases level arm. Since the moment capacity of the section is constant, decrase of the level arm causes increments of strength.
- One of the main purposes of this study was to compare the pushover and time-history procedures in terms of performance assessment. The displacements are obtained according to time history analysis with spectra compatible artificial accelerograms. Target displacement of the structure is also obtained according to Eurocode 8 with pushover analysis. Altough time-history analysis method gives accurate results; pushover analysis method provides a simpler application. According to results of this study, demand displacement is obtained as 3.36 cm under the applied seismic hazard level and target displacement of the structure is 13.534 cm. As a result, pushover procedure provides to be in the safe side for the shear wall direction of this building.

Finally, a few recommendations can be given for future studies. Seismic performance assesment of the building can be perfomed in the directions of composite moment frames. It is possible both with nonlinear-static and nonlinear dynamic methods. Additionally, the performance level of the structure can be evaluated in the element level too, with an investigation of rotations and rotation capacities of the structural components of the structure.

REFERENCES

[1] **Priestly, M. J. N.** (2000). Performance Based Seismic Design. *12th World Conference on Earthquake Engineering (2000)*, University of California, San Diego, USA.

[2] **Mwafy, A. M., and Elnashai, A. S.** (2001). Static Pushover versus Dynamic Collapse Analysis of RC Buildings. *Engineering Structures, **23** (2001),* 407–424. Department of Civil and Environmental Engineering, Imperial College, London SW7 2BU, UK.

[3] **Fajfar, P., and Gaspersic, P.** (1996). The N2 Method For Seismic damage analysis RC Buildings. *Earthquake Engineering and Structural Dynamics.,vol 25,* 31–46. Department of Civil Engineering, University of Ljubjana, Jamova 2, 61001 Ljubjana, Slovenia.

[4] **Saiidi, M., and Sözen, M. A.** (1981). Simple Nonlinear Seismic Analysis of R/C Structures. *Journal of the Structural Division, ASCE, 1981;* 107(ST5): 937-51.

[5] **ATC-40.** (1996). Seismic Evaluation and Retrofit of Concrete Buildings. *Applied Technology Council,* California, USA.

[6] **FEMA-273.** (1997). NEHRP Guidelines for Seismic Rehabilat, on of Buildings. *Federal Emergency Management Agency,* Washington, USA.

[7] **FEMA-356.** (2000). Prestandart and Commentary for the Seismic Rehabilitation of Buildings. *Federal Emergency Management Agency,* Washington, USA.

[8] **FEMA-440.** (2005). Improvement of Nonlinear Static Seismic Analysis Procedures. *Federal Emergency Management Agency,* Washington, USA.

[9] **ASCE 41-06.** (2007). Seismic Rehabilitation of Existing Buildings. *American Sociecty of Civil Engineers,* California, USA.

[10] **European Committee for Standardization.** (2004). Design of Structures for Earthquake Resistance- General Rules, Seismic Actions and Rules for Buildings. *Eurocode 8-1, EN-1998-1.* 23 April 2004, Brussels, Belgium..

[11] **McKenna F., Scott M. H., and Fenves, G. L.** (2008). Nonlinear Structural Analysis Using Software Design. *18th Analysis and Computation Specialty Conference, ASCE.*

[12] **Mazzoni, S., McKenna, F., Scott, M. H., Fenves, G. L., et. al.** (2007). Open System for Earthquake Engineering Simulation (OpenSees) Command Language Manual. 1 July 2007.

[13] **Sheikh S. A., and Üzümeri, S. M.** (1981). Analytical Model for Concrete Confinement in Tied Columns. *Journal of the Structural Division, ASCE, 1981.*

[14] **Mander, J. B., Priestley, M. J. N., and Park, R.** (1988). Theoretical Stress-Strain Confined Concrete. *Journal of the Structural Division, ASCE,* 114(8), 1804-1826.

[15] **Saatçioğlu, M., and Razvi S. R.** (1992). Strength and Ductility of Confined Concrete. *Journal of the Structural Division, ASCE, vol. 118 no.6*, pp. 1590-1607.

[16] **Bangash, M., Y. H.** (1989). Concrete and Concrete Structures: Numerical Modeling and Applications. *Elsevier Science Publishers Ltd.,* ISBN 1-85166-294-4 London, (p. 4).

[17] **European Committee for Standardization.** (2003). Design of Concrete Structures – Part 1-1: General Rules and Rules for Buildings. *Eurocode 2-1-1, EN-1992-1-1.* 23 December 2003, Brussels, Belgium..

[18] **Karsan, I. D., and Jirsa, J. O.** (1976). Behavior of concrete under compressive loading. *Journal of Structural Division, ASCE,* 95(ST12).

[19] **Popovics, S.,** (1973). A Numerical Approach to the Complete Stress-Strain Curve of Concrete. *Cement and Concrete Research, vol. 3,* pp. 583-599.

[20] **Lowes, L., Lehman, D., Turgeon, J., Birely, A., Pugh, J., Kuchma, D., Hart, C., Marley, K.** (n.d.). Seismic Behaviour, Analysis and Design of Complex Wall Systems. *NEES Small-Group Project.* NFS Grant CMMI-0421577.

[21] **Comité Euro-International du Béton** (1996). RC Elements Under Cyclic Loading: State of the Art Report. *Thomas Telford Services,* ISBN 0 7277 2086 4, London, UK (p. 60).

[22] **Popov, E. P., and Balan, T. A.** (1998). Engineering Mechanics of Solids. *Prentice-Hall Inc., 2nd Edition,* ISBN 0-13-726159-4, New Jersey, USA, (p. 66, 67).

[23] **Riley, E. F., and Zachary, L. W.** (1989). Intro. to Mechanics of Materials. *John Willey and Sons Inc,* Sigapore, (p. 52, 147).

[24] **Andriyana, A.** (2008). Failure Criteria for Yielding, *Centre de Mise en Forme des Mat´eriaux, CEMEF UMR CNRS 7635,* Paris, France.

[25] **Taucer, F. F., Spacone, E., and Filippou F. C.** (1991). A Fiber Beam-Column Element for Seismic Response Analysis of Reinforced Concrete Structures. *Eathquake Engineering Research Center College of Engineering, University of California,* Report No: UCB/EERC-91/17 Berkeley, USA.

[26] **Terzic, V.** (2011). Force-Based Element vs. Displacement-Based Element. December 2011.

[27] **European Committee for Standardization.** (2004). Design of Steel and Concrete Composite Structures –Part 1-1: General Rules and Rules for

Buildings. *Eurocode 4-1-1, EN-1994-1-1.* December 2004, Brussels, Belgium..

[28] **Foliente, G. C.** (1995). Hysteresis Modeling of Wood Joints and Structural Systems. *Journal of Structural Division, ASCE, vol. 121, no.6*, pp. 1013-1022.

[29] **Baber, T. T., and Noori M. N.** (1985). Random Vibration of Degrading Pinching Systems. *Journal of Engineering Mechanics, ASCE, vol. 111, no. 8,* pp. 1010-1026.

[30] **Haukaas, T., and Kiureghian, A. D.** (2004). Finite Element Reliability and Sensitivity Methods for Performance-Based Earthquake Engineering. Pacific *Eathquake Engineering Research Center (PEER), College of Engineering, University of California,* PEER Report 2003/14 Berkeley, USA.

[31] **Chopra, K. A.** (1995). Dynamics of Structures: Theory and Applications to Earthquake Engineering. *Prentice-Hall Inc.,* ISBN 0-13-855214-2, New Jersey, USA, (p. 565).

[32] **Gasparini, D.A., Vanmarcke, E.H.,** (1976). Simulated Earthquake Motions Compatible with Prescribed Response Spectra. *Department of Civil Engineering, Massachusetts Institute of Technology, Cambridge,* Research Report R76-4, MA, USA.

[33] **Demonceau, J. F., Hoang, L. V., Jaspart, J. P., Sommariva, M., Maio, D., Zilli, G., Demofonti, G., Ferino, J., Pournara A. E., Varelis, G. E., Papatheocharis, C., Perdikaris, P., Pappa P. Karamanos S. A., Ferrario, F., Bursi, O. S., Zanon G.** (2011). Performance-Based Approaches for High Strength Tubular Columns and Connections under Earthquake and Fire Loadings. *Research Programme of the Research Fund for Coal and Steel.* Project ATTEL.

[34] **Fassin, M.** (2011). Analisi Dinamica non Lineare di Strutture Composte Acciaio-Calcestruzzo Realizzate in Elementi Tubolari di Acciaio ad alta Resistenza, *M.Sc. Thesis,* University of Trento, Italy.

[35] **Oyen, P. E.** (2006). Evaluation of Analytical Tools for Determining the Seismic Response of Reinforced Concrete Shear Walls, *M.Sc. Thesis,* University of Washington, USA.

[36] **European Convention for Constructural Steelwork** (1986). Recommended Testing Procedure for Assessing the Behaviour of Structural Steel Elements under Cyclic Loads. *ECCS Technical Committee 1-Structural Safety and Loadings Technical Working Group 1-3, Seismic Design,* Brussels, Belgium.

[37] **Gelfi, P.** (2011). Civil Engineering Free Software developed with the cooperation of the students of the author. University of Brescia, Italy. http://dicata.ing.unibs.it/gelfi/software/programmi_studenti.html

APPENDICES

APPENDIX A: Drawings of the Structure
APPENDIX B: Input data
APPENDIX C: Analyses Results

APPENDIX A: Drawings of the Structure

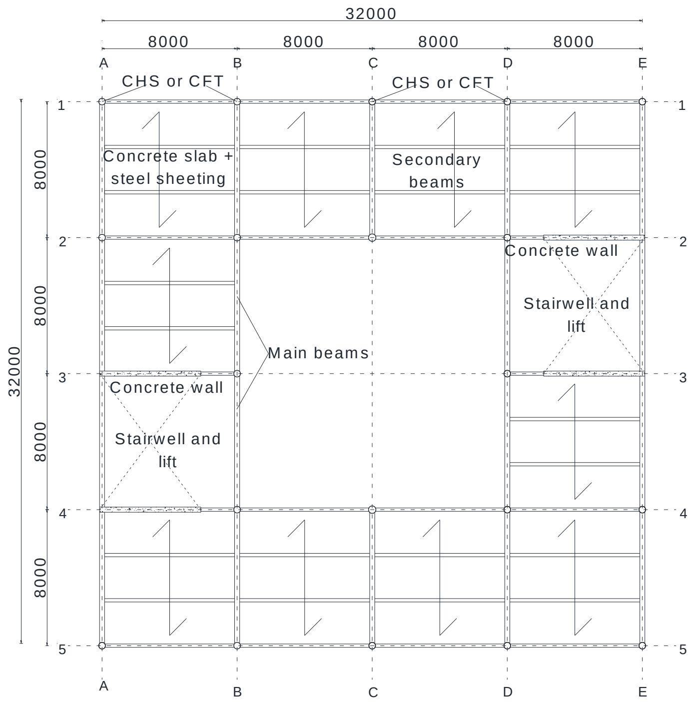

Figure A.1 : Plan view for the ground floor of 3D structure.

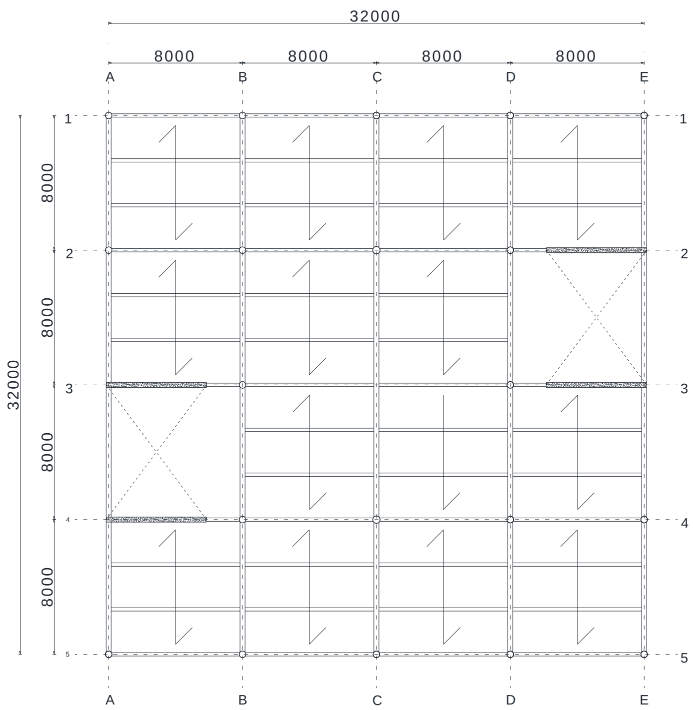

Figure A.2 : Plan view for the 4th floor of 3D Structure.

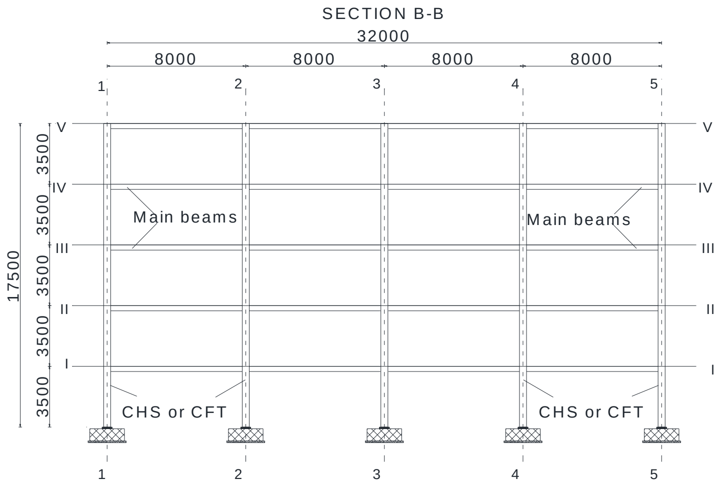

Figure A.3 : Sectional view for axis B-B of the 3D structue.

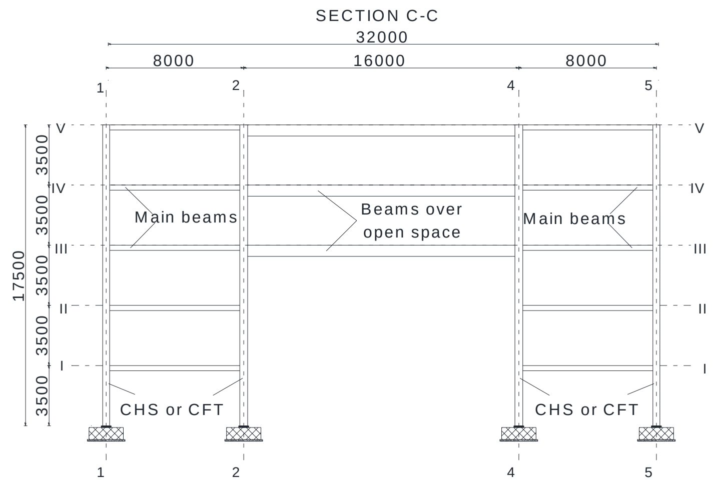

Figure A.4 : Sectional view for axis C-C of the 3D structue.

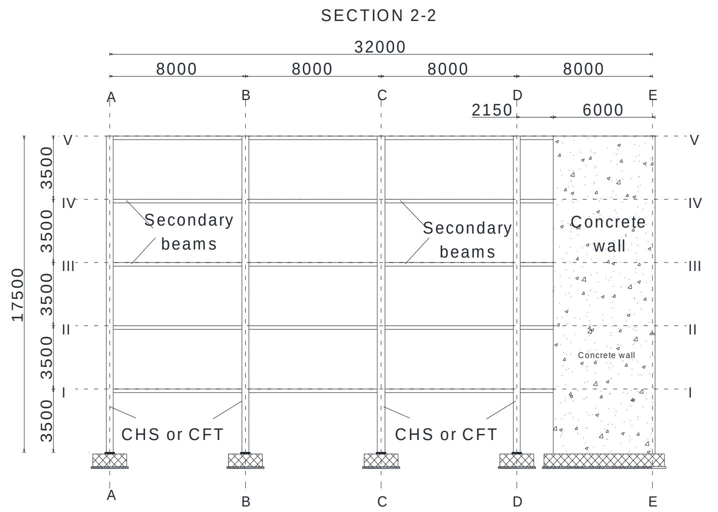

Figure A.5 : Sectional view for axis 2-2 of the 3D structue.

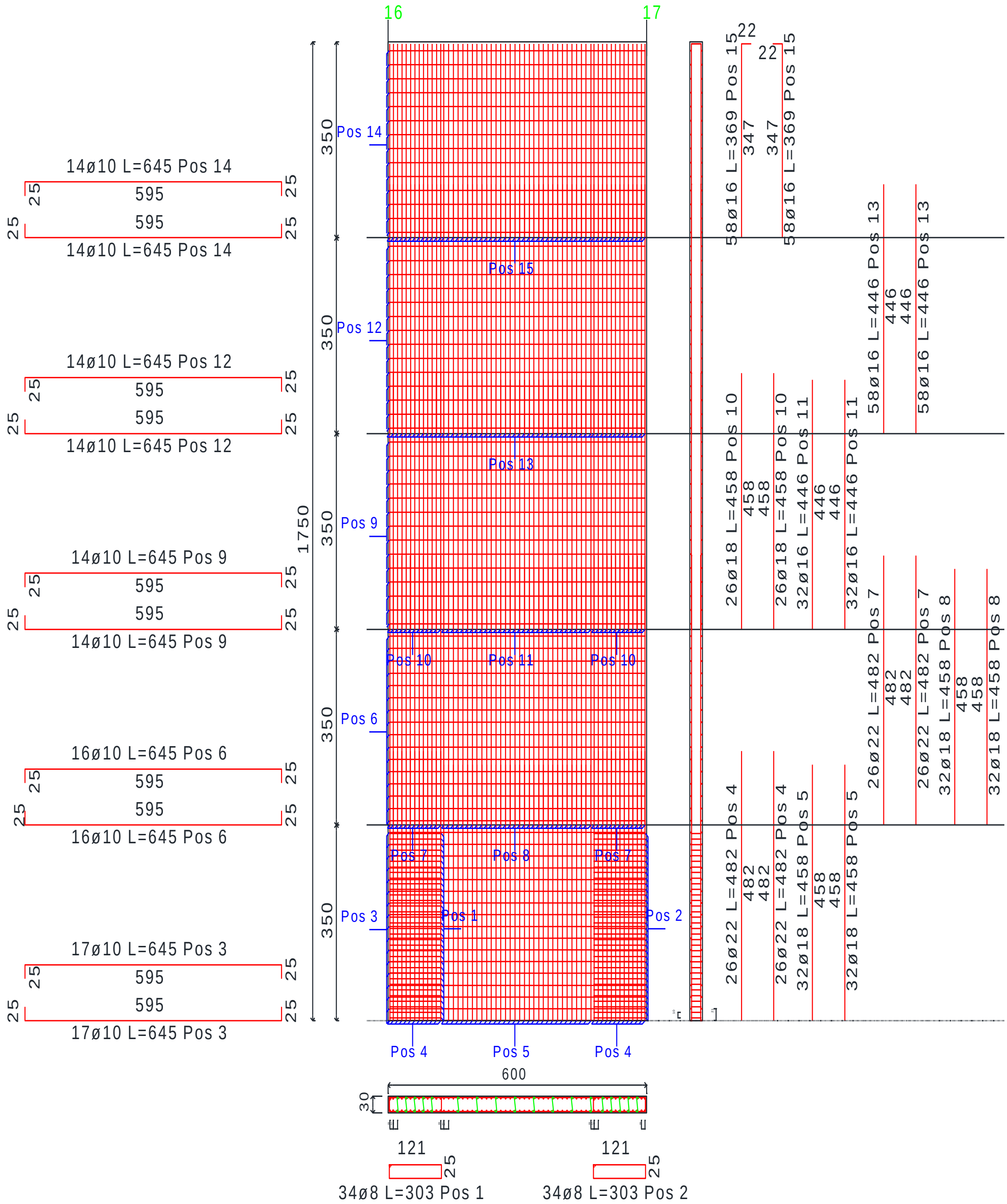

Figure A.6 : Reinforcement details of RC shear walls.

Table A.1 : Reinforcement details of RC shear walls.

Floor	Reinforcement			
	Longitudinal		Transversal	
4	116Ø16		28Ø10	
3	116Ø16		28Ø10	
2	52Ø18	64Ø16	28Ø10	
1	52Ø22	64Ø18	32Ø10	
Base	52Ø22	64Ø18	34Ø10	68Ø8

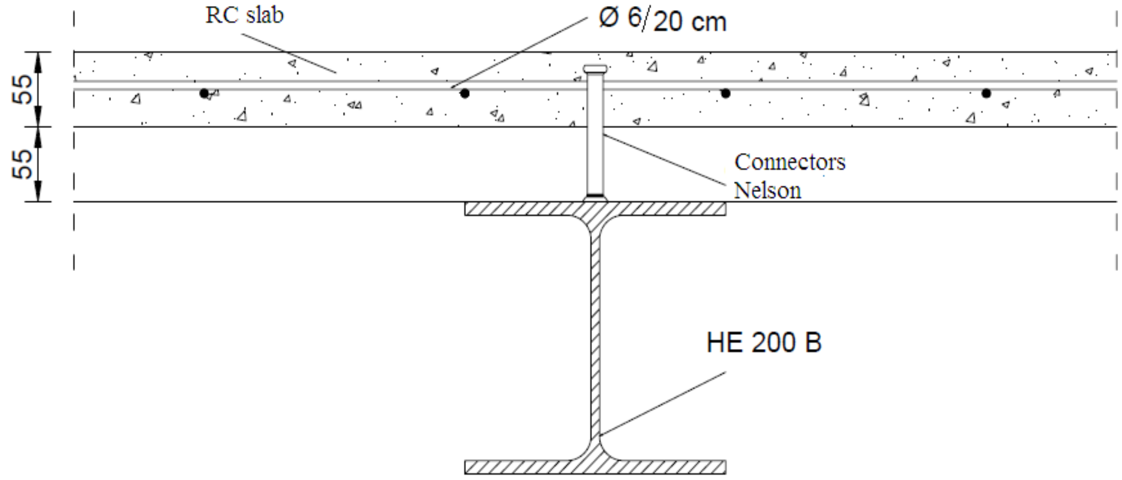

Figure A.7 : Sectional view for composite secondary beams [34].

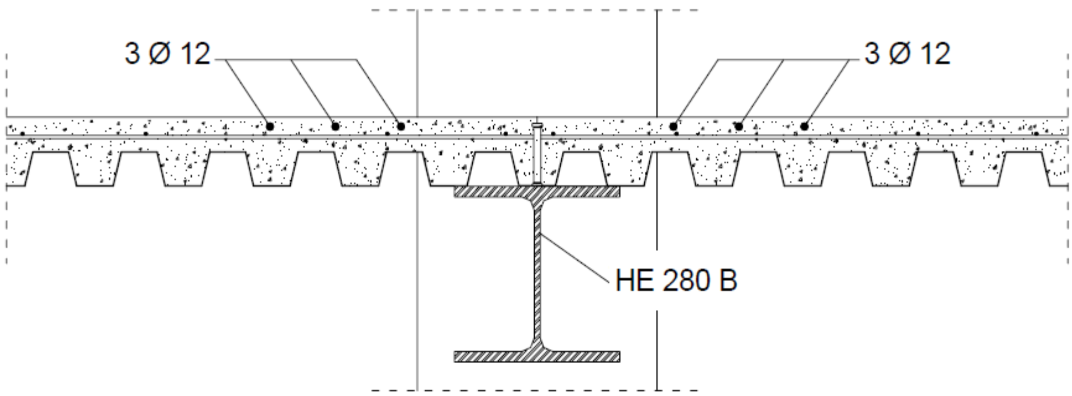

Figure A.8 : Sectional view forcomposite primary beams [34].

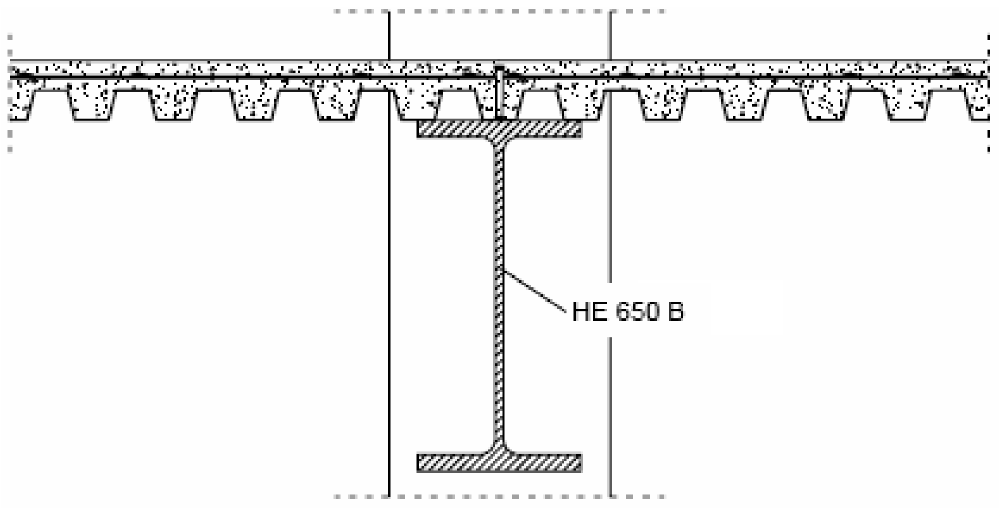

Figure A.9 : Sectional view for the beams above the open space [34].

APPENDIX B: Input Data

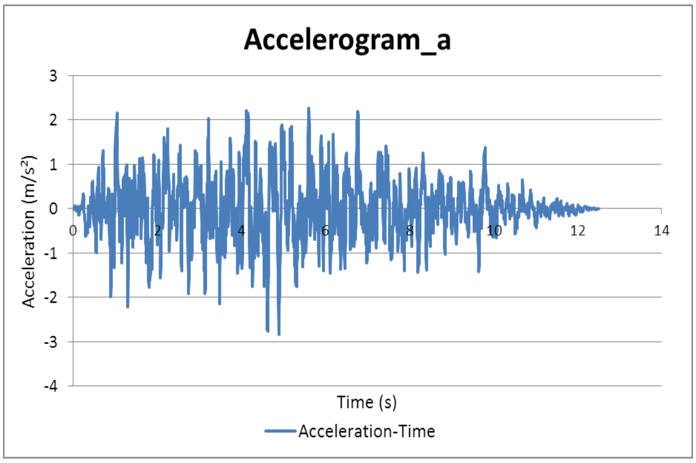

Figure B.1: Artificial accelerogram_a for time-history analysis.

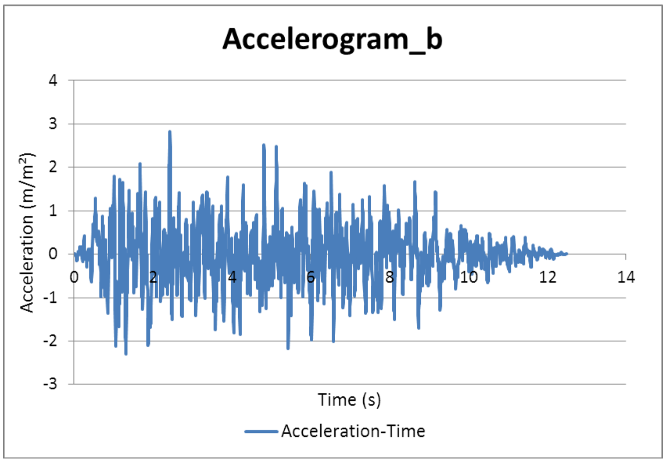

Figure B.2: Artificial accelerogram_b for time-history analysis.

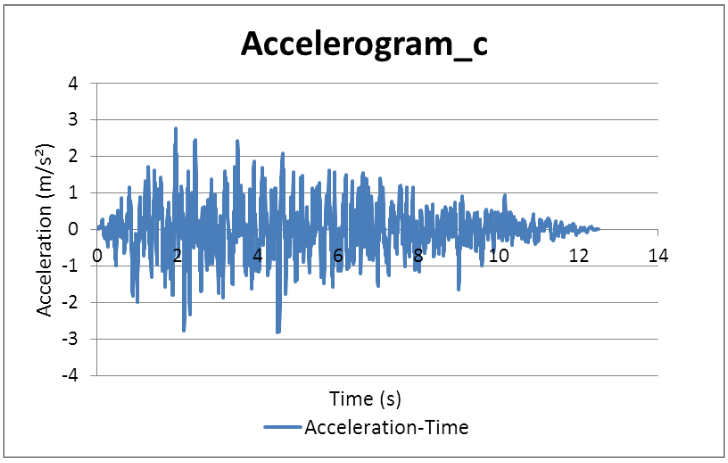

Figure B.3: Artificial accelerogram_c for time-history analysis.

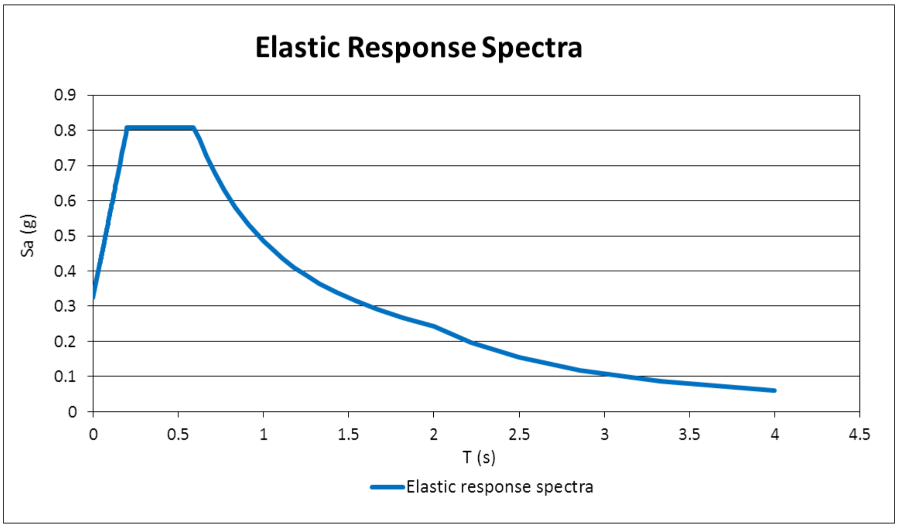

Figure B.4: Elastic Response Spectra of the Structure in Terms of *g*.

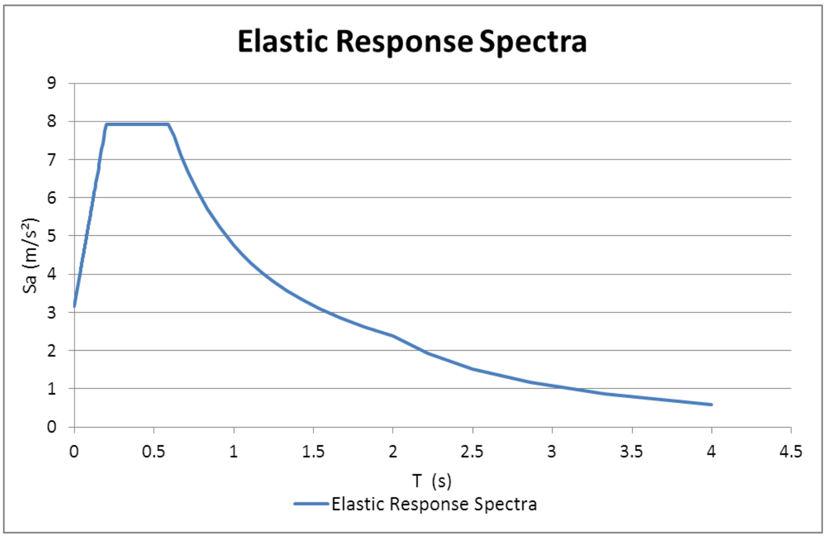

Figure B.5: Elastic Response Spectra of the Structure (m/s²).

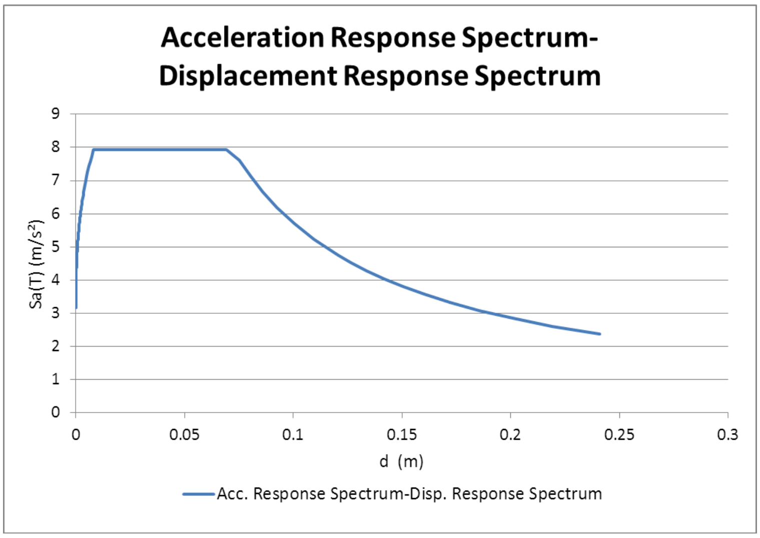

Figure B.6: Acceleration Response Spectrum vs. Displacement Reponse Spectrum.

APPENDIX C: Analyses Results

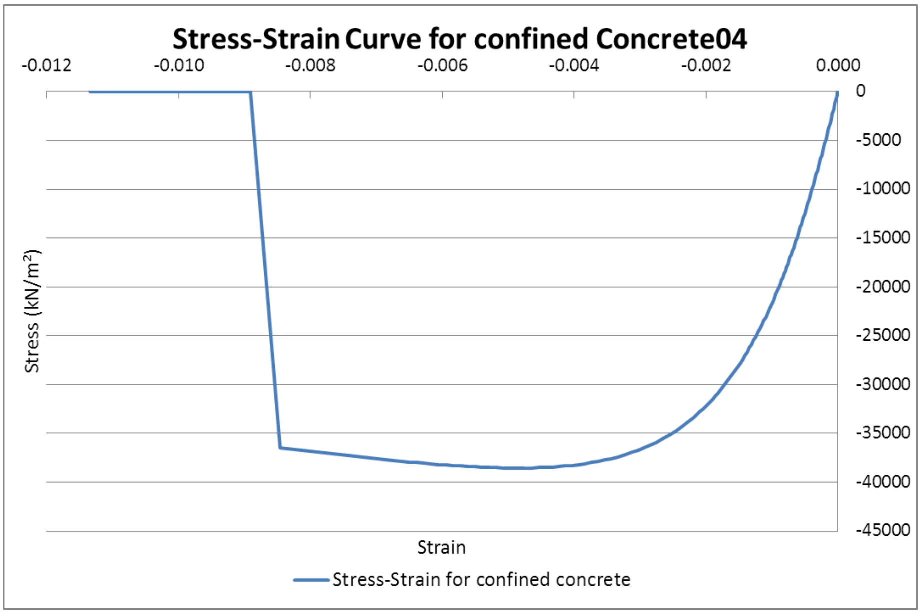

Figure C.1: Stress-starin curve of fiber defined with confined concrete04 model.

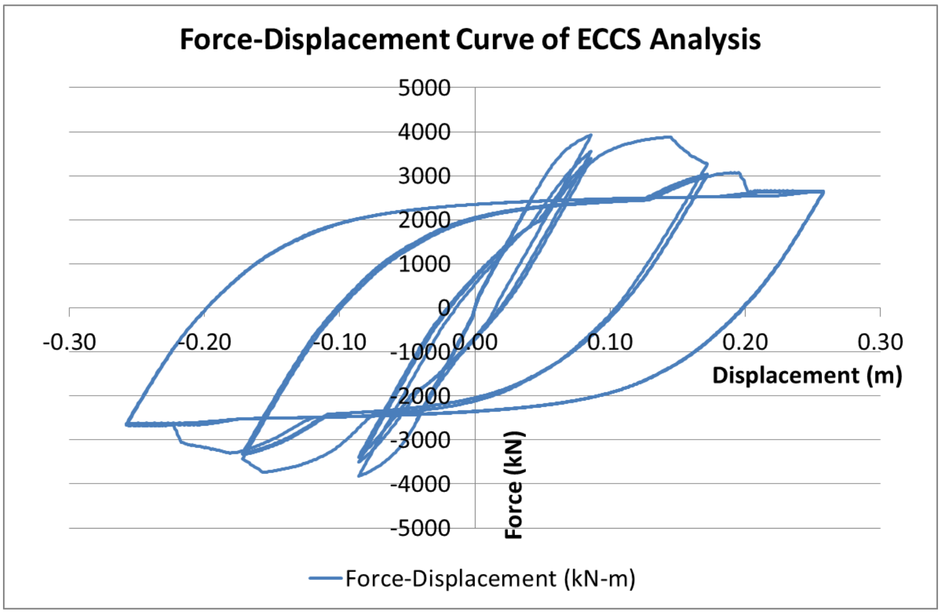

Figure C.2: Force-displcement curve of shear wall for ECCS loading.

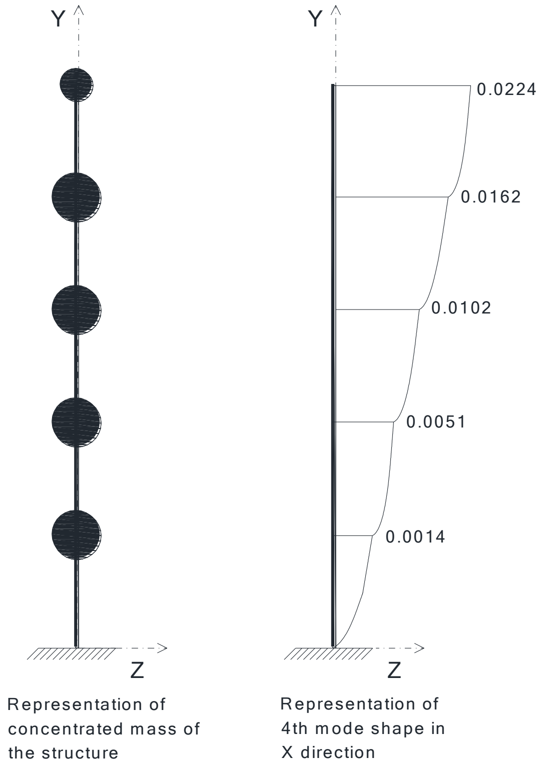

Figure C.3: Representation of concentrated mass and 4th mode shape of the structure.

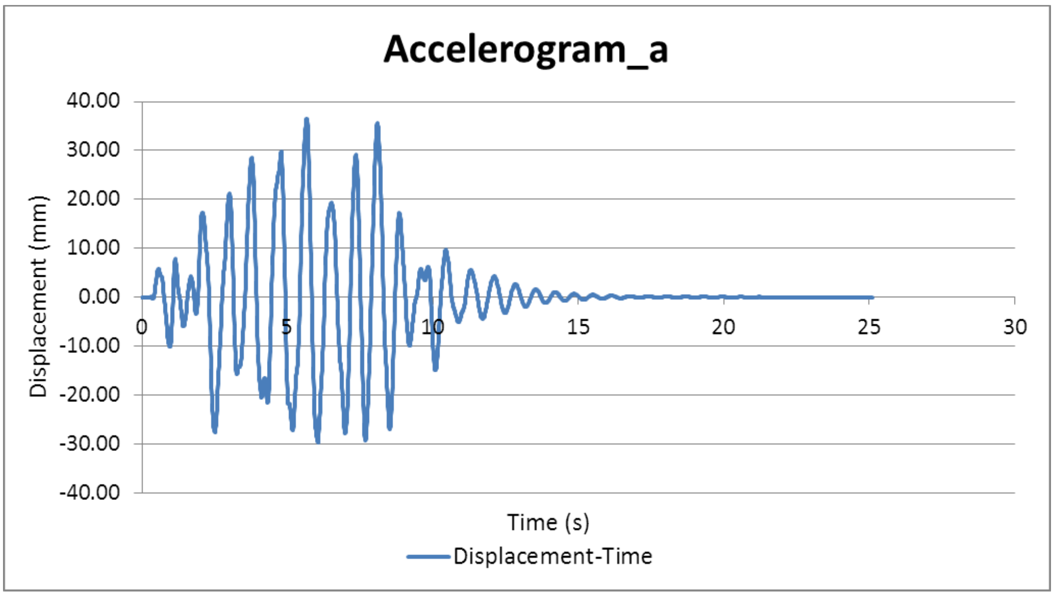

Figure C.4: Displacements of the roof (control node) of the structure for accelogram_a

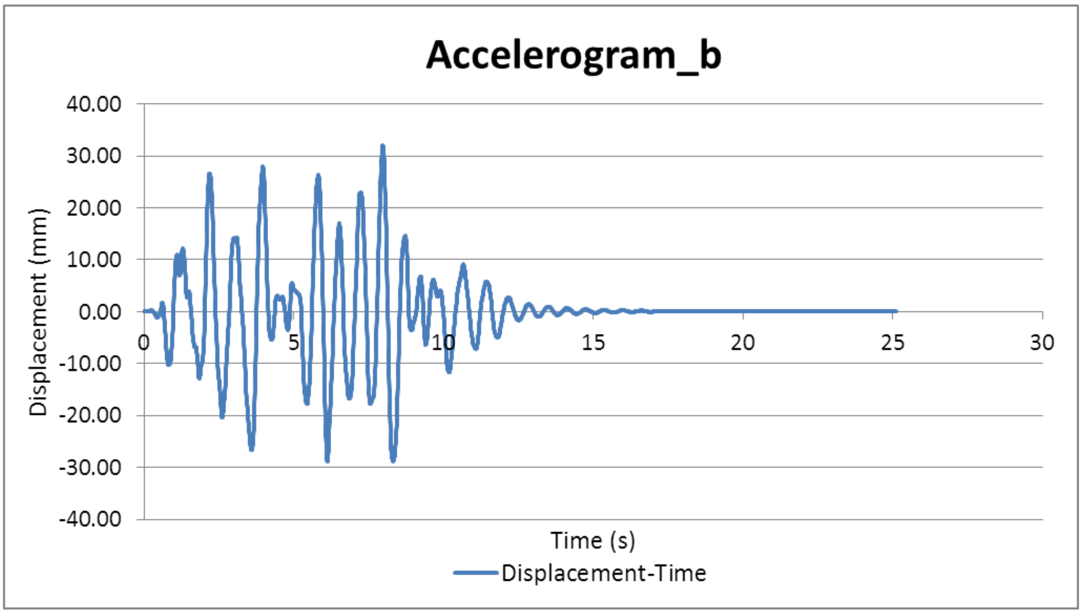

Figure C.5: Displacements of the roof (control node) of the structure for accelogram_b

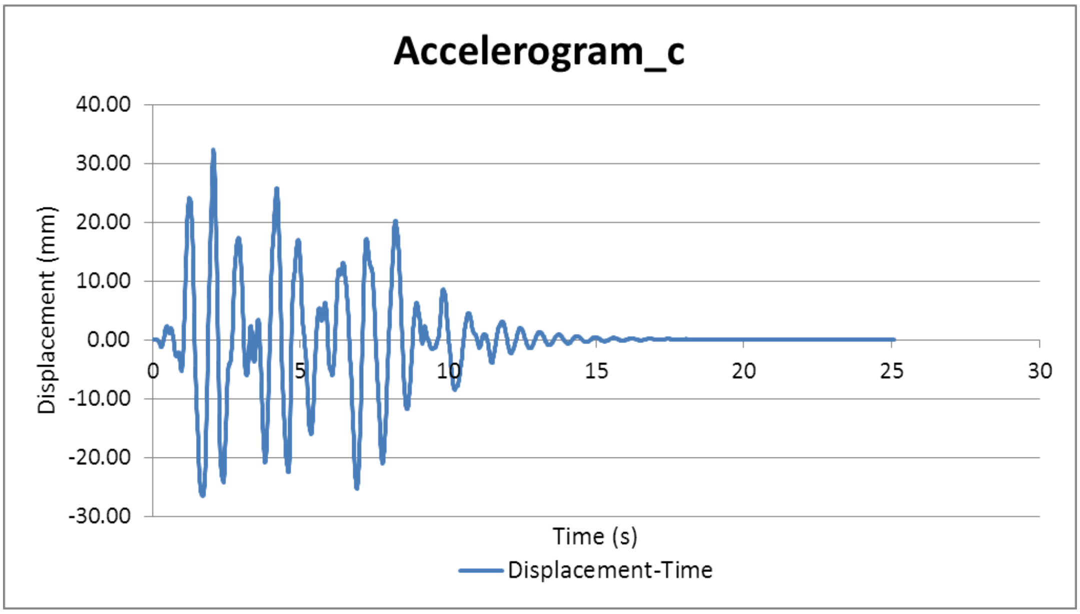

Figure C.6: Displacements of the roof (control node) of the structure for accelogram_c

CURRICULUM VITAE

Name Surname: Ragibe Ece Yükselen

Place and Date of Birth: Antakya, 16.03.1989

E-Mail: yukselenr@itu.edu.tr

B.Sc.: Istanbul Technical University, Civil Engineering Programme.

Professional Experience:
University of Trento, Italy. Research for Master's Thesis *(Sept. 2013-March 2014).*
Parlar Engineering and Consulting. Structural Design *(Feb. 2013-Augst 2013).*
Cecen Steel Construction Componay. Structural Design *(Sept. 2012-Jan 2013).*
Cakit Engineering and Consulting. Structural Design *(July 2011-Sept. 2012).*